Interpretations of Data and Mechanisms for Hippocampal Pyramidal Cell Models

Lyle J Borg-Graham*
Equipe Cognisciences
Institut Alfred Fessard - CNRS
91198 Gif-sur-Yvette, France

April 16, 1997 (Corrections March 22, 1998)

A Chapter in "Cerebral Cortex, Volume 13: Cortical Models"
Edited by P. S. Ulinski, E. G. Jones and A. Peters, New York: Plenum Press, 1998

Abstract

Biophysically detailed models of single neurons which draw on a wide variety of experimental and theoretical foundations are increasingly important in the understanding of the functional role of various cellular mechanisms. In this paper, such an approach is detailed for pyramidal neurons of the hippocampus. Included is a review of the experimental literature, descriptions of biophysical models appropriate for the analysis of single cell behaviour, a comparative review of several published models, and parameters for an updated model of this cell type.

*lyle@cogni.iaf.cnrs-gif.fr, Tel: (331) 69 82 34 13, Fax: (331) 69 82 34 27

Contents

1 Introduction **6**
- 1.1 Neuron Model Evolution - Following Electrophysiology . . . 6
- 1.2 Neuron Model Evaluation - Following the Parameters . . . 7
- 1.3 Why Hippocampus? . . . 7
- 1.4 Organization of This Chapter . . . 7

2 The Database for Single Neuron Models **8**
- 2.1 Voltage Clamp Versus Current Clamp . . . 8
- 2.2 Single Channel Versus Macroscopic Currents . . . 9
- 2.3 Type of Preparation . . . 9
- 2.4 Kinetic and Pharmacological Dissection . . . 10
- 2.5 Temperature Dependence . . . 10
- 2.6 Age Dependence . . . 11
- 2.7 Hippocampal Subfield Dependence . . . 11
- 2.8 Differences in Firing Properties Between Sharp vs. Patch Recordings . . . 11
- 2.9 The Measured Voltage . . . 12

3 Strategies for Single Neuron Models **12**
- 3.1 Building the Model . . . 12
- 3.2 Parameter Searching . . . 12
- 3.3 Model Robustness and Validation - As Robust As Nature? . . . 13
- 3.4 The Purpose of Modelling - Testing Speculations . . . 13
- 3.5 Tools for Compartmental Models . . . 14

4 Anatomy and the Model: Data and Methods **14**
- 4.1 Reducing Branching Cable Structures and the Placement of Channels . . . 15
- 4.2 Dendritic Tree Reduction from the Raw Anatomy . . . 15
- 4.3 Accounting for Dendritic Spines . . . 16
- 4.4 Modelling the Axon . . . 17
- 4.5 Anatomy of the Working Model . . . 17

5 The Linear Model: Data and Methods **17**
- 5.1 Reproduction of Linear Properties . . . 18
- 5.2 Measured Properties of the Resting State . . . 18
  - 5.2.1 Considering A Somatic Shunt . . . 18
- 5.3 Analytical Methods and Results . . . 19
  - 5.3.1 Analysis of Dendritic Transients . . . 19
  - 5.3.2 Pitfalls Evaluating Linear Parameters Derived from Intracellular Measurements . . . 19
  - 5.3.3 Combined Experimental and Modelling Results . . . 20
- 5.4 Numerical Methods: Morphoelectrotonic Analysis of Dendritic Trees . . . 21
- 5.5 How Far Can We Take Linear Dendritic Models? . . . 21
- 5.6 Model Linear Parameters . . . 21

6 Phenomenological Templates **22**
- 6.1 Morphology of the Potentials Preceeding the Spike . . . 22
  - 6.1.1 Rectification Around the Resting Potential . . . 22
  - 6.1.2 The Pre-Hyperpolarization between Repetitive Spikes . . . 22
- 6.2 Morphology of the Action Potential . . . 23
  - 6.2.1 Action Potential Threshold: Absolute and Relative to Holding Potential . . . 23
  - 6.2.2 Action Potential Rate of Rise and Fall . . . 24
  - 6.2.3 Action Potential Amplitude and Duration . . . 24
- 6.3 Where Does the Spike Start? . . . 24
- 6.4 Morphology of the After-Potentials . . . 25
  - 6.4.1 The Fast After-Hyperpolarization . . . 25
  - 6.4.2 The After-Depolarization . . . 25
  - 6.4.3 The Medium After-Hyperpolarization . . . 26

6.4.4 The Slow After-Hyperpolarization . . . 26
6.4.5 The Slow After-Depolarization and Plateau Potentials . . . 27
6.5 Differences in Firing Properties Between HPCs and Other Cell Types . . . 27
6.6 Regular Firing Characteristics - Adaptation and f/I Characteristics . . . 28
6.7 Mechanisms for Bursting . . . 28
6.7.1 Is the Dendritic Tree Important for Bursting? . . . 28
6.7.2 Constraints for the Slow Depolarization Mechanism Underlying Bursts . . . 29
6.7.3 Is Ca^{2+} Entry the Key? . . . 29
6.7.4 Bursting in the Hippocampal Network . . . 30
6.7.5 So What Causes Bursting? . . . 30
6.8 D Spikes . . . 31
6.9 Dendritic Channels and "Hot Spots" . . . 31

7 Review of Hippocampal Models **31**
7.1 Single Cell Models Emphasizing Intrinsic Non-linear Properties . . . 31
7.1.1 Models of Traub and Colleagues . . . 31
7.1.2 Borg-Graham, 1987 Model . . . 32
7.1.3 Wathey, Lytton, Jester, and Sejnowski 1992 Model . . . 33
7.1.4 Pongracz, Poolos, Kocsis, and Shepherd, 1992 Model . . . 33
7.1.5 Warman, Durand and Yuen, 1994 Model . . . 33
7.1.6 Models of Jaffe et al., 1994, and Migliore et al., 1995 . . . 34
7.1.7 Other Single Cell Models . . . 34
7.1.8 Recapitulation on the Working Model . . . 35
7.1.9 On-line Parameters of Reviewed Models . . . 35
7.2 Models Emphasizing Interactions Between Synaptic Processes and Intracellular Ion Dynamics 35

8 Channel Models **35**
8.1 Linear Conductance: Driving Force From Equilibrium Thermodynamics . . . 36
8.1.1 Setting E_{rev} for Ohmic Channel Models . . . 36
8.2 Intrinsic Non-Linearity of Pore Conduction . . . 36
8.3 Channel Gating *à la* Hodgkin and Huxley: Independent Voltage-Dependent Gating Particles 37
8.4 An Extended Hodgkin and Huxley Model . . . 37
8.4.1 Comparison to the Original Hodgkin-Huxley Equations . . . 38
8.4.2 Parameters of the Single Barrier Gating Model . . . 38
8.4.3 Relationships Between the Extended Hodgkin-Huxley Model Parameters and $x_\infty(V)$ and $\tau_x(V)$ . . . 39
8.4.4 Determining the Number of Particles in Hodgkin-Huxley Models . . . 39
8.5 Activation versus De-Activation; Inactivation versus De-Inactivation . . . 39
8.6 The Hodgkin-Huxley Model: Some Conclusions . . . 40
8.7 Channel Gating as Dynamical Systems *à la* Markov Models . . . 40
8.7.1 Markov Mechanisms Can Decouple the Timecourse of Activation/Inactivation Signals and Functional Channel State Transitions . . . 40
8.7.2 Linear Markov models based on the Hodgkin-Huxley model . . . 41
8.8 Ca^{2+}-Dependent Gating . . . 41
8.8.1 The Barrett, Magleby and Pallotta 1982 Model . . . 41
8.8.2 The Moczydlowski and Latorre 1983 Model . . . 41
8.8.3 A Simple Kinetic Model . . . 42

9 Ionic Concentration Dynamics **42**
9.1 The Data on Ca^{2+} Concentration Dynamics . . . 43
9.1.1 Ca^{2+} Influx Via Voltage-Gated Ca^{2+} and Synaptic Channels . . . 43
9.1.2 $\Delta[Ca^{2+}]$ From Current-Evoked Spikes . . . 43
9.2 Determinants of the Resting $[Ca^{2+}]_{in}$ . . . 44
9.3 Considering Intracellular Ca^{2+} Stores . . . 44
9.4 Membrane Pumps . . . 44
9.4.1 The Sodium Pump . . . 44
9.4.2 Ca^{2+} Pumps, and Models of Ca^{2+} Removal . . . 45

9.4.3 Pump Model for the Working Model . . . 45
9.5 Buffer Models . . . 45
9.5.1 Instantaneous Buffer Model . . . 46
9.6 Models of Ca^{2+} Diffusion . . . 46
9.7 The $[Ca^{2+}]_{in}$ System in the Working Model . . . 47
9.7.1 A Multi-Compartment Ca^{2+} System with Instantaneous Buffer . . . 47
9.7.2 Consequences of the Soma/Short-Cable Model: Adjusting Ca^{2+} Channel Current Influx For $[Ca^{2+}]$ Integration . . . 48

10 HPC Sodium Channels **48**
10.1 Electrophysiology of Sodium Channels in Mammalian Central Neurons . . . 49
10.1.1 Interpretations Based on the Sah et al. 1988b Data . . . 49
10.1.2 I_{Na} Modulation . . . 49
10.1.3 I_{Na} - Fast, Slow, Persistent Components? . . . 49
10.1.4 Stability and the "Window Current" . . . 50
10.1.5 Na^+-only Spikes . . . 50
10.1.6 The Sub-threshold/Threshold Regime . . . 50
10.1.7 Relating I_{Na} Kinetics to Spike Properties and the PHP . . . 51
10.2 Comparison of I_{Na} Models from the Literature . . . 51
10.2.1 Hodgkin-Huxley Type I_{Na} Models . . . 51
10.2.2 A Model with Multiple Hodgkin-Huxley Type I_{Na} Channels . . . 52
10.2.3 Evaluating Published Markovian Kinetic Models . . . 52
10.3 An *ad hoc* Markovian Model . . . 52
10.3.1 A Variable Threshold Without A Large Window Current . . . 52
10.3.2 Accounting for the Persistent Na^+ Current . . . 53
10.3.3 Shortcomings of the I_{Na} Model . . . 53

11 HPC Calcium Channels **53**
11.1 T-, N-, R-, P-, Q- and/or L-type: How Many Ca^{2+} Channels Are There in HPCs? . . . 53
11.2 Electrophysiology of Calcium Channels . . . 54
11.2.1 I_{Ca} Modulation . . . 54
11.2.2 Characteristics of Calcium Spikes . . . 54
11.2.3 Kinetics of Activation and Inactivation of Ca^{2+} Currents . . . 54
11.3 HPC Model Ca^{2+} Channels . . . 55
11.3.1 Models With A Single Type of Ca^{2+} Channel . . . 55
11.3.2 Models Incorporating Three Types of Ca^{2+} Channels . . . 56
11.4 Major Properties for the Working Model Ca^{2+} Channels . . . 56

12 HPC Potassium Channels **56**
12.1 The Slow Subthreshold K^+ Current: I_D . . . 57
12.1.1 A Model of I_D . . . 57
12.2 The Delayed-Rectifier K^+ Current: I_{DR} . . . 57
12.2.1 A Model of I_{DR} . . . 58
12.3 The Fast Transient Repolarizing K^+ Current: I_A . . . 58
12.3.1 A Model of I_A . . . 59
12.4 The Fast Ca^{2+}-Dependent Repolarizing K^+ Currents: I_C and I_{CT} . . . 59
12.4.1 A 3 State Markov Model for I_{CT} with Voltage and Ca^{2+} Dependent Transitions . . . 60
12.5 The Slow Ca^{2+}-Dependent K^+ Current: I_{AHP} . . . 61
12.5.1 A Model of I_{AHP} . . . 61
12.6 Is the Variance in Kinetics Between I_{CT} and I_{AHP} Due to Unique Pools of Ca^{2+}? . . . 62
12.7 The Muscarinic K^+ Current: I_M . . . 63
12.7.1 A Model of I_M . . . 63
12.8 Anomalous Inward Rectification and Other K^+ Currents . . . 63
12.8.1 Anomalous Inward Rectification . . . 64
12.8.2 A Serotonin-activated Inward Rectifier . . . 64
12.8.3 $I_{K,rest}$, $I_{T,slow}$, $I_{K(slow)}$ . . . 64

13 Non-Specific Cation and Chloride Currents **64**
13.1 The Hyperpolarization-Activated Sag Current: I_Q/I_H 65
13.1.1 A Model of I_H 65
13.2 The Persistent Cl^- Current: $I_{Cl(V)}$ 66
13.3 The Ca^{2+}-dependent Non-Specific Cation Currents: I_{ADP}, I_{CAN}, I_{ACPD} 66

14 Simulations of HPC Properties with the Working Model **66**

List of Figures

1 Anatomies of Hippocampal Pyramidal Cells and Models 79
2 Consolidation of Dendritic Segments 80
3 Example of The Reduction of a Full Anatomical Description 81
4 The Reduced Anatomy has Similar Linear Properties as the Original 82
5 Linear Response of the Working Model 82
6 Landmarks for Phenomenological Templates 83
7 The Single Spike of the Working Model 84
8 Voltage Clamp Properties of I_{Na} Models 85
9 State Diagrams of Markov Gating Models Used for I_{Na} and I_{CT} in the Working Model . . . 86
10 Properties of the Working Model 4 State Markov I_{Na} Model 87
11 Simulations of the Modulation of Single Spikes by the Major Repolarizing Currents 88
12 Simulations of the Spike Trains 89
13 Simulations of Spike Trains with Whole Cell Patch Parameters 90
14 Simulations of the Modulation of Spike Trains 91
15 Simulations of the Development of the mAHP and the sAHP and $[Ca^{2+}]_{in}$ During Spike Trains 92
16 Simulations of the Role of I_D in Delaying the First Spike of a Train 93
17 Simulations of the f/I Characteristic 93

List of Tables

1 Measured and Modelled Linear Parameters 94
2 Measured and Modelled Single Spike Parameters 95
3 Measured and Modelled $[Ca^{2+}]_{in}$ Parameters 95
4 Summary of Channels in the Working Model 96
5 Parameters for the Extended Hodgkin-Huxley Model Gating Particles in the Working Model 96
6 Parameters for I_{Na} Markov Model Gating in the Working Model 97
7 Parameters for I_{CT} Markov Model Gating in the Working Model 97
8 Parameters for I_{AHP} Ca^{2+}-Dependent Gating in the Working Model 97

1 Introduction

A neuron model organizes, collates, and directs our expanding electrophysiological and biophysical knowledge. This chapter reviews single neuron models, with hippocampal pyramidal cells (HPCs) as the reference, emphasizing the integration of electrophysiological data and biophysical theory into a cohesive hypothesis. We discuss the process of translating data into specific mechanistic hypotheses. We critically review the parameters and mechanisms that have been used in several models published to date, comparing their predictions with the data and against each other. A final goal is the description of an updated HPC model that may be a reference for future refinement and elaboration.

1.1 Neuron Model Evolution - Following Electrophysiology

Single neuron models, inspired by the remarkable success of Hodgkin and Huxley (1952b), have evolved in fits and starts in parallel with advances in experimentally-based (wet) understanding. Happily, the tools for both approaches have become more sophisticated and easier to use - consider the widespread use of patch clamp setups and sophisticated neuronal simulator programs (cf. sharp electrode protocols and SPICE).

Unhappily, while in the experimental realm natural constraints can be relied upon - barring gross mishandling of the data, brain tissue sets the rules - the Garbage In Garbage Out maxim in computer science is a ubiquitous gnat in simulations. Thus, for wet experiments biology sets the "equations", and the job of the electrophysiologist is to be clever and careful enough to read the results. With dry experiments, the experimenter-programmer defines both the input and the black box, exposing the result to a much greater possibility of error.

The success of the Hodgkin-Huxley model of the squid axon and the associated Na^+ and K^+ channels was due to at least two reasons. First, there was a scientific design in which experiment and theory were directly intertwined (with good fortune, Hodgkin 1976). Second, the system under scrutiny was relatively simple and well measured, with two dominant and separable non-linear components and very good space clamp of a large accessible structure. All the model parameters were taken directly from data (more or less, in the case of gating particle exponents) and, in retrospect, it is not completely suprising that such a model reproduces "itself" so well.

On the other hand, applying the Hodgkin-Huxley approach or extensions of it to neurons in which many, or in fact most, of the parameters are not directly measurable has been more problematic. This difficulty stems from at least the following factors. First, it is difficult to constrain the free parameters of non-linear dynamical systems in order to uniquely reconstruct some data set - a minimal data set is hard to specify and there is the possibility of multiple formal solutions. Second, most non-linear modelling is accomplished with fairly easy to apply, robust numerical methods; thus it is not too hard to get something that "looks" reasonable, even when bugs linger in the code or understanding.

That being said, detailed, carefully constructed and qualified single cell models can yield useful insights, suggest testable predictions, and assist in quantitative comparison of data from different sources that describe the same phenomena (Borg-Graham, 1987c, Bower and Koch, 1992). The intent of this chapter is to point out some of the pitfalls as well as useful strategies in this process.

The ultimate utility of these models is for understanding the role of individual cells, particular channel types, or other mechanisms in brain physiology and pathology. For example, the identification of several membrane currents as the principle effector of various components of the voltage response of a cell - e.g. I_{CT} and the fAHP, I_{AHP} and the sAHP - is well-established. Correlations between instrinsic, low-level phenomena and disease states have been reported, e.g. alteration of various phases of spike repolarization and repetitive firing characteristics in scrapie-infected mouse HPCs (Johnston et al., 1997). More ambitious proposals include assigning specific membrane potentials, and by implication their causitive membrane currents, to cognitive phenomena, e.g. the proposal by Lisman and colleagues as to the role of the sADP in short-term memory in hippocampus (Jensen et al., 1996b).

Although much progress remains for the predictive success of this level of model (see for example Goldstein and Colatsky, 1996 in relation to channel models), given the increasing confluence of experiment and theory, this is indeed an exciting time for this fundamental component in the evolving field of computational neuroscience.

1.2 Neuron Model Evaluation - Following the Parameters

In this chapter we shall review both the experimental basis for model parameters and the interpretation of these parameters in various published models. In the process of analyzing the modelling reports, it became clear that a significant obstacle was the difficulty of reproduction, independent of any issues associated with specific interpretations of the electrophysiological data - essentially every model analysed within this review (including the author's previous work!) presented various degrees of internal inconsistencies at the parameter or equation level. In some cases, consultations with the authors resulted in the necessary corrections (e.g. typographical errors); in others, careful analysis and adjustment of model parameters bore fruit. We believe that the essential problem is that of reliable communication of the large parameter sets characteristic of these sorts of models. To this end, the parameters presented here are available on-line in the Surf-Hippo neuron simulator distribution (Borg-Graham, 1995; see Section 3.5). Readers wishing to use the mechanisms described in this chapter thus have convenient access to the relevant parameters, with the benefit that updates to the on-line parameters will be made as warranted by future work or contributions from other workers.

A recent collection of papers describing single neuron models, including hippocampus (Claiborne et al., 1992 and Brown et al., 1992), is found in McKenna et al. (1992). Segev (1992) discusses various issues regarding the level of detail appropriate for single cell models, and a review of models focusing especially on computations in dendritic trees has been written by Mel (1994).

1.3 Why Hippocampus?

Models of many cell types, and just about every brain region, have appeared in the last decade. Models of hippocampal cells are of particular interest because the electrophysiological literature on these cells and the hippocampal region is especially rich - HPCs are among the most studied cell type of the mammalian brain, and the circuitry of the hippocampus is known to a large degree. While there are certainly functional physiological differences between cortical cells of different areas, and between cells within the same area (see Section 2.7 for how this applies to the hippocampus), choosing the HPC as a representative, canonical cortical pyramidal cell is not unreasonable.

The data and models in this chapter derive mainly from studies of HPCs in the CA1-CA3 regions in rat and guinea pig. Data from both sharp electrode and patch electrode recordings will be considered and compared, with the majority of cases being from the *in-vitro* brain slice preparation. Occasionally, specific references will be made to data and models of non-pyramidal hippocampal neurons (interneurons, cells of the dentate gyrus), cortical pyramidal neurons and other neurons - such references are intended to be illustrative, not definitive.

1.4 Organization of This Chapter

There are several interrelated themes to this chapter:

- Model components - anatomy, linear properties, channel models, concentration dynamics
- Review of HPC electrophysiology
- Review of HPC models
- New model structure and parameters

We focus on a single cell model that reproduces the intrinsic behaviour of a neuron, whose elements include the linear membrane properties and the variety of voltage and 2nd messenger gated channels which shape a cell's response. The discussion is primarily on properties observed from responses to intracellular current or voltage stimulation, as opposed to synaptic stimulation; occasionally we will mention single neuron models in the context of network models. Likewise, our view of the neuron here is in the context of relatively short time scale dynamics, under the assumption that the basic architecture is stable. The resulting model could serve as a starting point for looking at longer time scale phenomena, such as plasticity.

We start with a review of the electrophysiological methods from which model data is derived, since parameters relevant to a given mechanism or phenomenom can strongly depend on the experimental protocol. We then present a discussion of neuron model methodology, the components that go into single cell models, and what these models may be used for. This is followed by a discussion of the morphological component

of cell models, and estimates of the linear properties of HPCs. Next, the phenomenological templates that constrain model mechanisms in HPCs are presented, including the important issue as to what makes some cells burst and others not. Next, we review some of the published models of HPCs, with emphasis on single cell models. This is followed by descriptions of various models of channel biophysics and concentration dynamics, with a review of the data regarding activity driven changes in intracellular Ca^{2+}. We then describe electrophysiological data and models concerning sodium channels, calcium channels, potassium channels and other channels of HPCs. We close the chapter with selected examples of model simulations.

At various points in this chapter we will propose parameters and show results for a relatively simple HPC model, referenced to as the Working model. This model is intended to illustrate some of the issues discussed in the chapter, and sample simulations will be shown of some key behaviours - all traces in this chapter are from either this model or examples of more elaborate passive anatomical models.

We assume that the reader has an introductory exposure to cable theory, compartmental modelling techniques and electrophysiology - throughout the text we shall mention appropriate background references.

2 The Database for Single Neuron Models

A reconstruction of the neuron's electrical properties is a test of the electrophysiologist's basic, reductionist starting position: the total response of a neuron arises from an ensemble of channel types, each of which is characterized by protocols designed to describe it it individually using some combination of electrical (voltage clamp or current clamp), pharmacological and kinetic isolation. Many mechanisms contribute to particular characteristics, and it is of considerable interest to understand which of these mechanisms are physiologically modulated (Kaczmarek and Levitan, 1987). Observed variability of the cell response may have a profound implications on the computational role of the neuron - one goal of a model may be to determine what variability is "real" and what is a function of the experimental setup.

In this section we describe some of the characteristics and limitations of the experimental procedures from which model parameters are derived. Different experimental techniques can give different values of model parameters, therefore it is quite important to understand the variety of procedures in order to better integrate data for different sources. Useful introductions to practical electrophysiological technique can be found in Kettenmann and Grantyn (1992), The Axon Guide (Sherman-Gold, 1993), and in Neher and Sakmann (1995).

In reality, isolation of specific mechanisms is rarely, if ever, completely possible, notwithstanding the issue of the potential lability of channel properties under various recording contexts (*in-vivo*, slice, culture, electrode type, etc.). An integrative model, therefore, must incorporate the available data with a certain flexibility - all the models referenced here base their channel models with varying degrees of fidelity to the literature. The model parameters that we will develop in this chapter are molded in this context, that is as a hypothesis of specific mechanisms which may suggest additional tests, and are constructed so that parameter evolution is as incremental as possible.

2.1 Voltage Clamp Versus Current Clamp

In an ideal electrophysiology world voltage clamp data would supply parameters of voltage-dependent parameters directly, and the reconstruction of current clamp protocols would follow accordingly. But despite the necessary working assumption by electrophysiologists that voltage clamp will yield a "purer" picture of channel behaviour, the direct insertion of voltage clamp data plus assumptions of kinetic mechanisms (in particular the Hodgkin-Huxley model, Section 8.3) into current clamp simulations typically fails. The reality is that for all but a very limited set of circumstances, the available voltage clamp data can only provide a framework for parameter estimation.

There are two reasons for this. The first has to do with limitations inherent in the various types of voltage clamp preparations, which include intact cells or reduced preparations (cultured or isolated cells). The major problem with intact cells is that accurate voltage clamp is limited to membrane near the point of electrode penetration, so that currents arising from distant, poorly clamped membrane may distort the results. Model-based discussions of these sorts of errors are given by Müller and Lux (1993), in the context of voltage-dependent membrane, and Spruston et al. (1993), looking at synaptic events (see also Johnston and Brown, 1983). On the other hand, in the reduced preparations the control of membrane voltage is better but the isolation or culturing methods may alter the cellular properties. For example, occasionally reports using the reduced preparations include representative current clamp behaviours, and the spike characteristics and firing patterns typically are quite different from what is considered "normal" (e.g. Sah et al., 1988b).

The second reason derives from the fundamental challenge for any experiment for elucidating phenomenological mechanisms: the decision as to which are the most important dimensions of the experimental parameter space. In other words, since usually it is impossible to measure everything, the primary question in experimental design is how best to place the bet. When electrophysiological mechanisms are analyzed with voltage clamp methods, the protocols are designed assuming a kinetic model, even implicitly; thus measurements are specifically chosen in order to characterize that model. For measuring membrane currents, the model is usually the Hodgkin-Huxley model. However, there is increasing evidence from both single channel data and macroscopic channel modelling that this kinetic model is inadequate for certain currents (see Section 8). For this reason, and since the system is non-linear, it is quite possible to miss important characteristics if they are not measured explicitely (the great advantage of linear systems analysis, of course, lies in the comprehensiveness of the impulse response).

In summary, since our aim is to describe a model that reproduces functional characteristics, we place an emphasis on the reproduction of properties seen under current clamp. Voltage clamp data is used to estimate parameters, but not necessarily for direct reproduction, unless that data was obtained under more or less "normal" conditions.

2.2 Single Channel Versus Macroscopic Currents

In a similar vein, in principle one should be able to record single channel properties and then apply the results to whole cell models. However, this has not been accomplished to date, suggesting at least that there may be significant alterations in channel behaviour when going from the single channel recording environment to the "natural" state. We have tried this approach for some descriptions of Na^+ channels (Section 10.2.3) with limited success at reproducing expected macroscopic current behavior (see also Destexhe et al., 1994).

2.3 Type of Preparation

Electrophysiological protocols for measuring electrical properties of neurons *in toto* and specific currents use a wide variety of preparations, each with its own advantages and disadvantages. Interpretation of data must take into account how the relevant protocol compares to that corresponding to reproduced behaviour. As stated at the beginning of the chapter, the assumed standard condition is the slice preparation, using either sharp or whole cell patch (Sakmann and Neher, 1995) electrodes. Note of course that this standard, dictated by the primacy of this preparation in the literature, is rather arbitrary if we are eventually interested in undestanding the "true" state of the cell. Consequently, we can assume that if the slice (Alger et al., 1984) is the benchmark preparation, then data from, progressively, acutely isolated cells, cultured slice (Thompson and Gähwiler, 1992), and finally cultured cells may require more flexibility in the interpretation. Likewise, perforated patch[1] and on-cell (cell-attached) patch recordings (Marty and Neher, 1995) are incrementally further removed from the control case.[2] Similar considerations apply to the age of the animal, species, and the hippocampal subfield in which the HPCs are found (for example, the degree in which properties of CA3 cells may be definitive of CA1 cells, or vica-versa, may depend on the specific mechanism under consideration). Additional considerations for interpreting sharp versus patch electrode recordings are discussed in Section 2.8. A review of the variables implicit in the techniques for slice electrophysiology is given by Reid et al. (1988).

From the point of view of parameter estimation of specific channel properties, the slice preparation allows recordings of cells with minimum disruption of the membrane properties and morphology, with the disadvantage of limited access for pharmacological manipulations and poor control of membrane voltage. Isolated cells, on the other hand, allow better control of the cell's extracellular environment, and better voltage clamp due to truncation of the dendritic tree. It follows then that recordings from isolated cells will tend to emphasize somatic membrane properties, rather than dendrites, an important consideration when postulating the existence of a given dendritic channel based on isolated cell studies. While cultured preparations may offer better access and control than intact or isolated preparations, these techniques may significantly alter the expression of biophysical mechanisms. A further caveat with the culture technique is that direct identification of pyramidal cells *per se* is not possible.

[1] In principle the perforated patch technique may give a better picture of the "true" physiological condition, however it as yet cannot be considered the standard since the literature using this technique is relatively sparse.

[2] On the other hand, in theory single channel measurements from the cell-attached configuration should provide the most unambiguous picture of detailed channel kinetics.

2.4 Kinetic and Pharmacological Dissection

Pharmacological and kinetic techniques are often used to isolate individual non-linear components of the cell response. Neither method is perfect, since both the sensitivities to various drugs or chemicals and the time scales for activation/inactivation may overlap. In the case of pharmacological studies, it is also quite important to consider the side-effects of a given "cocktail" in the interpretation of published results.

For example, the choice of the electrode solution is a critical factor in determining which currents will be observed. Certainly the standard procedure is to include or exclude specific ingredients in the pipette with this in mind. This situtation is more critical in the case of whole cell patch recordings, because of dialysis of the intracellular medium by the pipette solution. For example, Zhang et al. (1994) have done a recent systematic study on the effect of various whole cell pipette solutions on one hallmark of the HPC response, the slow after-hyperpolarization (sAHP, Section 6.4.4). The authors found that the sAHP (and associated accommodation) was very similar to classical results when the patch electrodes were filled with $KMeSO_4$, whereas other commonly used patch pipette solutions attenuated this response. The $KMeSO_4$ patch recordings were also very similar to $KMeSO_4$-filled sharp electrode recordings presented in the study.

While adding some pharmacological agent or blocking ion, either to the bath or pipette solution, is the more obvious way of isolating specific currents, manipulation of the effective concentration of a permeant ion can also be an important part of a given protocol. For antagonist actions, replacement of an ion with an impermeant one may be used. For example, while extracellular Cs^+ is known to be a specific blocker of I_Q/I_H (Section 13.1), recording with an electrode solution whose principal cation is Cs^+ ("cesium loading") has a general K^+ channel blocking action, simply because there are no K^+ ions to flow out, and K^+ channels typically have a low permeability to Cs^+.

Increasing the gradient of K^+ or Na^+ is often used to enhance the respective currents, but the already high gradient of Ca^{2+} requires other strategies. One approach is to replace Ca^{2+} with Ba^{2+}, which has a higher permeability than Ca^{2+} in many Ca^{2+} channels - in the later discussion on Ca^{2+} channels there will be references to both measurements made of Ca^{2+} currents and Ba^{2+} currents (via Ca^{2+} channels) for this reason.

Another factor in the expression of various neuronal properties is the pH of external environment, and the buffer system used in the preparation. While a modulation in pH *per se* is linked to various pathological states in brain tissue, and concomitant changes in firing behaviour, the dependence on buffer system is of particular relevance to the *in-vitro* situation, and the subsequent interpretation of reported experiments. Church (1992) has examined this for rat CA1 pyramidal cells in the slice, and found several properties which depend on whether an HCO_3^--CO_2 or HEPES-buffered medium is used. He found that a switch from the former to the latter system caused a fall in E_{rest}, a rise in spike threshold, a reduction in R_{in}, and a reduction in rectifying responses around E_{rest}. All major phases of after-hyperpolarizations following spikes (fAHP, mAHP, and sAHP; see Section 6.4) were also reduced, and consistent with these reductions was a reduction in spike adaptation. The HEPES-buffer also blocked current-evoked bursting activity in those cells that burst under the HCO_3^--CO_2-buffer.

2.5 Temperature Dependence

In general the kinetics of biophysical mechanisms are temperature dependent, and this dependency has been characterised in a variety of theoretical descriptions (see discussions in Tinoco et al., 1978 and Hille, 1992). A major, and difficult, consideration in integrating data from different sources is taking this dependency into account, since it is often the case that a model's data base may include experimental conditions with temperatures ranging over 10°C.

While a few studies of channel kinetics have included temperature as an experimental variable, in general the Q_{10} of a mechanism must be postulated ($Q_{10} \approx 3$ is a typical assumption). All Working model parameters presented in this chapter will be nominally adjusted for room temperature, but additional refinement to account for temperature will be necessary.

One of the few explicit studies on temperature and HPC responses was reported in Thompson et al. (1985). They describe a strong temperature dependence of R_{in} (see Table 1), various spike characteristics (see Table 2), afterpotentials (see Section 6.4.4), and spike adaptation, for temperatures ranging from 27 to 37°C. Briefly, they found that E_{rest} and the amplitude of the initial spike in response to a current step was not significantly changed by the temperature, but that reducing the temperature increased both the sAHP and the adaptation of spike trains, and reduced the spike amplitude for spikes after the first spike in a train.

2.6 Age Dependence

Various cell properties depend on the age of the preparation, in particular at early developmental stages (e.g. see work on the characterization of K^+ currents with early development by Spigelman et al., 1992), or very old animals (e.g. see Landfield and Pitler, 1984; Thibault and Landfield, 1996; Campbell et al., 1996).

There is a somewhat implicit correlation between properties recorded with patch electrodes and the age of the animal, since in general patch recordings are done on younger animals (before P25 in rat), whereas sharp electrode recordings are done at essentially any age.

2.7 Hippocampal Subfield Dependence

Are there fundamental differences in the electrophysiology between pyramidal cells in the various hippocampal subfields? The traditional view is that certain basic firing types correlate with subfield: regular-spiking cells predominate in CA1 (Schwartzkroin, 1977b), and bursting cells are mainly in CA3 (Bilkey and Schwartzkroin, 1990). A more refined view from Masukawa et al. (1982) was that bursters are found in both subfields, but primarily on their lateral borders (CA1a, CA1c, CA3a, and CA3c), while the medial parts (CA1b, CA3b) showed regular spiking responses.

Clearly there are (sub)regional specializations, but whether these imply fundamental differences in the cells' intrinsic mechanisms is still open to question. The recent result of Jensen and colleagues (Jensen et al., 1994; see Section 6.7) that an apparently normal looking regular spiking cell can be induced to look like a bursting cell by (among other things) lowering $[K^+]_o$ is an indication that the differences are more quantitative than qualitative. Along these lines are the demonstrations by models of Traub et al. (1991) and Migliore et al. (1995) showing how non-drastic quantitative modifications in the distributions of non-linearities in the same basic structure could account for the various electrophysiological types.

2.8 Differences in Firing Properties Between Sharp vs. Patch Recordings

In Section 5.2.1 we will discuss the different "passive" properties of HPCs recorded with sharp microelectrodes versus whole cell patch electrodes. It is also important to consider whether or not there is a difference in firing properties between the two techniques. To date this question has not been specifically addressed in the literature, other than the paper by Zhang et al. (1994) discussed above.

A very basic and perhaps obvious point to keep in mind is that the size of stimulus currents used for whole cell patch recordings is typically on the order of a fifth of that used in sharp electrodes, because input resistances with patch electrodes tend to be higher than that for sharp electrode recordings (Section 5.2.1). Thus, for example, current clamp recordings using sharp electrodes will typically use stimuli on the order of 0.5 to 2.0 nA to elicit spike trains, while with patch electrodes similar responses are evoked with typically 0.1 to 0.5 nA.

In the perforated patch recordings by Spruston and Johnston (1992) the examples shown of firing patterns for the pyramidal cells deviate from the classical pattern. Spikes were followed be strong hyperpolarizations that are more reminiscent of interneurons (see discussion of PHPs in Section 6.1.2) and thus look very "non-pyramidal". Since these trajectories reflect activation of significant conductances, and can have a strong effect on various firing properties, this discrepancy may be more than anecdotal. For this reason it may be of interest to examine in more detail particular characteristics of perforated patch recordings (this pattern can be seen in sharp recordings, however, e.g. Deuchars and Thomson, 1996).

A careful analysis of current clamp artifacts intrinsic to the design of several popular patch-clamp amplifiers has been presented recently by Magistretti et al. (1996). They show that the additional feedback loop in these circuits introduces significant distortions of fast events, in particular action potentials, including overestimation of spike amplitude and after-hyperpolarizations. Interestingly, due to the simpler input stage design of the classical "bridge-mode" amplifiers of the sort typically used with sharp microelectrodes, a practical result is that these signals are more faithfully recorded using the "older" amplifier design (note that the study of Spruston and Johnston, 1992, used an AxoClamp amplifier, which is a "bridge-mode" design).

Magistretti et al. proposed a modification to the patch clamp amplifier circuit to circumvent this problem. In summary, quantitative analysis of current clamp patch electrode recordings must take into account the hardware used to a greater extent considering that this issue was probably somewhat taken for granted previously. For the purposes of this chapter, with respect to quantitative parameters of spikes we shall place more emphasis on data made with sharp recordings.

2.9 The Measured Voltage

A final consideration in reviewing electrophysiological data is the accuracy of measured voltages in light of two main types of artifacts. The first is the presence of a tip potential which derives from the different ionic composition of the intracellular milieu and the electrode solution, which may or may not be correctly estimated. The second artifact arises from the resistance of the electrode generating a voltage drop when current is passed. This property may be compensated for by either bridge circuits or by switched clamp protocols, but perfect compensation is difficult especially when the currents are large. In sum, these artifacts can generate errors on the order of a few millivolts, depending on the experiment, and should be considered in the quantitative evaluation of measured cell properties.

3 Strategies for Single Neuron Models

Single cell behaviours that we may choose to model form a large dimensional space, considering the possible variables which define the context of the model (form of the input, chemical/pharmacological milieu, temperature, species, cell type, etc.). Basic subsets of the model behaviour include the linear or quasi-linear properties of the cell and the basic firing patterns observed in the slice preparation in response to intracellular current injection or activation of extrinsic (afferent or orthodromic) pathways. As mentioned earlier, in this chapter we shall primarily, but not exclusively, consider intrinsic stimulation.

3.1 Building the Model

If we assume that the mechanisms that determine single spike characteristics are shared to some degree with those that determine repetitive firing, then a resonable strategy is to start small and work up. Thus, in constructing a single cell model a first step can be to reproduce a single, isolated spike, and then extend the description to match various repetitive firing characteristics. Tractability encourages this initial hierarchy, especially since it is quite common for the set of model parameters that satisfy one behaviour to be disjoint from that which reproduce another. In particular, since parameters that work well at one time scale may fail on another time scale, the process of parameter fitting is profoundly iterative.

Concentrating on reproducing responses to current stimulation assumes that derived mechanisms will respond correctly to properly characterized synaptic input. Thus we assume that dividing the modelling effort into two distinct parts - synaptic versus non-synaptic mechanisms - is a reasonable strategy, despite the obvious direct overlaps between the two (e.g. synaptic channels with voltage dependencies).

Often an additional assumption for single cell models is that many channel properties can be reproduced to a good first approximation by neglecting dendritic channel distributions and placing all non-linearities at the soma (see Section 4). A related issue, when considering synaptic input, is the non-linear effect of the dendritic tree on synaptic integration (see Section 5.5).

It is important to emphasize that these considerations imply that models built with reduced representations of input/output mechanisms - e.g. at one extreme integrate-and-fire models, with perhaps simple adaptive mechanisms - may neglect crucial elements. This is a difficult question, since large network models require some simplification in order to be testable in any practical way. We have the view that the development of reduced models, appropriate for network models, should be made after careful analysis of the more complete type of model described here, with as full an understanding as possible of what may be lost by the simplification.

3.2 Parameter Searching

As alluded to earlier, a non-linear system of many parameters is likely to have many local error minima with respect to the reproduction of a given behaviour. At some point it becomes important to decide (usually implicitly) which minimum is closet to the "best" solution. To my knowledge no formal method for avoiding this problem exists (but there are attempts - see Bhalla and Bower, 1993, also Foster et al., 1993). Therefore a specific choice of parameters for these models should be considered as a possible solution, open to the possibility of further refinement. Indeed, as will be demonstrated in this chapter, the parameters of published models tend to be quite distinct from one another, and tend to work only in a limited testing domain.

Of course, the very notion of an "error" in the output of a simulation implies that there is some specific data that we are trying to reproduce. One of the goals of this chapter is to present the quantitative variation

of a few aspects of HPC output, at least to provide a neighborhood of behaviours for which single cell models may be designed to match. Certainly this list is incomplete, and it is difficult to say *a priori* whether or not these aspects are crucial for what a neuron is *really* doing.

3.3 Model Robustness and Validation - As Robust As Nature?

Assuming that we have chosen something to reproduce, quantitative fitting of cell models to data is hampered by the fact that first, biology is probably quite variable and second, biological measurements are definitely variable. This situation is often exacerbated by the experimental design and/or presentation of data in the literature, which may not be well matched for the derivation of model parameters (Bower and Koch, 1992, Foster et al., 1993).

For example, quantitative parameters are almost always presented as averages ($\pm$s.d.) over a group of cells. However, these statistics say nothing about the intrinsic variability of *each* cell. This information may be even more important when more than one parameter, say A and B, is measured: model parameter estimation may be very different if there is a significant covariance between A and B.

A related issue is parameter sensitivity, or fragility, of a given model. In some respect the biology of neurons is not very fragile, in that many basic behaviors at the cellular level are maintained over some non-zero range of parameters (e.g. temperature, extracellular constituents, measurement techniques). The problem is to predict the relationship between the sensitivity of neuronal phenomena to that of experimental parameters, and the sensitivity of model behaviour to that of model parameters.

In our work we use the following *ad hoc* criteria with respect to parameter precision (and by implication set a criteria for robustness): every model parameter is constrained to at most 3 significant figures, with the majority having only one or two significant figures. This is a bit more conservative than allowing the unit step of a given parameter correspond to the likely range of the parameter divided by 30 to 300 (Sokal and Rohlf, 1981).[3]

Another test of model design is the consistency of parameter precision for a particular mechanism. Different mechanisms may have different intrinsic precisions, thus it may be reasonable for a cell model to have components defined with single digit precision (e.g. R_m or C_m), with others defined with higher precision, especially sensitive non-linear mechanisms. This is related to the fact that neuron models represent stiff systems, that is they display dynamics on a very wide range of time scales (Mascagni and Sherman, 1998). In any event, the free parameters that define a specific mechanism should have more or less the same precision. For example, some of the reviewed models include mechanisms in which the precision of the parameters of a single mechanism ranges from one to five significant digits (e.g. "10" and "18.975" in the definition of I_C kinetics in Traub et al., 1991 - see Section 7.1.1). This range suggests a parameter sensitivity that may be unrealistic, and perhaps a choice of an unlikely mechanism.

3.4 The Purpose of Modelling - Testing Speculations

At minimum, a neuron model should reproduce the data base from which it was built, that is the templates used for determining model parameters. It is at this step that the original model of Hodgkin and Huxley succeeded brilliantly, and in doing so showed the plausibility of their speculations on channel kinetics. Next, the generalizability of the model should be tested against other, independent sets of data. Such tests have led to various and sometimes drastic revisions to the Hodgkin-Huxley squid axon model (e.g. Patlak, 1991; see also Pallotta and Wagoner, 1992); the success of the published HPC models at this stage is spotty. If a model does not pass this stage, then the *raison d'être* of models, generating testable predictions, becomes barely tenable - at best the flawed theory encapsulated in such models may still yield intriguing predictions.

[3] For example, if we are specifying the reversal potential of a current, then the range of values from first principles is roughly 100mV. This implies that the precision of this parameter should be on the order of .3 to 3 mV - e.g. a value of -72 is reasonable, but -72.25 is probably over-specified. If the test behaviour is significantly affected by a change from -72 to -72.2, this may indicate that some part of the model (hopefully related to this parameter in an obvious way) is poorly constructed.

The relevant precision of a given model parameter is also indicated by the error in any reported measurements; more specifically, the measurement gives a lower bound on the likely biological, true precision. For example, if the reversal potential in the example above was reported as -72.3$\pm$0.1mV, we might consider that this parameter is quite fixed in the real system. On the other hand, a reported value of -72.3$\pm$4.2mV could mean either that there is a lot of variation in the fundamental mechanism or there is a large variation inherent in the measurement technique.

3.5 Tools for Compartmental Models

Both analytical and numerical techniques have been applied in the analysis of neuron models. Analytical approaches are more commmonly used for the analysis of linear mechanisms (discussed in Section 5.3 and elsewhere), although some work has been done for non-linear mechanisms (see Jack et al., 1983). Numerical techniques are much more common, due to their applicability to a variety of non-linear mechanisms, and their overall ease of use. These techniques are exemplified by compartmental models of neurons (see review in Segev et al., 1989), in which the branching cable structure of the cell is approximated by a series of isopotential compartments interconnected with resistors. All of the single cell models that we discuss in this chapter are of this type.

The descriptions by Hines (1984) of $O(n)$ integration of tree circuit topologies, as naturally found in individual neurons, and mid-step solving of time-dependent non-linear elements (e.g. voltage-dependent gating particles) are exploited by most modern simulators, and have been vital contributions in making simulations of detailed anatomies practical. Hines and Carnevale (1994) have written a short review of numerical methods appropriate for neuronal modelling; a more detailed discussion may be found in Mascagni and Sherman (1998).

There are now several compartmental model simulation packages in the public domain designed for the computational neuroscience community, including NEURON (Hines, 1992), GENESIS (Bower and Beeman, 1994), and the program used for the simulations presented in this chapter, Surf-Hippo (Borg-Graham, 1995). Each of these progams, which can handle both single neuron models and networks, runs on Unix workstations and x86 boxes (PCs). A recent survey of tools is given by De Schutter (1992), although current availibility of public domain tools is better found using the WWW.

As mentioned earlier, the necessity for numerical methods has one major drawback: formal verification of even moderately complicated neuron models is not possible. One approach to verification is by the cross-validation of models using independent tools, possibly written in different languages and with major or minor differences in algorithms. This becomes practical with the increasing availability of sophisticated public domain packages.

For example, GENESIS allows various numerical integration methods, which may point out particular instabilities in a given formulation. Surf-Hippo is one of the few complete packages written in Lisp, as opposed to C. Lisp has the advantage that the user is communicating directly with the Lisp interpreter environment, and thus has complete access to all components of a simulation. Simulation scripts, a necessity for serious parameter searching, are also written in Lisp, whose flexible and powerful syntax is arguably more transparent than most other languages. Surf-Hippo allows both fixed and adaptive time step integration - using an adaptive time step can give much faster run times for typical simulations, with the option of verifying selected results using the more conservative fixed time step integration. Surf-Hippo can simulate both non-ideal and ideal voltage clamp, in the latter case by effectively dividing the circuit into two parts around the clamped node. The ideal voltage clamp algorithm not only allows analysis of voltage clamp protocols without the complications of a finite source series resistance, but because the method is very stable it also makes for much faster simulations. Both GENESIS and Surf-Hippo can simulate recordings from extracellular electrodes, that is measurement of the field potential, assuming a purely resistive, homogeneous extracellular medium.

Recently, a set of benchmarks ("Rallpacks", after Wilfrid Rall) have been proposed that are specifically tailored for neuron simulations (Bhalla et al., 1992). These include benchmarks for which analytical solutions are available (signal propagation in linear dendritic trees), and non-linear structures based on the "canonical" Hodgkin-Huxley Na^+ and K^+ channel equations. This last test is an example of the technique of cross-validation mentioned above, where solutions (waveforms) have been published for comparison. The results of the Rallpack benchmarks for NEURON, GENESIS, and Surf-Hippo are comparable.

The graphical user interfaces for NEURON, GENESIS, and Surf-Hippo are quite sophisticated, an important point for practical work. For example, Surf-Hippo allows automatic saving of edited model parameters into files which are both loadable and human readable. This feature helps to avoid errors in saving results at any time during a simulation session. "Point-and-click" histology rendering in these packages (with 3D anatomical representations in NEURON and Surf-Hippo) allow easy modification of cell models.

4 Anatomy and the Model: Data and Methods

The circuit topology of the single cell model - the mapping of the cell anatomy to a compartmental model - can have a range of complexity, depending on the question being addressed. As illustrated in Figure 1,

this complexity may range from a few compartments to a circuit with several thousand compartments, corresponding to the level of detail typically found in anatomical studies (for a general discussion see Turner and Schwartzkroin 1984).

There are essentially two stages of the mapping. The first concerns the representation of the branching structure of the dendritic (and possibly axonal) tree, and may be described in terms of cable sections (regular or tapering cylinders). The second stage translates the connected cables into connected isopotential compartments.

4.1 Reducing Branching Cable Structures and the Placement of Channels

The classical work of Rall (reviewed in Rall et al., 1992) on the analysis of linear dendritic trees included the derivation of his "3/2" rule for the collapsing of a set of daughter branches and their parent branch into a single cylinder with the same proximal input impedance.[4] Unfortunately, HPC anatomy does not appear to conform to these restrictions: for example, Turner et al. (1995) quote a range of average values for $d_r^{3/2}$ in CA3 HPCs between 1.25 to 3.36 (Turner and Schwartzkroin, 1980, reported similar results for CA1). It must also be emphasized that this technique is based on linear structures.

Nonetheless, it is often reasonable to reconstruct basic cell properties using soma-centric models with simplified dendritic trees, for example a soma/short-cable model consisting of a single compartment soma with one or two unbranched dendritic cables. Under some conditions it may even be reasonable to estimate parameters using a single compartment model.

On a practical level estimating parameters of distributed non-linearities is much more difficult than when a point-distribution is assumed - a first approximation of somatic responses to somatic stimuli restricts non-linearities to the soma. Here the dendritic tree is a linear load for the soma, and as such a simple cable (with on the order of five compartments, Borg-Graham, 1987b) can be constructed whose linear input impedance approximates the full tree very well (Turner, 1984b).

In addition, until recently almost all quantitative measurements of electrical properties were derived from somatic impalements (early exceptions in hippocampus include Wong et al., 1979, Benardo et al., 1982 and Masukawa and Prince, 1984). Such measurements suggest a first interpretation with a soma/short-cable model.

However, simulated responses to dendritic input using models with vastly simplified dendritic trees must be interpreted very carefully. Simulating non-somatic input by stimulating the "dendrite" in these sorts of structures (e.g. Traub et al., 1991) in the best case assumes a linear response to simultaneous stimulation at a set of locations with a fixed electrotonic distance from the soma, an unrealistic experimental situation. In the more realistic case, the contribution of the local dendritic non-linearities would be highly dependent on the local input impedance at the site or sites of stimulation. Thus, even if experimental simultaneous stimulation at equidistant sites could be assumed, their composite response could not be lumped together in a model by stimulation of a single location in a short cable geometry. A compromise approach is to model a local patch of dendrite in fine detail, while representing the rest of the tree in a much more schematic fashion. An example of this approach is given by Holmes and Levy (1990) in a model of synaptic interaction with internal Ca^{2+} in a dentate granule cell.

In summary, the short cable representation of the dendritic tree can at least represent the dendritic linear impedance load on the soma, and at most, with careful interpretation, may provide a substrate for a first approximation of the somatic view of intrinsic dendritic non-linear mechanisms, and possibly the integration of synaptic input.

4.2 Dendritic Tree Reduction from the Raw Anatomy

Assuming a defined branching structure, various algorithms may be employed to transform anatomical coordinate data into a compartmental model (e.g. Stockley et al., 1993). The simplest approach, of course, is a one-to-one mapping, where there is one compartment (dendritic segment) for each anatomical location, with the location and dimensions of that compartment taken as some function of the associated anatomical point and either one or two adjacent points.

For most practical simulations this produces an over-detailed representation since typical anatomical studies include on the order of thousands of dendritic locations and associated diameters. Here we describe

[4] An equivalent cylinder is possible if the electrotonic length of all the daughter branches are the same and they have identical terminations, and if the ratio, $d_r^{3/2}$, of the sum of the daughter diameters, each raised to the 3/2 power, to the parent branch diameter raised to the 3/2 power, is equal to one.

one method for reducing such a description into fewer compartments, with the minimum number given by twice the number of branch points in the dendritic tree, plus the number of dendritic trunks. The motivation for this method is to preserve both the 3-dimensional shape of the neuron and the electrotonic properties of the tree as best as possible.

The reduction is iterative and operates on a pair of segments at a time. Starting from the soma and working down each proximal trunk, two consecutive segments, call them A and B, are combined into one if there is no other segment common to both (i.e. the connection is not a branch point) *and* if the electrotonic length of the candidate replacement segment is less than that set by some *a-priori* criteria (i.e. a parameter L_{max}). The process continues distally - if A and B were combined in the previous step into a segment AB, the next pair consists of AB and the segment distal to the original segment B (call it C). Otherwise, the next pair to be considered is B and C. Figure 2 illustrates the procedure on a short chain of dendritic segments.

The parameters of the replacement segment are derived according to the following constraints:

1. The total axial series resistivity of the two original segments is conserved.
2. The total membrane impedance (area) of the two original segments is conserved.
3. The end points of the new segment correspond to the non-common end points of the original two segments.

In order to meet these constraints an additional parameter for each segment must be introduced, which we are choosing to be a coefficient, a, of the cytoplasmic resistivity that is used when determining the segment intracellular axial resistance (the default value for a is 1). This coefficient and the dimensions of the new segment are calculated as follows. Let l_i be the segment length, d_i the segment diameter, and a_i the coefficient for the segment axial resistivity, where i is p, d, or n for the proximal, distal, or new segment, respectively. As stated above, the length of the new segment, l_n is fixed by the far endpoints of the original proximal and distal segments. Conservation of membrane area (that is, conservation of membrane capacitance and resistance) gives:

$$d_n = \frac{(l_p \times d_p) + (l_d \times d_d)}{l_n}$$

Conservation of axial resistance gives:

$$a_n = \frac{(l_p \times a_p)/d_p^2 + (l_d \times a_d)/d_d^2}{l_n/d_n^2}$$

This technique yields a new segment whose cable parameters are similar to the concatenation of the two parents. However, the actual proximal input impedance of the new segment will always be greater than or equal to the input impedance of the former segment pair, since the membrane impedance is now farther away electrically from the proximal end of the new segment, relative to the membrane impedances of the original pair. Thus, the input impedance of a transformed (consolidated) tree will always be greater than or equal to the original tree, and the difference in the impedances will be greater the larger the consolidation (equivalently, the larger the L_{max}).

This algorithm is implemented in the Surf-Hippo simulator (Borg-Graham, 1995). An example is illustrated in Figures 1 and 3, where a CA1 cell anatomy description with 3205 points is reduced to a 193 compartment model. Somatic and dendritic responses for the two models to current stimulation at each soma and similar positions in the dendritic tree are compared in Figure 4. This figure shows that both centripetal and centrifugal passive propagation, and local input impedance, are very similar for the two models.

4.3 Accounting for Dendritic Spines

HPCs are covered with thousands of dendritic spines. Depending on the question being addressed, spines may be incorporated in a compartmental model with either explicit representations (e.g. a few compartments per spine, Zador et al., 1990, Schiegg et al., 1995), mixed implicit and explicit representations, where a subset of spines (e.g. for which synaptic input is applied) have detailed represention, with the membrane properties of the remainder of the tree adjusted for spine membrane area (Holmes and Levy, 1990), or purely implicit spine representation via membrane parameter adjustment (see Major et al., 1994). On the other hand, it is not uncommon for single cell models with partial or full anatomical representations to omit spines all

together (e.g. the model of Jaffe et al., 1994, Section 7.1), even when synaptic input is an explicit part of the model (e.g. the models of Traub et al., 1994, Wathey et al., 1992, and Migliore et al., 1995, Section 7.1).

As mentioned, a simple method for incorporating the centrifugal view of dendritic spines, while maintaining the overall geometry of the dendritic tree, is to adjust R_m and C_m to account for the membrane area of the spines (Holmes and Levy, 1990; see also discussion in Holmes and Rall, 1992b). This method assumes that the voltage drop across the spine neck is negligible (for non-stimulated spines).

For example, in a study of the electrotonic properties of rat CA1 HPCs, Mainen et al. (1996) estimated an average cumulative spine area of $2.85\mu m^2/\mu m$ of dendritic length (Harris et al., 1992). For the cells analyzed in this study, this constant factor resulted in an average 52% increase in the total membrane area of the cell.[5] Similar parameters for spine incorporation were used in the analysis of CA3 HPCs by Major et al. (1994).

4.4 Modelling the Axon

Axon modelling is all the more difficult since data on their non-linear structure is scant, probably less than that for dendrites. Of course, the original Hodgkin-Huxley model was of an axon, and the first application of non-linear compartmental models was applied to the Hodgkin-Huxley squid axon model (Cooley and Dodge, 1966) . Unfortunately, there is much less quantitative data for mammalian axons for which to build similar models (see discussion in Segev et al., 1992).

Another obstacle to realistic axon modelling in the case of HPCs is that axon morphologies are often not included in the available anatomical data. One exception is the study by Major et al. (1994), where the axon arborization was traced with the same fidelity as the dendritic tree (the CA3 32da cell in Figure 1).

We can use this anatomy to estimate the contribution of the axonal arbor to a linear model of the cell. As given in this study, assuming a homogeneous membrane resistivity R_m of 200KΩcm^2 and an intracellular resitivity R_i of 270Ωcm, the somatic input resistance is 267MΩ. The total dendritic/axonal tree resistance is 277MΩ, and the input resistance of the axon alone is 1,555MΩ. Thus, in this particular cell if the axon is ignored the somatic input resistance becomes 321MΩ, a 20% increase. We may note that this difference may be an upper bound, since any myelination of the axon would be expected to greatly increase the appropriate R_m (this possibility may also mean that the estimated "overall" R_m in this study may be an overestimate).

Most published single cell models ignore the axon completely; a few reproduce the contribution to the cell response by a simplified version of an axon, including I_{Na} and I_K for somewhat schematic action potentials (e.g. the models of Traub et al., 1994, and Pongracz et al., 1992, Section 7.1).

In summary, *for the linear model*, neglecting the axon may not be wholly unreasonable. For the full non-linear model, on the other hand, the validity of this assumption remains an open question. For example, it has been proposed that inhomogenous densities of Na^+ channels and/or different types of Na^+ channels with respect to the soma, dendrites, and axon, can account for details of the location of spike initiation and threshold; we will return to this point in Section 6.3. The default assumption is that the contribution of axon non-linearities to the somatic response can be approximated by "moving" those non-linearities to the soma, essentially the same approximation that may be made with respect to dendritic non-linearities as above.

4.5 Anatomy of the Working Model

The anatomy of the Working model is that used in the earlier soma/short-cable model by the author (Borg-Graham, 1987; Section 7.1.2, see in Figure 1 as the BG87 model). The parameters of this structure are a soma diameter of 35μm, a dendrite length of 1200μm, and a dendrite diameter of 12μm.

5 The Linear Model: Data and Methods

In this section we summarize the basic data on the linear properties of HPCs, and discuss various reports and interpretations of these properties.

[5] However, some of the interpretations in this paper may be problematic since the authors do not take into account the effect of a soma shunt from sharp microelectrodes, as described in Section 5.2.1.

5.1 Reproduction of Linear Properties

Perhaps the most basic properties of neurons are those that characterize the resting state of the cell, that is the somatic input resistance R_{in}, the main time constant τ_0, and the resting potential E_{rest}. The first two parameters implicitly assume linear characterizations of what is, of course, a profoundly non-linear system (see Section 4). For practical purposes, unless specifically defined otherwise, R_{in} is taken from the small signal response around rest (within about 5 millivolts), and τ_0 is the slowest time constant characterizing the small signal impulse response.

The R_{in}, τ_0 and E_{rest} of a cell model are determined by the model geometry, the specific membrane resistivity R_m, the reversal potential E_{leak} associated with R_m, the cytoplasmic resistivity R_i, the specific membrane capacitance C_m, and membrane conductances activated at rest which can change the *effective* membrane resistance and reversal potential. For a given model R_i and C_m are typically time-invariant and assumed constant over the entire cell (for exceptions, see model discussions in Sections 7.1.1, 7.1.4, and 7.1.5). On the other hand the effective R_m and E_{leak} of the linear model may deviate from the intrinsic values of these parameters by consideration of an electrode shunt, which we will discuss shortly, and activated channels or synapses. Thus the modulation of one of the many identified non- or weakly voltage-dependent channels found in neurons, in particular those modulated via 2nd messenger pathways over time scales that are long (tens of seconds) compared to intrinsic firing patterns can change the effective R_m and E_{leak}. Although we will not model these channels explicitly, examples of this type of channel in HPCs will be mentioned in the chapter. Synaptic effects, more relevant when reproducing the *in-vivo* state, can include that of tonic, or "background" synaptic activity (recent *in-vivo* data on this point in visual cortex is given in Borg-Graham et al., 1996; a model-based study of this question for neocortical cells may be found in Bernander et al., 1991). For all of these mechanisms - shunts, non-voltage-dependent channels and background synapses - the functional sequale may be captured by a static modulation of R_m and E_{leak}. In other words, these factors need not be considered in the dynamic structure of the model circuit. The participation of explicitely modelled channels that are open around the resting potential will also, certainly, influence the final value of E_{rest}, but these effects are not lumped into the linear model parameters.

A linear system approximation of the dendritic tree has been quite productive: linear cable theory has been applied in great detail to neurons (review in Rall et al., 1992). For example, as we discussed in Section 4, a first approximation to the distribution of non-linearities in a single neuron model places them on the soma, with the dendrites being linear (and ignoring the axon). This is an especially attractive strategy for evaluating dendritic tree properties given the elegance of linear systems theory. Thus in a practical sense it is useful to assume that the electrical properties of dendritic membrane can be thought of as a set of non-linearites on a linear substrate, where the linear portion is the dominant current path near rest (but see discussion in Section 5.5).

5.2 Measured Properties of the Resting State

In Table 1 measured values of E_{rest}, R_{in} and τ_0 are listed from various reports, including data from both CA1 and CA3 HPCs, as well as dentate granule cells for comparison. This table illustrates a key difference between recordings made with fine-tipped, or "sharp" microelectrodes, and those made with whole-cell patch electrodes, specifically that the latter gives significantly higher estimates for R_N and τ_0 than the former. On the other hand, the resting potential does not seem to depend much on the recording technique.

5.2.1 Considering A Somatic Shunt

A parsimonious explanation for the difference in R_{in} and τ_0 is that the sharp electrode introduces a shunt, or leak, at the recording site (see analysis in Staley et al., 1992). The whole-cell patch technique is thought to give a more accurate picture of the cell impedance because the gigaseal prevents an electrical shunt. While patch electrodes may vary certain membrane properties due to fast dialysis of the cell interior with the electrode solution, the high resistance is stable from the beginning of the recording (Borg-Graham, unpublished data from *in-vitro* turtle retina and *in-vivo* cat visual cortex). Similar high impedances are also seen with perforated patch electrodes which preclude dialysis (Spruston and Johnston, 1992, Marty and Neher, 1995).

When appropriate, a somatic shunt must be considered in deriving various linear parameters from impulse or step responses, that is by including it in the somatic membrane resistance. An example of how the assumption of a homogeneous R_m (i.e. neglecting the local shunt) can result in incorrect parameter estimation is given below in Section 5.3.2.

The problem still remains, however, for how to account biophysically for the cell's apparent resistance to the assumed non-specific permeability of a sharp electrode shunt. Typical values of the shunt are estimated on the order of $50M\Omega$, which is in the neighborhood of the cell's "intrinsic" impedance. A simple voltage divider analysis would predict that a non-specific shunt would reduce the cell resting potential by about half, yet this is not observed. Various candidate mechanisms have been proposed for the apparent paradox, including the up-regulation of either membrane-bound ion pumps or K^+ channels with reversal potentials below rest (Jones, 1989; Staley et al., 1992).

5.3 Analytical Methods and Results

The extensive literature of Rall laid the foundation for methodologies of cable analysis which are specifically appropriate for linear properties of dendritic trees (for a review see Rall, 1989 and Rall et al., 1992; also Jack et al., 1983). Turner and colleagues have presented extensive studies on the electrotonic analysis specifically on hippocampal dendritic trees, both under normal conditions (Turner and Schwartzkroin, 1980 and 1984, Turner 1984a and 1984b, and Turner et al., 1995) and pathological conditions (Pyapali and Turner, 1994).

5.3.1 Analysis of Dendritic Transients

Classically, closed form solutions for the behavior of transient signals in linear dendrites, for example the speed of a signal, have been difficult to obtain. Recognizing that the major obstacle arose from the *definition* of the quantity of interest, Agmon-Snir and collegues (Agmon-Snir and Segev, 1993, Agmon-Snir, 1995, Zador et al., 1995) observed that when a given parameter was described as a linear measure (specifically, in terms of moments of the waveform), the analysis was greatly facilitated. For example, the usual definition of "speed" is the time it takes for the *peak* of signal to get from point A to point B. However, the peak is a non-linear measurement; in this report the landmark for measuring speed was the center of gravity of the waveform (the ratio of the first and zeroth moments), a linear measure.

5.3.2 Pitfalls Evaluating Linear Parameters Derived from Intracellular Measurements

Assumption of a homogeneous R_m, for example when using the Rall model of equivalent cylinders, has in the past given erroneous estimates of cell properties. This can be illlustrated by examining the often cited report of Brown et al. (1981). In this paper analysis of the somatic current step response was based on the critical assumption that the cell could be approximated by the soma/short-cable model with a homogeneous membrane time constant. Essentially three parameters were derived from hyperpolarizing current steps (responses assumed linear) of hippocampal pyramidal cells: a homogeneous R_m, L (the electrotonic length of the short cable approximation) and ρ (ratio of dendritic and somatic conductance). The response to a current step at the soma of this structure can be represented by a linear combination of exponential terms:

$$V_f - V = \sum_{i=0,\infty} C_i \exp(-t/\tau_i)$$

where V is the response at the soma relative to rest, V_f is the steady-state soma voltage, τ_0 is the membrane time constant ($\tau_0 = R_m C_m$), and the remaining τ_i's are shorter time constants due to charge redistribution down the dendrite cable. Standard exponential peeling techniques were used to estimate the first few terms of this expression, which were then used in three different methods to estimate the cable model parameters. Measured somatic R_{in} averaged about $39M\Omega$, and τ_0 about 19 milliseconds (means from CA3 cells). R_m was then derived from the measured τ_0: since C_m was taken to be $1.0\mu F/cm^2$, this immediately gives R_m equal to $19K\Omega\, cm^2$. With R_i assumed to be $75\Omega\, cm$, these techniques resulted in average values of ρ as 1.2 and L as 0.93.

To see how well this procedure works, it is straightforward to "reverse-engineer" a soma/short-cable geometry based on the above parameters. For this we need to derive the the radius of the soma, a_{soma}, the radius of the dendrite, a, and the length of the dendrite, l. The first step is to derive a_{soma}. G_{soma} is given by ρ and R_{in} - since

$$\rho = \frac{G_{dendrite}}{G_{soma}}$$

and

$$G_{dendrite} + G_{soma} = \frac{1}{R_{in}}$$

then

$$G_{soma} = \frac{1}{R_{in}(1+\rho)}$$

This gives $G_{soma} = 11.7$ nS. The radius of the soma is then calculated from G_{soma} and R_m:

$$a_{soma} = \sqrt{\frac{R_m G_{soma}}{4\pi}}$$

This results in $a_{soma} = 42\,\mu m$. With λ as the electrotonic space constant of the cable, R_{in} is a function of G_{soma}, l and a, given by:

$$R_{in} = \left(\frac{1}{r_a \lambda}\tanh(L) + G_{soma}\right)^{-1} \tag{1}$$

where the first term on the right is the input resistance of a finite cable with an open circuit termination (e.g. Equation 4.11 in Jack et al., 1983), and where

$$L = l/\lambda$$

and

$$\lambda = \sqrt{\frac{R_m a}{2R_i}}$$

Estimates for l and a may be obtained by calculating R_{in}, L, and ρ, over a range of l and a with Equation 1, and finding the best fit to the experimentally derived values for R_{in}, L, and ρ. This procedure gives $l \approx 1800\mu$m and $a \approx 3\mu$m. The resulting geometry is shown in Figure 1, compared against other model geometries and actual cell anatomies. The most striking feature of the geometry derived from this report is the estimated soma radius of 42 μm, whereas a more realistic value is on the order of 15 μm (this difference gives about a eight-fold difference in soma surface area). Clearly the parameters reported in this paper cannot correspond to the actual cell properties, stemming from the non-consideration of the somatic shunt.

Holmes and colleagues present a more theoretical analysis of the sorts of errors illustrated by the above example (Holmes et al., 1992, Holmes and Rall, 1992a). In another paper of this series, Holmes and Rall (1992b) develop a general approach for estimating electrotonic dendritic structure, that does not rely on equivalent cylinder approximations.

5.3.3 Combined Experimental and Modelling Results

Using different analytical approaches, two recent studies (Spruston and Johnston, 1992, Major et al., 1994) carefully estimated linear membrane properties of hippocampal cells from patch clamp recordings.

Spruston and Johnston (1992) used the perforated path technique on CA1 HPCs, CA3 HPCs and dentate gyrus cells. In this paper it was assumed that the perforated patch recordings precluded a somatic shunt, and therefore R_m could be estimated directly from τ_0. Assuming a value of $1.0\mu F/cm^2$ for C_m, this gave an R_m of 28 and $66K\Omega\,cm^2$ for CA1 and CA3 HPCs, respectively.

One interesting finding from this study concerned the prediction that with a somatic shunt the longest time constant of a step response is less than the intrinsic membrane time constant. Estimates for parameters of a soma/short-cable model were evaluated from the data using analytical techniques similar to those of Brown et al. (1981), as discussed earlier, but with an explicit consideration of a somatic shunt term. These results were checked against independent estimates derived from numerical simulations of a soma/short-cable model. Spruston and Johnston showed that realistic values for the soma/short-cable model parameters, constrained by their experimental measurements, quantitatively supported the role of a soma shunt in the apparent discrepancy in the relationships between τ_m and R_N in sharp versus whole-cell recordings. The estimates presented in this paper were consistent with predictions shown in a linear model by Borg-Graham (1987b). In this study the benchmark τ_0 (from Brown et al.) was taken to be 19 milliseconds - allowing an inhomogeneous R_m gave an (non-unique) estimate of 40 and 2.5 $K\Omega\,cm^2$ for the dendritic and somatic

regions, respectively; thus the measured τ_0 of 19 milliseconds underestimated the 40 millisecond τ_m of the dendrites (C_m was taken as $1.0\mu F/cm^2$).

Major and colleagues have derived analytical expressions for the analysis of arbitrary characterized, linear dendritic trees (Evans et al., 1992)[6]. Major et al. (1994) applied these methods to their data from CA3 HPCs, and used an optimization procedure to match responses to short current pulses from specific cells to the their anatomies by varying R_m, C_m and R_i, taking into account estimates for the pipette contribution to the response. This resulted in estimates for R_m of 150-200KΩcm^2, R_i of 170-340 Ωcm, and C_m of 0.7-0.8 μF/cm^2.

Since this study was constrained by quantitative anatomy, as opposed to an assumption of the equivalent cylinder implicit in the soma/short-cable model, and since the recordings were made with whole cell patch electrodes, thus minimizing the somatic shunt, these estimates may represent the best picture to date of the resting properties of the HPC electrotonic structure. It is interesting, then, to note that the estimates for R_m and R_i are significantly higher, and for C_m significantly lower, than those used in most previous studies. One caveat may be that the techniques used in this paper required fairly long recording times (around 30 minutes, for reduction of noise) and thus washout effects, as mentioned in the paper, may have biased the cell properties.

5.4 Numerical Methods: Morphoelectrotonic Analysis of Dendritic Trees

Zador and Brown and their colleagues (Zador, 1993, Zador et al., 1995, Tsai et al., 1994, Carnevale et al., 1995) have developed a numerical technique known as the morphoelectrotonic transform. This results in a vivid anatomical rendering of the dendritic tree based on the frequency dependent transfer impedance between each point in the tree and a fixed reference point. This visualization emphasizes the point that steady-state electrotonic signal transfer is much larger than that for signal frequencies typical of synaptic events. The major limitation of this linear transform is that it is applicable for current, not conductance inputs, and thus is difficult to apply to synaptic integration under more realistic conditions.

5.5 How Far Can We Take Linear Dendritic Models?

As the ubiquity of voltage-dependent properties in dendrites becomes more apparent (Johnston et al., 1996), it is not obvious how much we can safely extrapolate from purely linear representations of dendritic structure. For example, even a small-signal linear approximation must consider the evidence for voltage-dependent mechanisms that are activated near rest, serving to "clamp" the resting potential (see Section 6.1, and later discussions of I_D, I_M, I_{AHP}, I_Q/I_H and $I_{Cl(V)}$).

In addition, even if the dendritic membrane is reasonably voltage-independent for small signals (on the order of several millivolts), analyzing the integration and transmission of synaptic signals requires consideration of the non-linear interactions *between* synapses since they are modulated conductances (Koch et al., 1983), and it is hard to imagine synapses being activated alone in a functional context. Specifically, the expected interactions between synapses put a severe restriction on the transmission properties predicted by purely linear methods (e.g. with the use of linear moments and the morphoelectrotonic models, discussed earlier). In summary, it is quite important to determine whether functionally relevant synaptic input *ever* operates in a linear regime.

Nonetheless, despite its limitations the linear model forms the necessary backbone for the estimation of non-linear properties.

5.6 Model Linear Parameters

The following summarizes typical default values for linear parameters, both measured and derived, with the parameters of the Working model in parentheses:

- Resting potential: -65mV ($E_{leak} = -65$mV, $E_{rest} = -65.7$mV)
- Input resistance R_N: 40MΩ (sharp recordings) to 200MΩ (patch recordings) (39MΩ)
- Time constant τ_0: 20ms (sharp recordings) to 100ms (patch recordings) (14.4ms)
- Estimated membrane capacitance C_m: 0.7 $\mu F/cm^2$ (0.7 $\mu F/cm^2$)

[6]Note that in formulations of the simple soma/short-cable model, the dimensions of model are some of the parameters estimated from analysis the voltage response (refer to the reverse-engineered model presented earlier).

- Estimated membrane resistivity R_m: 150 to 200kΩ cm^2 (dendrite: 40kΩ cm^2, soma: 2500Ω cm^2)
- Estimated cytoplasmic resistivity R_i: 150 to 250 Ω cm (200 Ω cm)

The small signal step response of the Working is shown in Figure 5. The value for the dendritic R_m in the Working model is probably an underestimate, and the low somatic R_m reflects a somatic shunt from a sharp recording. This value also results in a slightly low τ_0.

In all the simulations presented in this chapter, simulations start from a holding potential of -65mV, corresponding to the value assigned to E_{leak} (an exception is the demonstration of I_D shown in Figure 16). Simulation of the "true" E_{rest} in the Working model by letting the system relax (over about 20 seconds) to steady-state from the holding potential of -65mV gives E_{rest} equal to -65.7mV, primarily due to a small activation of I_{CaT}, which in turn raises the resting level of $[Ca^{2+}]_{in}$ enough to slightly activate I_{AHP}.

6 Phenomenological Templates

The shapes of action potentials, the trajectories of the membrane voltage prior to and after the spike, and the responses of a neuron to long-lasting inputs, are complex, variable, and vary significantly between different types of cells. In contrast to the modulation of non- or weakly voltage-dependent channels, or assumptions of tonic synaptic activation, mechanisms with a strong voltage or Ca^{2+} dependence and fast kinetics need to be explicitly considered in the model.

This section describes the main properties of HPC responses, generally under control conditions, that are relevant to single cell models, and issues concerning dendritic channels. Experimental manipulations of these properties, in particular as used to isolate specific membrane currents, will be discussed here and in later sections detailing the different currents.

We start with a quantitative review of the various potentials that precede and follow the individual spike, illustrated in Figure 6. We then discuss the site of spike initiation in the cell, the differences in firing patterns of various cell types, the characteristics of repetitive firing in regular spiking (non-bursting) cells, the characteristics and mechanisms for bursting, and so-called "D" spikes. We conclude this section with a short discussion on dendritic channel properties.

6.1 Morphology of the Potentials Preceeding the Spike

In this section we discuss the responses to current steps that precede spikes, both starting from the resting state and the voltage trajectories between spikes during repetitive firing.

6.1.1 Rectification Around the Resting Potential

Subthreshold inputs which change the membrane potential by more than plus or minus several millivolts begin to activate a variety of time-dependent non-linearities. For hyperpolarizing current steps, this is manifested as a depolarizing sag due to a slowly-developing (typically about 100 millisecond time constant) inward rectification. For depolarizing current steps, depending on the conditions, there may be either an inward rectification (so that the apparent input resistance becomes larger, e.g. Hotson et al., 1979) or an outward rectification (e.g. Storm, 1988b). Hyperpolarization-activated inward rectification (see Section 13.1) and depolarization-activated outward rectification (see Sections 12.1, 12.3 and 12.7) serve to stabilize the resting potential; in addition, time dependent inactivation of depolarization-activated outward rectification may act to integrate excitatory synaptic input over time. For depolarizing current steps in particular, the holding potential (or equivalently, the effective resting potential) of the neuron will to some degree determine which membrane currents will be available for shaping the subthreshold response; however, it is not always clear from the literature what determines the dominant mechanism (e.g. inward or outward rectification) in a given experiment.

6.1.2 The Pre-Hyperpolarization between Repetitive Spikes

For isolated single spikes, the next characteristic of interest is the spike threshold, discussed in the next section. For repetitive firing another important characteristic is the lowest voltage that precedes a spike, which we will refer to as the pre-hyperpolarization (PHP). PHPs are usually referred to as after-hyperpolarizations - we use the term PHP to emphasize the constraints imposed by this potential on the firing mechanisms for subsequent spikes, in particular the removal of I_{Na} inactivation, which we discuss in Section 10.1.7. In

essence, it may be better to view this potential not so much as the spike's aftermath but rather as its overture.

A conspicuous difference between the firing of HPCs (and typically cortical pyramidal cells) and other neurons is that in pyramidal cells the difference between PHPs and spike threshold is typically less than 10 millivolts, while in other cells this difference is usually at least 10 to 20 millivolts, a classical example being the spike train of the squid axon. Hippocampal and cortical interneurons exhibit a similar large differences between the PHP and threshold. During pyramidal cell bursts, the PHP may be almost eliminated, with little difference between the apex of the repolarization and the threshold for the subsequent spike, but for our purposes we will concentrate on the PHP characteristics during the repetitive spikes of regular firing cells.

A further characteristic of pyramidal cells is that the threshold of the *first* spike of a spike train is often below subsequent PHPs, whereas in non-pyramidal cells the combination of a generally deeper PHP and a generally smaller threshold difference between initial and later spikes in a train result in PHP profiles that are more hyperpolarized than the thresholds of all the spikes in the train. We also note that there are exceptions to these characteristics of PHPs in HPCs (see Section 2.8), but otherwise this means that recovery of spike current inactivation can occur at potentials above the lowest spike threshold. A general discussion regarding differences in firing properties between pyramidal (specifically, spiny) cells and interneurons (specifically, non-spiny) cells in the hippocampus may be found in Scharfman (1993).

In the study by Lanthorn et al. (1984), various characteristics of repetitive firing in CA1 HPCs were reported. This study described "slow prepotentials", a depolarizing ramp between spikes whose starting point is the PHP. Interestingly, the difference between the PHP and the spike threshold during steady-state repetitive firing was quite stable (about 6.7 millivolts), whereas the difference between the peak of the fAHP (see below) and the spike threshold became larger with higher spike rates (roughly 5mV with 400 millisecond interspike interval, and about 10mV for a 100 millisecond interspike interval; refer to Figure 4 in Lanthorn et al., 1984). If the peak of the fAHP is relatively fixed in absolute terms (Jensen et al., 1996, discussed later), then this suggests that there is a fixed relationship between the PHP and the spike threshold over some voltage range. Such a relationship is consistent with a Na^+ channel whose kinetics provide a variable threshold which is a function of the previous repolarization (see Section 10.1.7).

The PHPs of faster spike trains can be compared in the paper by Thompson et al. (1985). In Figure 6 of this report, spike trains with steady state interspike intervals of 19 milliseconds (elicited at 37°C) and 27 milliseconds (elicited at 27°C) had steady-state PHP to threshold differences of 7.5 millivolts. Again, the difference between PHP and subsequent appears stable in a given cell, in this case with respect to both temperature and firing rate.

6.2 Morphology of the Action Potential

Here we shall discuss quantitative parameters for action potentials including voltage threshold, rate of rise and fall, and the spike amplitude and duration. Table 2 summarizes these parameters from various references.

6.2.1 Action Potential Threshold: Absolute and Relative to Holding Potential

The reporting of threshold values is problematic since there is rarely a precise definition given in the literature - indeed, there is no such thing as a definite threshold that can be interpreted out of context, for example without specifying the current stimulus level or firing mode. Unambiguous definitions of the threshold include the point at which the slope of the voltage trace exceeds some *ad hoc* value (e.g. 50mV/ms, Andersen et al., 1986), or the point corresonding to the maximum of the second derivative (e.g. Mainen et al., 1995). The thresholds listed in Table 2, measured from either isolated spikes or the initial spikes in spike trains, range from about -55 to -45 millivolts. Most of these values are estimated "by eye". From this table we can see that the difference between the holding potential and single spike threshold is also variable, ranging from about five to 15 millivolts.

The threshold for firing in HPCs tends to be more abrupt relative to non-pyramidal neurons. Quantitative data on this characteristic, such as the time course of the second derivative, would be useful for the determination of model parameters (in particular I_{Na} kinetics), but for the moment this data is lacking in the literature. In some reports (e.g. Storm 1987a), the sharpness of the threshold can be appreciated by the almost passive character of just-subthreshold current step responses, however, this phenomena is not always observed (see Section 6.4.2).

Another observation that may be made concerning spike threshold is that typically the threshold for the initial spike of a train from a regular firing cell is several millivolts less than later spikes, with a total span of 5 to 10 mV (Andersen et al., 1986). Of course the thresholds for spikes within a burst span even a greater range (on the order of 20mV). All of these characteristics are most directly related to the voltage dependence for the activation of fast Na^+ channels, and to a lesser (but important) extent to the inactivation properties of these channels.

Action potential threshold is a function of where in the cell the excitatory stimulus occurs. Andersen et al. (1986) reported that the thresholds of somatic spikes evoked by either somatic current injection or stimulation of synaptic inputs on the proximal apical dendrite were about three millivolts higher (around 15mV above the resting potential) as compared to those evoked by stimulation of inputs to the distal apical dendrite (around 12mV above the resting potential). These results were interpreted as evidence for regenerative properties of the HPC dendrite.

6.2.2 Action Potential Rate of Rise and Fall

Rates of rise and fall may be taken as the maxima or the average slope between the relative positions (e.g. $10 - 90\%$) of the spike; of course the latter measure depends on the definition of threshold. The dV/dt for the spike upstroke is a good indicator of the minimum magnitude of the inward currents (i.e. without taking into account opposing outward currents), estimated from the *effective* capacitive load that must be charged. The effective capacitance arises from the somatic capacitance plus the capacitive component of the dendritic tree's input impedance as seen from the soma. On the other hand, the rate of fall for the spike gives a somewhat weaker estimate of the magnitude of the outward currents during repolarization - this is more complicated than the estimation of depolarizing current since there is more likely to be residual inward currents active, and the slower rate of fall means that the cell conductance has to be considered more carefully (see discussion in Storm, 1987a). Unfortunately, the dV/dt for the spike is not readily available in the literature for later spikes during repetitive firing, information which would be useful in reconstructing the kinetics of I_{Na} for repetitive firing.

In Table 2 the values for the rate of rise range from about 200 to 400 mV/ms, and for the rate of fall from about 40 to 100 mV/ms.

6.2.3 Action Potential Amplitude and Duration

Spike amplitude is usually measured from the spike threshold, and sometimes from the resting potential - obviously the former measure can be more problematic due the ambiguity of threshold. As seen in Table 2 the peak of the spike under control conditions can reach from about +20 to +35mV; assuming a typical value of E_{Na} as around +60mV (Hille 1992) this large range suggests that spike amplitude is determined mainly by inactivation properties of I_{Na}, in addition to the activation properties of the repolarizing currents, rather than E_{Na}.

Spike duration, as reported in the literature, may be taken from either the threshold-crossing to when the voltage recrosses the threshold (the "base" of the spike), or the width at half-amplitude. Using the latter measure, which is less sensitive to firing mode, spike duration varies from about 0.5 to 1.5 milliseconds.

Figenschou et al. (1996) describe Ca^{2+}-dependent cholinergic overall depression of the spike waveform (including increase of threshold, slower rise, slower repolarization, spike broadening, and amplitude reduction) which are not readily attributed to modulation of Ca^{2+} currents or the slow Ca^{2+}-dependent K^+ current I_{AHP}. The authors postulate that the effect may be due to activation of a pathway involving PKC that in turns modulates either Ca^{2+} channels, Na^+ channels, or both.

6.3 Where Does the Spike Start?

The precise location of spike initiation is classically taken as the axon hillock, or initial segment. There has been increasing interest in the spike generating properties of dendrites (e.g. Benardo et al., 1982, Stuart and Sakmann, 1994, Andreason and Lambert, 1995). Under various conditions "ectopic" spikes (those arising from other locations) may occur, for example in certain *in-vitro* models of epileptogenesis (Stasheff et al., 1993), or with certain strengths of synaptic input to the apical dendritic tree (Turner et al., 1991). The report by Stasheff et al., in particular, combined electrophysiological measurements with simulations to show that under their conditions the ectopic spikes were arising from axon terminals. Other modelling studies have examined this question (Moore et al., 1983, motorneurons; Mainen et al., 1995 and Rapp et al., 1996,

neocortical pyramidal cells) with the general conclusion that excitable dendrites under certain conditions can start the spike.

It may be that the relationships between the PHP and spike threshold, among others, can be explained in part by the spiking behaviour of structures with distributed channels, for example the consequence of a higher density of Na^+ channels in the initial segment that is electrically decoupled from the soma (Mainen et al., 1995 and Rapp et al., 1996). However, for the Working model we shall interpret the data in the context of a somatic channel model, and therefore apply these constraints solely to the determination of channel kinetics.

6.4 Morphology of the After-Potentials

The trajectory of the voltage after the spike has several prominent features, all of which vary under different conditions, in particular whether the spike is isolated or part of a repetitive train.

6.4.1 The Fast After-Hyperpolarization

The first one or two milliseconds of spike repolarization under control conditions has a distinct fast phase followed by an abrupt transition that can preceed either a slower repolarization or a depolarization. Classically, when the transition leads to a depolarization, the transition is referred to as the fast after-hyperpolarization (fAHP), with the peak of the fAHP assigned to the voltage of the transition. This peak can vary in relation to other landmarks such as the holding potential and the spike threshold. Although there is some variability between different references, it is important to consider quantitative measurements of the fAHP since the speed of the event (indicative of a large current) suggests that the underlying mechanism has a significant role in shaping the cell's overall response.

Two of the earlier studies focusing on the fAHP were that of Storm (1987a) and Lancaster and Nicoll (1987), both done on rat CA1 cells in the slice, demonstrating the Ca^{2+} dependence of the fAHP. In an example trace under control conditions Storm showed a peak of the fAHP (-67mV) which was quite a bit below both the spike threshold (-45mV) and the resting potential (-62mV); this paper reports an overall range of -60 to -65mV for the fAHP peak. Similar values are seen in an example shown in Lancaster and Nicoll (fAHP peak of -67mV, threshold -55mV, and resting potential -63 mV).

The values in these studies are in contrast with pooled data for regular-firing cells in rat CA1 slice in a more recent study (Jensen et al., 1996). Here, with a resting potential of about -63 mV, the peak of the fAHP (about -53mV) was higher than the spike threshold (about -56mV). This paper also reported the point of maximum repolarization after the initial spike in bursting cells and called this an fAHP. Although this term is more typically used in the context of regular firing cells, it is interesting that Jensen et al. found no significant difference between this measure and the regular firing cell's fAHP.

This variance in the peak fAHP relative to the spike threshold may be seen in traces of many papers, and applies to both single spikes and the initial spikes during repetitive firing (e.g. see Deuchars and Thompson, 1996 for both types). A more consistent characteristic is that during repetitive firing the fAHP is only seen in the first one or two spikes, with occasional smaller fAHPs showing up later in the train. This diminution of the fAHP during repetitive firing is not simply a result of the higher baseline voltage for the later spikes, since Jensen et al. (1996) show that the peak of the fAHP of single spikes is remarkably insensitive to the holding potential (up to $\pm$8mV around the true resting potential). Spigelman et al. (1992), however, show such a dependence in rat P26 CA1 HPCs.

We may note that although not mentioned in the paper, a figure in Thompson et al. (1985, ref. Figure 5) showed a possible strong dependence on fAHP inactivation with temperature - a prominent fAHP was evident throughout a spike train at 37°C, whereas the more typical diminution of the fAHP was seen in a spike train recorded at 29°C. Although the experiments of Storm (1987a) were done over a wide range of temperatures (28-33°C), there was no mention of an fAHP temperature dependence. The experiments of Lancaster and Nicoll (1987) were done at 29-31°C.

6.4.2 The After-Depolarization

After single evoked spikes, the shift in trajectory after the fAHP has been designated the after-depolarization (ADP) or the depolarizing after potential (DAP). Probably the first term is more useful since this phase may be either a continuation of the spike repolarization consisting of a simple "passive" decay down to the resting potential, or a distinct "active" positive-going depolarization of several millivolts, which may then decay to rest or be immediately followed by either addtional spikes or a full-fledged burst. We will make the

distinction that the ADP is that portion of the voltage trajectory after a single spike which is simply above resting potential, and that a *depolarizing* ADP (DADP) includes a positive going component.

The issue of whether the ADP is passive or active has been the subject of some interest, in particular as the ADP leads to further spikes for bursting cells. Several studies (e.g. Traub, 1982 and Storm et al., 1987 in hippocampus) have pointed out that the distributed capacitance of the dendritic tree would contribute a small passive inward current to the soma after a fast and local spike repolarization. The parameters of the Working model predict such a current for at least a small fast DADP (Figure 7). However, the time course of the passive contribution is on the order of a few milliseconds, appropriate for some depolarizing effect at the beginning phase of the DADP, but too fast for the longer DADPs (10-20 milliseconds) often seen in the literature. More prominent DADPs probably reflect the activation of various somatic conductances during this phase, which would further limit the effect of the passive dendritic current. Finally, the concurrent activation of channels present in the proximal dendrite (Johnston et al., 1996) would argue against a significant capacitive (passive or linear) component. This possibility is not considered in the Working model prediction since here the dendrite is linear.

An active ADP in some CA1 HPCs (those which tend to burst, see below) has been identified as due to a TTX-sensitive Na^+ current (Jensen et al., 1996 and Azouz et al., 1996). This ADP was seen both after single spikes and as a prolonged decay after subthreshold current pulses.

6.4.3 The Medium After-Hyperpolarization

At the end of a stimulus that elicits one or more spikes there is a medium after-hyperpolarization, or mAHP, which increases with the number of spikes and lasts on the order of one hundred milliseconds. Storm (1989) described the properties of the mAHP in detail, showing that the size of the mAHP grows roughly linearly with the number of spikes in a train, increasing from about one millivolt with a single spike to about five millivolts with seven spikes.

The mAHP is attenuated by cholinergic agents (Storm, 1989), and both Storm and a later study by Williamson and Alger (1990) showed that when a train of action potentials were elicited from a cell depolarized from rest, the mAHP had a substantial Ca^{2+}-dependent component. For example, when cells were held between -49 to -57mV, the amplitude of the mAHP with control saline was about four millivolts. When Ca^{2+}-blockers (nifedipine or Cd^{2+}) were added, or external $[Ca^{2+}]$ was reduced, the amplitude decreased to around two millivolts. Manipulations that increase Ca^{2+}-influx (addition of BAY K 8644, raising external $[Ca^{2+}]$) increased the amplitude of the mAHP to about six millivolts. Conversely, spike trains evoked from hyperpolarized levels ended in an mAHP that was antagonized by Cs^+.

It is not unusual for the peak of the fAHP to be within millivolts of the peak of the mAHP for single evoked spikes. For repetitive firing, a similar relation is observed between the fAHP and the minimum voltage between spikes - that is the PHP described earlier, which might be considered the analogue to the mAHP for repetitive firing (ref. Figure 2B in Deuchars and Thomson, 1996).

6.4.4 The Slow After-Hyperpolarization

The slow after-hyperpolarization (sAHP) is a Ca^{2+}-dependent after-potential classically seen after a train of current-induced action potentials. As described by Hotson and Prince (1980) the sAHP has a magnitude of up to several millivolts below the resting potential, may peak with a delay up to 500 milliseconds after the spike train, and can last over a second. These authors also showed that the magnitude of the sAHP saturates abruptly when measured as a function of either current stimulus duration or amplitude (e.g. sAHP saturation with a 125 millisecond 0.5nA current stimulus). The magnitude of the sAHP is also strongly dependent on the resting potential - in this paper the amplitude of the sAHP of cells with a resting potential between -65 and -70mV was increased by up to five millivolts when the cells were depolarized five to ten millivolts. In some cells with a low resting potential of around -70mV no sAHP was observed unless a steady depolarizing current was applied.

Although the sAHP is typically discussed in terms of firing accommodation after several spikes, the sAHP is present after a single action potential. For example, Storm (1987a) showed a single spike evoked sAHP which peaked at about 1.5mV below an imposed resting potential of -65mV. Another example from Storm (1987b) showed a five millivolt sAHP after five spikes (resting potential not given). Another quantitative analysis of the sAHP by Storm (1989) included the dependence of the sAHP amplitude with the number of spikes, showing, as with the mAHP, a roughly linear relationship from about 0.5mV after one spike to a little over three millivolts with seven spikes (resting potential not given). In this paper the sAHP was also studied with a hybrid clamp protocol, in which voltage clamp was imposed immediately after current clamp evoked

spikes (Lancaster and Adams, 1986). This technique showed a rectification of the sAHP current, possibly consistent with the GHK permeation model (Section 8.2), as the voltage clamp potential approached the reversal potential of about -100mV. The linear portion of the IV characteristic intersected the voltage axis at an effective reversal potential of about -85mV. Similar results were reported by Lancaster and Adams (1986).

As mentioned earlier, Thompson et al. (1985) reported that a reduction in temperature increased the sAHP; in one example the sAHP peak amplitude after a train of six spikes increased from about two millivolts at 36°C to about four millivolts at 32°C (resting potential apparently -57mV). The authors suggested that a facilitation of a Ca^{2+}-dependent K^+ current could account for the changes, caused by both an increase of Ca^{2+}-entry per spike and a slowing down of the removal of intracellular Ca^{2+}.

An increase in Ca^{2+} entry could be a result of a broader spike (giving more time for Ca^{2+} channel activation), while a decrease in Ca^{2+} removal may be a function of a temperature dependence on a Ca^{2+} pump. However, if a slowing down of channel kinetics (e.g. I_{Na} inactivation and/or repolarizing K^+ channel activation) can account for the broadening of the spike, then it remains to be demonstrated whether any expected concomitant slowing of the Ca^{2+} channel kinetics would not offset an increase in total Ca^{2+} influx caused by the longer depolarization. It will be interesting in the future to examine such tradeoffs with simulations, also taking into account the different Q_{10}'s of channel conduction and channel kinetics.

6.4.5 The Slow After-Depolarization and Plateau Potentials

In the presence of cholinergic agents a Ca^{2+}-dependent slow after-depolarization (sADP), roughly seven millivolts and lasting on the order of one hundred milliseconds or longer, may be observed in CA3 HPCs after a spike train instead of the sAHP (Caeser et al., 1993). In CA1 HPCs application of cholinergic agonists can reveal either an sADP or a long lasting (seconds) plateau potential of about -20mV after a spike train (Storm, 1989; Fraser and MacVicar, 1996). Both potentials require Ca^{2+} and Na^+ in the bath solution; they may be related to hippocampal seizure activity, also known to be facilitated by cholinergic agents. Contrary to the conclusions from Figenschou et al. (1996), data in the paper by Fraser and MacVicar (Figure 1A, not commented in the discussion) suggest that $20\mu M$ of carbachol irreversibly blocks the fAHP.

6.5 Differences in Firing Properties Between HPCs and Other Cell Types

Physiologically, HPCs (and spiny cortical cells) are divided into two major classes, regular firing (or regular spiking) and bursting cells (for a review of the firing patterns in neocortical cells see Connors and Gutnick, 1990). These classes refer to the pattern of action potentials in response to both short and sustained current injections. Regular firing cells respond with spikes for only as long as the stimulus, in a regular, adapting manner. Bursting neurons, on the other hand, typically respond to a short stimulus (e.g. suprathreshold for several milliseconds) with several spikes riding on a slow depolarizing "hump" lasting on the order of one hundred milliseconds (e.g. Wong and Prince 1978). Sustained stimuli tend to elicit an initial burst followed by either an adapting "regular" firing pattern or additional bursts. The morphology of individual bursts is variable, but usually show a diminution of height and an increase in duration of the fast spikes riding the hump. Quite often, the repolarization of the somewhat fat and slow final spike is continuous with the repolarization of the slow hump. The mechanisms that determine these firing patterns may or may not overlap those that shape individual spike waveforms, and we will mention several theories as to the crucial burst mechanism (see Section 6.7).

The most conspicuous difference between current-evoked spike trains of HPCs (as well as spiny, presumably excitatory cortical neurons) and hippocampal interneurons (as well as non-spiny, presumably inhibitory cortical neurons) is that the former show either adapting regular firing or bursting behaviour, while the latter tend to show non-adapting ("fast-spiking") regular firing. Note that the term fast-spiking also refers to the fact that the spikes of interneurons tend have a shorter duration than that of pyramidal cells. There are also various subtle differences between the responses of HPCs and other cell types, for example in the details of the morphology of the action potential and the after-hyperpolarizations, which are beyond the scope of this chapter. However, it is worthwhile to note that these differences may reflect differences in channel distribution and electrotonic structure, as well as fundamental difference in channel types. This latter point should be kept in mind in the discussion later on specfic channel properties of HPCs, in that the details of a given current identified in HPC may not be the same for a similar current in another cell, even if the current in question is referred to with the same name. Finally, it may very well be that a particular channel type described in hippocampus may be unique to this structure.

6.6 Regular Firing Characteristics - Adaptation and f/I Characteristics

Adaptation (*deaccelerando* over the spike train) in regular firing HPCs varies, but in general is mediated by two main mechanisms, one primarily Ca^{2+}-dependent (via I_{AHP}) and the second primarily voltage-dependent (via I_M). A common way to represent the pattern of repetitive firing in response to steady current injection is with the so-called "f/I" plot, which plots the instantaneous firing frequency (the reciprocal of the interspike interval) at some point in the spike train against stimulus intensity. f/I plots for the first few interspike intervals tend to show three components as the stimulus is increased, corresponding to the primary (relatively flat), secondary (relatively steep), and tertiary (relatively flat) ranges, similar to motorneurons (Lanthorn et al., 1984). f/I plots for steady-state firing, on the other hand, tend to lack an intermediate steep portion of the firing curve as a function of stimulus strength.

The adaptation in regular spiking HPCs can be extreme, such that firing can be momentarily suppressed for some intermediate range of stimulus strengths. The report by Lanthorn et al. (1984) and others (e.g. Madison and Nicoll, 1984, Lancaster and Nicoll, 1987) show that the interruption of firing occurs after about 200 milliseconds of repetitive firing for stimuli which typically generate about five to ten spikes during this initial period. This suppression is a relatively robust phenomenon, occurring over a range of stimulus strengths from about 0.5 to 1.5nA (outside of this range Lanthorn et al. show no pause). The pause in firing is transient, lasting a few hundred milliseconds (Lanthorn et al., 1984), after which there is typically a non-adapting spike train.

6.7 Mechanisms for Bursting

The characteristics of bursting in central neurons and the underlying mechanisms has historically attracted much interest. Computational roles for bursting have been proposed (e.g. Lisman, 1996), and bursting is associated with pathological states. In particular, bursting in the hippocampal slice under various conditions has served as a model system for studying epilepsy (for a review see Alger, 1984).

Despite certain differences in the proportion of cells that burst in CA1 and CA3, it is not clear whether there is a fundamentally different bursting mechanism between HPCs in these two regions, or for that matter for other bursting cells in the CNS. Most likely there is some overlap in the responsible mechanisms, given that there are several plausible and mutually compatible candidates. Although bursting in epilepsy models is typically associated with synaptic activation (especially under protocols in which GABAergic inhibition is blocked), the association with current-evoked bursts and other evidence indicate that the fundamental burst mechanisms are intrinsic. Key mechanisms or conditions for bursting in HPCs that have been proposed from experimental work include:

- Ca^{2+} entry/spikes (Wong and Prince, 1978, Wong and Prince, 1981, Konnerth et al., 1986).
- Dendritic Ca^{2+}-spikes (Wong et al., 1979).
- Cholinergic agonists (Bernardo and Prince, 1982a).
- Low extracellular Ca^{2+} (e.g. Haas et al., 1984, Azouz et al., 1996).
- Persistent TTX-sensitive Na^{+} current (Jensen et al., 1996, Azouz et al., 1996).

Bursting may also depend on the holding potential: in cells which normally respond with bursts, long current steps applied from hyperpolarized levels tend to result in regular firing patterns (Wong and Prince, 1981; see also examples in Scharfman, 1993). Interestingly, thalamic neurons show the opposite behavior, in that they tend to burst only after being hyperpolarized (see for example McCormick and Pape, 1990). This points out the fact that different cell types could very well rely on different mechanisms for bursting.

Several cell models have examined the role of dendritic Ca^{2+} spikes as the mechanism underlying bursting, some of which are described later in the chapter (Traub and Llinas, 1979, Traub, 1982, Traub et al., 1991, Traub et al., 1994; Rhodes and Gray, 1994 for neocortical pyramidal cells). The HPC model by Migliore et al. (1995), described later, focused on the relative balance of Ca^{2+}-independent K^{+} currents as determining whether a given structure would burst or not.

6.7.1 Is the Dendritic Tree Important for Bursting?

Various attempts have been made in order to relate firing pattern with morphology (for a recent model-based analysis, see Mainen and Sejnowski, 1996). For example, Bilkey and Schwartzkroin (1990) reported a positive correlation between the incidence of bursting and the length of the apical dendrite in CA3 cells.

However, bursting in CA3 cells does not require an extensive dendritic tree, since bursts are observed in acutely isolated cells with just apical dendrites (data in Wong et al., 1986, referenced in Traub and Miles, 1991, fig 2.4; also Traub et al., 1991). Also, any conclusions from modelling studies of the role of the electrotonic structure and channel distribution depend critically on the choice of channel models. For example in the study by Mainen and Sejnowski it is not obvious that the channel models are directly relevant to HPC mechanisms.

6.7.2 Constraints for the Slow Depolarization Mechanism Underlying Bursts

If the mechanisms for the spikes during the burst are roughly the same as that for regular spikes, then the inward current underlying the slow depolarizing potential must be strong enough to drive a input impedance that is significantly lower than the resting state because of the activation of the various repolarizing currents. Since these currents that are active during the later stages of spike repolarization are probably on the order of hundreds of picoamperes or more, this sets a lower bound on the size of the depolarizing current.

Under these assumptions, the major problem with attributing the slow depolarization to the classical persistent Na^+ current I_{NaP} (French et al., 1990, see Section 10.1.3) is that the size of this current, on the order of a few hundred pAs at around -53mV (the voltage at the end of the first burst spike repolarization, e.g. Jensen et al., 1996), is too small, even if we assume that this current activates instantaneously. Similar conclusions apply to Ca^{2+} channel mediated slow depolarizations, using estimates of Ca^{2+} channel kinetics that reproduce other firing patterns (e.g. Ca^{2+} spikes), as discussed below.

6.7.3 Is Ca^{2+} Entry the Key?

The classical explanation of a Ca^{2+} current generating the slow depolarization underlying bursts, at least in CA3 cells, was supported by studies such as Wong and Prince (1978, 1981). In these reports, either extracellular Mn^{2+} or low extracellular Ca^{2+} arrested burst firing, and focal application of Ba^{2+} restored a burst-like component. However, the effects of extracellular Mn^{2+}/low Ca^{2+} often developed over an hour after application, and from the figures in the paper apparently were accompanied by increases of more than 10 millivolts in spike threshold. These results suggest that the effect of the Ca^{2+} manipulation may be mediated by local membrane interactions, i.e. shifts in the voltage "seen" by the Na^+ channels via charge screening by divalent ions (the effect of divalent ions on neuronal membranes is discussed in Hille, 1992). Since the Na^+-dependent component of the active ADP is quite sensitive to the holding potential (Jensen et al., 1996), such shifts might serve to inactivate the slow Na^+ component. The slow depolarization with Ba^{2+} (whose time course shown in Wong and Prince, 1981 was at least twice as long as the control burst depolarization) may be due to the higher permeability of Ba^{2+} through Ca^{2+} channels providing enough current to support a regenerative event.

Also, estimates of Ca^{2+} channel density (see Section 11) constrained by Ca^{2+} spike data do not predict I_{Ca} mediated slow depolarizations - this phenomena in models discussed later (Traub et al., 1991, Traub et al., 1994) included Ca^{2+} channel dendritic densities which were probably unrealistically high, as well as Ca^{2+} channel biophysics that possibly overestimated I_{Ca}. Thus, the evidence seems to be against a role for Ca^{2+} influx supplying the necessary *charge* for the burst depolarization.

Madison and Nicoll (1984) showed the contemporaneous development of initial bursts and reduction of accommodation to long pulses in CA1 cells with EGTA-filled electrodes. They proposed the appearance of a burst resulted from a Ca^{2+} spike facilitated by an increased driving force for Ca^{2+} (EGTA $\Rightarrow$ lower $[Ca^{2+}]_{in}$). However, the reduction in current predicted by a GHK permeation model (as probably appropriate for Ca^{2+} currents, Section 8.2) due to Ca^{2+} accumulation at the potentials in the range of this hump is small, and probably cannot account for suppression of a regenerative Ca^{2+} potential. On the other hand in this paper application of the Ca^{2+} channel blocker Cd^{2+} only shows a reduction in accommodation, without a *de-novo* burst.

One differential effect of EGTA versus external Ca^{2+} blockers (e.g. Mn^{2+}, Co^{2+}, Ni^{2+} or Cd^{2+}) with respect to Ca^{2+}-dependent mechanisms is that the former blocks I_{AHP} and not I_C (because of high affinity of I_C to Ca^{2+} influx), whereas the latter blocks both because of global Ca^{2+} current block (e.g. Storm, 1987a). It could be that the mechanism underlying the burst has a similar sensitivity to Ca^{2+} entry as I_C.

Finally, the most conspicuous evidence against the hypothesis that Ca^{2+} is necessary for bursting is found in the recent report by Azouz et al. (1996). This paper shows that burst firing in CA1 HPCs is resistant to inorganic Ca^{2+} blockers, and in some cases was even enhanced. CA1 bursts also persisted in 0 Ca^{2+}, 2mM Mn^{2+} bath solutions. On the other hand, application of TTX in 0 Ca^{2+}, 2mM Mn^{2+} bath solution progressively blocked bursts in response to sustained current steps, before blocking the remaining

full amplitude spikes. This latter finding was cited by the authors as evidence for a distinct persistent Na^+ current underlying the burst slow depolarization.

6.7.4 Bursting in the Hippocampal Network

With respect to the hippocampal slice as a model for epilepsy, the low-Ca^{2+} preparation is used to study non-synaptic epileptiform activity (e.g. Haas et al., 1984, Roper et al., 1993), providing further evidence against the hypothesis that substantial Ca^{2+} entry is a necessary component of intracellular bursts.

Synchronous bursting, e.g. that associated with epileptogenesis, is a function of both intrinsic bursting properties and patterns of connectivity. Although normally associated with CA3, such patterns of activity can be seen in CA1 under various conditions. In particular, and relevant to the present discussion, when $GABA_A$ inhibition has been blocked with bicuculline synchronized bursts in CA1 can be seen when this region has been completely isolated from the rest of the hippocampus, as demonstrated by Meier and Dudek (1996). Such behaviour is further evidence for the role of intrinsic CA1 bursting mechanisms, particularly because the intracellular records show bursts with a classical morphology.

6.7.5 So What Causes Bursting?

Recent reports (Jensen et al., 1994, Jensen et al., 1996 and Azouz et al., 1996) show that CA1 HPCs with stereotypical regular firing patterns may be reversibly transformed into bursting cells under various ionic manipulations. For example, there is an up-regulation of bursting with increases in extracellular $[K^+]$ (Jensen et al., 1994), which is qualitatively different than simply an increase in excitability that would be expected in general with raised $[K^+]_o$. A similar result was reported by Andreasen and Lambert (1995) for dendritic recordings of CA1 HPCs: raising $[K^+]_o$ from 3.25 to 5.25mM converted a "regular" train of dendritic action potentials to bursts. Also, in this paper both dendritic bursts and slow Ca^{2+}-mediated dendritic spikes were found to be resistant to blockers of T- and L-type Ca^{2+} channels, leaving open the possibility for a necessary role of other types of Ca^{2+} channels in dendritic bursts (see Section 11)

The recently described Ca^{2+}-dependent non-specific cation currents in CA1 and CA3 cells may offer another explanation behind the apparent Ca^{2+}-dependence of bursting (Caeser et al., 1993; Fraser and MacVicar, 1996; see Section 13.3). The pH of the extracellular medium is also important: Church (1992) showed that bursting CA1 rat HPCs reversibly switched to regular firing when the buffer was changed from HCO_3^--CO_2 to HEPES (pH 7.4 throughout). In the same experiment, lowering the pH (under the HCO_3^--CO_2 buffer) to 6.9 also reversibly changed the cell to regular firing.

Taken together, these findings support the view that the apparent dichotomy between regular and bursting patterns is at base a reflection of a delicate, and quite possibly modulatable balance of non-linear mechanisms. We also note that explaining bursts requires not only identifying the mechanism or mechanisms underlying the slow depolarization, but also an adequate description of the fast I_{Na} kinetics that actually generate the spikes and the repolarizing mechanisms, which may be different than the regular firing case. All cell models that we have examined which generate some sort of burst utilize a Hodgkin-Huxley based description of I_{Na} with properties essential for the bursts, specifically, that the recovery of inactivation may occur at relatively depolarized potentials. However, as we shall discuss in Section 10, the use of this type of model overestimates steady-state Na^+ rectification, precisely because of the relatively depolarized inactivation curve.

It may be that bursting involves an interplay of I_{Na} inactivation that is less complete and K^+ current inactivation that is faster than that occurring during regular firing. This would be consistent with the proposal by Jensen et al. (1996) and Azouz et al. (1996) for a crucial role of a persistent TTX-sensitive Na^+ current, where the current may reflect a qausi-persistent kinetic state of I_{Na} distinct from the reported I_{NaP}.

The channels that we include in the Working model do not generate bursting responses. For example, the preliminary model of I_{Na} that we propose in Section 10.3 is not able to generate spikes originating from the more depolarized portion of the depolarizing burst envelope, and even though it has a persistent component that is similar to the classical I_{NaP}, the kinetics of this current are not sufficient to drive the hump. On the other hand, this I_{Na} model can be readily extended to provide for higher thresholds, and possibly more complicated kinetics of inactivation. Finally, it will be important to reevaluate channel kinetics in the Working model after the addition of dendritic and axonal channels in order to see how the behaviour of the distributed channels can contribute to bursting properties not evident with the somatic channel model.

In summary, bursting mechanisms in the cell models reviewed in this chapter do not seem to be consistent with all the available data. We feel that the bursting question is still open, and perhaps a refinement of the channel models described in this chapter will burst properly.

6.8 D Spikes

D ("Dendritic") spikes are fast five to 15 millivolt depolarizing events in HPCs that are robust to changes in the holding potential (Kandel and Spencer, 1961). D spikes may occur singly or in clusters (with a timing reminiscent of bursts), they may be either substhreshold or capable of eliciting full spikes, and they may be spontaneous or triggered by current injection (in which case they appear as later events of a burst).

In the context of single cell models, the important issue regarding D spikes is their relationship to intrinsic mechanisms; specifically, should our model be able to reproduce these waveforms in isolation? Although early explanations centered on the idea that D spikes were due to intrinsic dendritic mechanisms (Kandel and Spencer, 1961b, Schwartzkroin, 1977b), a more likely explanation is that these events are echos of single spikes or bursts from electrotonically-coupled cells, i.e. via gap-junctions (Jensen et al., 1996; for a discussion of electrotonic interactions in hippocampus, see Alger, 1984). We may note that none of the models discussed in Section 7.1 describe D spikes; also, attempts at reproducing these "mini-regenerative" waveforms in our more recent studies have argued against an intrinsic basis for them. Thus, in summary, it would appear that network interactions are crucial for this phenomena.

6.9 Dendritic Channels and "Hot Spots"

The data on the distribution of specific channels in the dendritic tree, though increasing, is far from complete. In our discussion of specific channel properties in Sections 10, 11 and 12 we will summarize some of the more recent key findings.

Certainly models can help focus this question, at least by proposing plausible density patterns. The practical problem is that without knowing precisely the kinetics of a specific channel, it is all the more difficult to establish reasonable predictions for its contribution in a distributed structure (Section 4.1). The more conservative models to date that deal with this question have tested uniform or fairly uniform dendritic channel distributions, and probably such constraints are consistent with the present state of knowledge regarding channel kinetics (e.g. the HPC model of Migliore et al., 1995, described in Section 7.1.6; see also the Purkinje cell model in De Schutter and Bower, 1994). Other HPC models (discussed in Section 7.1) have used much more *ad hoc* distributions of various channels in the dendrites, for example local concentrations in so-called "hot spots". Such distributions are equivalent to adding many more degrees of freedom to a model's parameter space, and as such make it more difficult to extrapolate general conclusions from the model behaviour.

7 Review of Hippocampal Models

We now present a brief review of HPC models, emphasizing those models oriented towards understanding intrinsic properties, and summarize the major results.

7.1 Single Cell Models Emphasizing Intrinsic Non-linear Properties

Several of the single cell models in this section have been referenced earlier in discussions of specific mechanisms, and later sections will do likewise (for convenience, these models will be labeled as described). Characteristics of different models will be taken both from the original reports and, in the case of the Traub91, Traub94, Warman94, Jaffe94 and Migliore95 models (see references below), from additional simulations run using Surf-Hippo.

7.1.1 Models of Traub and Colleagues

The work of Traub and colleagues (Traub and Llinas, 1977, Traub, 1982, Traub et al., 1991, Traub et al., 1994) comprise a progressive evolution of HPC models that have been particularly influential not only in describing hippocampal function, but in application to models of other cortical neurons. The more recent models (Traub et al., 1991, referenced to as the Traub91 model; Traub et al., 1994, referenced to as the Traub94 model; see Figure 1) are primarily based on CA3 HPC physiology. They include descriptions of six currents (I_{Na}, I_{Ca}, I_{DR}, I_C, I_{AHP} and I_A), based to varying degrees on voltage clamp data. These models also include strongly active dendrites. The Traub94 model included a moderately complex dendritic tree and axon, with significant variations of the kinetic descriptions and a different value of E_K (essentially making them models of *different* channels) for axonal I_{Na} and I_{DR} (Westenbroek et al., 1989). This model was used mainly to examine synaptic-evoked firing patterns under various conditions.

There was no emphasis in either model on the reproduction of single spike morphologies from the data. Especially, the morphology of the bursts generated by these models, which showed the fast spikes riding on the slow burst depolarization initially getting smaller and then getting larger, differ substantially from that which is typically seen in the data (Section 6.5).

A rather high value of C_m (3 $\mu F/cm^2$) and a rather low value of R_m (10,000 Ω cm^2) were used for the entire Traub91 model. In the Traub94 model, more conventional values for R_m and C_m were used for the soma and dendrites (50,000 Ω cm^2 and 0.75 $\mu F/cm^2$, respectively), but the axon membrane had a significantly lower R_m of 1000 Ω cm^2. R_i was also different in the soma/dendrites and axon in this model (200 Ω cm and 100 Ω cm, respectively). An essentially *ad hoc* pattern of dendritic channel densities was used in the models, with hot-spots of I_{Ca} and associated I_{DR} and I_C, in order to reproduce Ca^{2+} spikes. A minor difficulty in both models for quantitative comparison with data is that all potentials are given relative to the resting potential; in our analysis we have assumed an E_{rest} of -60mV.

Both the Traub91 and Traub94 models predicted bursts driven by a Ca^{2+} current and differential repetitive firing characterisitics that depended on somatic versus dendritic stimulation. The Traub94 model showed bursting evoked by antidromic stimulation, that was blocked by appropriately timed dendritic IPSCs. Reduction of dendritic I_{Ca} and I_C, and an increase in somatic I_{DR}, caused the Traub91 model to switch from burst firing, reminiscent of classical CA3 HPC properties, to adaptive repetitive firing, more like CA1 HPCs. Neither model has a stable resting potential, in that they require constant holding currents to avoid spontaneous firing. For example, the Traub94 model shows spontanteous bursting, even if the axon is removed (simulations not shown). When Ca^{2+} channels are blocked, this model fires spontaneous single spikes (simulations not shown).

The role of dendritic Ca^{2+} spikes was crucial in determining the behaviour of both of these models. However, the dendritic spikes predicted by the Traub91 model, in particular under control conditions, are larger than either the early dendritic recordings of either Wong et al. (1979) or Benardo et al. (1982), or recent recordings such as those of Spruston et al. (1995). The peak of these spikes in the model was about +40mV, as compared to about +10mV for the somatic (Na^+) spikes. In the Traub94 model dendritic Ca^{2+} spikes were somewhat smaller (about +20mV) and the somatic spikes somewhat larger (about +30mV).

It is likely that the magnitude of I_{Ca} in the models was overestimated, especially due to overestimation of the driving force (see Sections 11.2.3 and 11.3). We can consider the functional consequence of the predictions, namely that the excitability of the dendrites in these models predicted all-or-nothing responses which propagated throughout the tree, thereby greatly limiting the capability of the tree to act as a substrate for any subtlety in local synaptic interactions. These consequences are especially important in the critical evaluation of the many network models that have been built using these cell models (e.g. Traub and Miles, 1991, Traub et al.; 1996).

7.1.2 Borg-Graham, 1987 Model

An earlier single cell model (Borg-Graham, 1987a and Borg-Graham, 1987b, referenced to as the BG87 model), using a soma/short-cable model (Figure 1) with all channels at the soma, was developed by the author to explore a variety of channel properties in a single context. Analysis was restricted to somatic responses to somatic stimulation. The model, based on both CA1 and CA3 data, included eleven channels: three Na^+ channels (two fast transient channels, $I_{Na(Trig)}$ and $I_{Na(Rep)}$, and a persistent channel, $I_{Na(Tail)}$), six K^+ channels (I_{DR}, I_A, I_C, I_{AHP}, I_M and I_Q), and two Ca^{2+} channels (I_{Ca} and I_{CaS}). Linear parameters were chosen under the assumption that measurements of HPCs (from the sharp electrode recordings of Brown et al., 1981) could be accounted for by incorporating a somatic shunt. The two putative fast transient Na^+ channels were included to account for the available voltage and current clamp data in the context of the Hodgkin-Huxley model, which required a mechanism that allowed for both distinct thresholds of activation and removal of inactivation above the lowest spike threshold without significant steady-state rectification. The model included a description of the dynamics of $[Ca^{2+}]_{in}$ based on a colocalization of I_{Ca} and I_C channels. This structure was proposed to account for the fast kinetics of I_C as opposed to the slower, more integrative kinetics of I_{AHP}. Finally, the model used a reformulation of the Hodgkin-Huxley model that casts the Hodgkin-Huxley parameters in a more biophysical and intuitive way, an updated version of which is discussed in Section 8.4.

The inclusion of specific mechanisms - two fast Na^+ channels with distinct kinetics - for different spike thresholds suggested that selective regulation of those mechanisms could have useful computational consequences (specifically, variation of failure point, or lock-up, for large sustained inputs, Borg-Graham, 1987c).

While the BG87 model reproduced single spike morphology and many of the characteristics of single spike

modulation in response to various pharmacological procedures, it was less successful at reproducing patterns of repetitive firing. For example, while there was a strong adaptation and an sAHP mediated by I_{AHP} in the model, I_M played a minor role in the cell response, contrary to its more likely important contribution to regulation of repetitive firing (see Section 12.7). Also, there is no experimental evidence to support two distinct fast Na^+ channels: the Markovian I_{Na} model described in Section 10.3 collapses the functional characteristics of $I_{Na(Trig)}$, $I_{Na(Rep)}$ and $I_{Na(Tail)}$ into a single channel.

7.1.3 Wathey, Lytton, Jester, and Sejnowski 1992 Model

When the increase in EPSP slope associated with LTP is compared to the amplitude of the extracellularly measured population spike, there is often a larger increase in the latter relative to the former measurement. This relationship (E-S potentiation) was investigated by Wathey et al. (1992, referenced to as the Wathey92 model), with a detailed anatomical model of a CA1 cell (Figure 1) that included simple models, that is not necessarily matched to hippocampal properties, of somatic/axonal I_{Na} and I_K, with I_{Ca} distributed in hot spots in the dendritic tree. This paper described how the electrotonic relationship between the I_{Ca} locations and the locations of synaptic enhancement predicted whether the E-S potentiation was specific or non-specific to the potentiated synapses.

7.1.4 Pongracz, Poolos, Kocsis, and Shepherd, 1992 Model

Pongracz et al. (1992) examined the interaction of voltage-dependent NMDA receptors with a soma/short-cable structure cell model (apical and basal cables with five compartments each, and a two compartment axon). Somatic channels included I_{Na}, I_{DR}, I_{Ca}, I_{AHP} and I_C; all dendritic compartments included I_{Ca}, I_{AHP} and I_C, and dendritic hot spots included I_{Na} and I_{DR}. The proximal axonal compartment (the "initial segment") included I_{Na} and I_{DR} channels; the I_{Na} was of a slightly higher density than the soma. In order to speed up the response of the axon, the passive properties of the initial segment and distal axonal compartment were significantly different than the rest of the cell: R_m of 1,000 and 500 Ωcm^2 as opposed to 80,000 Ωcm^2, respectively, and C_m of 0 and 1 $\mu F/cm^2$ as opposed to 1 $\mu F/cm^2$, respectively. Notably, this model took into account the accumulation and removal of extracellular $[K^+]$ in a thin (200 Å) shell around each compartment - this was used to dynamically update the reversal potential of the K^+ currents and $GABA_B$ synaptic currents, but apparently not of the K^+ contribution to the leak battery. Intracellular Ca^{2+} accumulation in *very* thin (2 Å) compartmental shells was also considered, in a somewhat schematic way - a normalized $[Ca^{2+}]_{in}$ figured in the activation of the Ca^{2+}-dependent K^+ currents, but not in the driving force for the Ca^{2+} currents.

A key finding with the parameters used in this paper was that synaptic responses increased after repetitive input (concurrent activation of AMPA, NMDA, $GABA_A$ and $GABA_B$ synapses), in part due to external $[K^+]$ accumulation. Although model results were directly compared quantitatively with experimental data, the omission of any reference for the data made detailed comparison difficult.

7.1.5 Warman, Durand and Yuen, 1994 Model

Warman et al. (1994, referenced to as Warman94 model) constructed an CA1 HPC model that was similar in structure and intent as the earlier models, ie. analysis of interactions between multiple somatic channels (I_{Na}, I_{Ca}, I_{CT}, I_{AHP}, I_M, I_A, and I_{DR}) within a simple electrotonic structure (Figure 1). As in the BG87 model, the value of R_m for the soma was significantly lower than the dendrites to account for the somatic shunt. In addition, the somatic C_m was taken as 1 $\mu F/cm^2$, whereas the dendritic C_m was taken as 1.85 $\mu F/cm^2$, although the reason was not specified. This model further refined the channel models, with better success in reproducing accommodation characteristics. An earlier model from this group with similar intent was made for a dentate granule cell (Yuen and Durand, 1991).

As with the BG87 model, this model reproduces several aspects of single spike morphologies in response to the modulation of various currents. Also, in contrast with the likely underestimation of I_M in the BG87 model, a notable prediction of the model was that I_M prevents spontaneous repetitive bursting. This was a result of tonic activation of both I_M and I_{Na} at rest, suggesting in part that I_M played a major role in maintaining the resting potential. The resting activation of I_{Na} was related to a large "window current" for this channel, which also was the main current causing the slow depolarization underlying bursts (as compared to a Ca^{2+} current). While indeed there is some evidence for I_M activation at the resting potential (see Section 12.7), cholinergic suppression of this current does not necessarily lead to spontaneous activation.

This prediction of the model, though, may reflect more an overestimation of I_{Na} around rest, rather than an overestimation of I_M (see Section 10.1.4).

7.1.6 Models of Jaffe et al., 1994, and Migliore et al., 1995

Two related models with complicated dendritic structure from Jaffe et al. (1994, referenced to as the Jaffe94 model) and Migliore et al. (1995, referenced to as the Migliore95 model) focused mainly on reproducing the pattern of Ca^{2+} accumulation in the cell and patterns of repetitive firing.

The Jaffe94 model included I_{Na} limited to within 150μm of the soma, and I_{DR}, I_C, I_{CaT}, I_{CaN}, I_{CaL} in every cell compartment. In this model less attention was paid to the descriptions of channel kinetics, excepting those for the Ca^{2+} channels, since the analysis was constrained to the dynamics of $[Ca^{2+}]_{in}$ driven by uncomplicated spike trains. Although the morphology of the model was taken from a CA3 cell (Figure 1), model parameters were chosen to represent both CA1 and CA3 HPCs; the authors claimed that in their experience $[Ca^{2+}]_{in}$ profiles were essentially the same for the two types. This model was able to reproduce characteristics of $[Ca^{2+}]_{in}$ profiles consistent with data generated by this group, including a slower decay for somatic versus dendritic $[Ca^{2+}]_{in}$ that could be accounted for by the difference in surface to volume ratios.

The Migliore95 model, on the other hand, was specific to CA3 HPC properties. This model included a more complete repertoire of channels (I_{Na}, I_{CaT}, I_{CaN}, I_{CaL}, I_A, I_M, I_{AHP}, I_{DR} and I_C), and considered how various patterns of dendritic channel density in several detailed anatomical reconstructions of HPCs could generate regular versus bursting behaviour. Patterns of channel distributions were carefully constrained by placing fixed densities of Na^+ and Ca^{2+}-independent K^+ channels on the soma and the proximal apical dendrites (within 100μm from the soma), and by varying a fixed density of the remaining channels throughout the dendritic tree and the soma. A main result of the Migliore95 model was that given the model channel kinetics, similar rules for distributions of all channel types would predict regular or bursting behaviour for all the structures, despite some non-trivial variations in the dendritic morphology.

7.1.7 Other Single Cell Models

As mentioned in Section 2.1, Spruston et al. (1993) presented a model-based analysis of somatic measurement of events in the dendritic tree. This paper looked at both a detailed cell anatomy (in fact the same cell that was used in the Jaffe94 model) and soma/short-cable equivalents. The cell structures were completely passive. The main result was that under a wide range of reasonable model cable parameters, under somatic voltage clamp distant synaptic events will be significantly distorted.

Two recent studies (Sah and Bekkers, 1996 and Lipowsky et al., 1996) directly combined experimental and modelling analyses of non-linear dendritic properties, specifically with respect to the interaction between the propagation of synaptic potentials and dendritic channels. Both studies used simple soma/short-cable structures (including a basal and an apical dendrite), with various dendritic channels.

Sah and Bekkers (1996) examined the interaction between somatic and dendritic GABAergic IPSCs with I_{AHP}, and concluded that I_{AHP} is present in the proximal 200μm of apical dendrite. Since the I_{AHP} was taken to be voltage-independent (see Section 12.5), their I_{AHP} model was simply a fixed conductance waveform. No other channels, nor Ca^{2+} dynamics were included in the cell model. The proximal distribution of I_{AHP} was inferred by the response of this current to changes in voltage clamp holding potentials that was similar to that of IPSCs of known dendritic origin. The restriction of I_{AHP} to the apical tree was suggested since EPSPs evoked in stratum radiatum (thus arising from the apical tree) were shunted more by the sAHP than EPSPs evoked in stratum oriens (thus arising from the basal tree).

Lipowsky et al. (1996) investigated the role of dendritic persistent Na^+ current (I_{NaP}) on the amplification of EPSPs in CA1 pyramidal cells. The model included I_{Na}, I_{NaP}, I_{Ca}, I_C, I_{AHP}, I_M, I_{DR} and I_A, with parameters of the $[Ca^{2+}]$ dynamics and all channels other than I_{NaP} adapted from the Warman94 model. The description of I_{NaP} was taken directly from the experimental report of French et al. (1990). The key issue addressed by the model was the effect on subthreshold distal apical input by the inclusion of either somatic or dendritic I_{NaP}, and in fact the relevance of the model channels other than I_{NaP} and I_A was minimal to the results reported in this paper. Addition of dendritic I_{NaP} amplified and slowed the EPSP; subsequent incorporation of dendritic I_A resulted in EPSP waveforms that were well matched to the data. Although a simple dendritic structure was used (single cable), the fact that non-linearities were included only in the proximal ($< 200\mu$m of the soma) apical dendrite, and simulated synaptic input was quite distal (600μm from the soma), means that the issue of non-linearities local to the input was avoided.

7.1.8 Recapitulation on the Working Model

The Working model that we demonstrate in this chapter has the soma/short-cable geometry of the BG87 model, again with all non-linear mechanisms located at the soma. The model includes the following channels: I_{Na}, I_{CaN}, I_{CaT}, I_{CaL}, I_D, I_{DR}, I_A, I_M, I_{CT}, I_{AHP} and I_H. A multiple compartment Ca^{2+} concentration system is included in the soma, incorporating a Ca^{2+} pump and an instantaneous buffer.

7.1.9 On-line Parameters of Reviewed Models

Complete "turnkey" implementations of the Traub91, Traub94, Warman94 and Working models, and specific mechanisms of the Jaffe94 and Migliore95 models are included in the Surf-Hippo distribution.

7.2 Models Emphasizing Interactions Between Synaptic Processes and Intracellular Ion Dynamics

Although not specific to hippocampus, Qian and Sejnowski (1989, 1990) described a one-dimensional model of ionic flow in dendritic structures which takes into account coupled electromotive and diffusional flow, and which they used to predict voltage and concentration responses to synaptic input. These results were compared with that of a model based on electromotive flow only (the standard cable model, that is the type of circuit used by all other models described in this chapter), and that of a modified cable model which calculates, at each time step, the contribution of diffusional flow after electromotive flow has been evaluated. They showed that for large structures the contribution of diffusional processes is, as expected, negligible due to the small changes in concentration, while for small structures, such as spines, the incorporation of diffusional processes gave potentially significant differences from the cable model with respect to predicted concentration profiles and saturation characteristics in response to varying strengths of synaptic input. They also showed that the modified cable model accounts for much of these differences, providing that the synaptic input is not too great, with the benefit of being computationally much more efficient than the full diffusion formulation.

The models of Zador et al., (1990) and Schiegg et al. (1995, see Section 9.3) combined a detailed representation of a single spine with a simplified HPC dendritic structure to analyze Ca^{2+} dynamics in the spine microenviroment. Holmes and Levy (1990) presented a detailed compartmental model of a dentate gyrus neuron which focused on the interaction between Ca^{2+} influx via NMDA-mediated synaptic channels on explicit spine representations and detailed $[Ca^{2+}]_{in}$ dynamics relevant to conditions consistent with the expression of LTP. They found that transient saturation of local buffer in the spine head was necessary for $[Ca^{2+}]_{in}$ increases that were sufficient to account for LTP.

8 Channel Models

In this section we will describe various models for non-linear channel properties, including both voltage and Ca^{2+}-dependent channels. These models are at an intermediate level of biophysical detail, appropriate for describing whole cell currents.

For a given current I_X, the most common models for the underlying channel are based on the assumption of a gated, membrane-spanning ionophore, where the mechanism of conduction $f(V, \Delta[X])$ (flow of ions down a voltage gradient), and that of gating $h(V, t, ...)$ (voltage and/or ligand dependent modulation of conduction) are separable:

$$I_X = h(V, t, ...)\ f(V, \Delta[X])$$

Here V is the membrane voltage, t is time and $\Delta[X]$ represents the concentration gradients for the permeable ions of the channel. The ellipsis in the argument of $h()$ stands for the various ligand-dependent processes (e.g. Ca^{2+}-dependence).

Here we review two models of the conduction term $f(V, \Delta[X])$: ohmic (thermodynamic equilibrium conduction) and constant-field permeation (non-equilibrium conduction). We shall also describe two related models of the gating term $h(V, t, ...)$: the Hodgkin-Huxley model (and a reformulation of the original equation parameters), and Markov models (which include the Hodgkin-Huxley model as a special case). We shall also review models of Ca^{2+}-dependent gating. We shall see that in principle both conduction models for $f(V, \Delta[X])$ have a non-linear negative feedback characteristic which in certain cases has important functional

consequences; therefore the non-linearity of neuronal ionic currents can arise from *both* the conduction term and the channel gating term.

8.1 Linear Conductance: Driving Force From Equilibrium Thermodynamics

In most cell models channel conduction is taken as ohmic (linear), with the driving force determined by the membrane voltage, $\Delta[X]$, and the relative permeabilities of the ions that pass through the channel. The general form of the ohmic model is:

$$f(V, \Delta[X]) \;=\; \overline{g}_X \; (V - E_X)$$

where, assuming that the units of $f()$ are in nanoamperes, $\overline{g}_X$ is the absolute conductance in μS and E_X is the reversal potential for the channel, the latter given by either the Nernst equation if only one ion is involved, or the Goldman-Hodgkin-Katz (GHK) voltage equation (e.g. Hille, 1992) for more than one ion (voltages in millivolts). In this model, the non-linearity of the conductance term arises implicitely from the Nernst or GHK equation-based estimate of the driving force E_X coupled with a non-zero change in $[X]$ with respect to I_X. Thus, the more current, the more the concentration gradient is reduced, resulting in negative feedback. In practice, many cell models that use the ohmic description neglect changes in concentration, under the assumptions that these activity-driven changes are small.

The use of the Nernst equation for the driving force in the ohmic model is based on the assumption of thermodynamic equilibrium; strictly speaking this corresponds to the situation in which no current is flowing. Thus this description is more appropriate for those ions in which the concentration gradient is not very high and the integrated currents are small compared to the relevant concentrations. These conditions are approximated for K^+ and Na^+, which is similar to saying that these ions are closer to equilibrium. Although widely used (as in all the non-Ca^{2+} channel descriptions we shall present here), the validity of this approximation for describing non-equilibrium conditions (that is, when the neuron is *doing* something electrically) has not been systematically tested.

8.1.1 Setting E_{rev} for Ohmic Channel Models

The most basic way to determine the ions associated with a particular channel experimentally is by estimating the reversal potential and relating that value to that expected from the Nernst or GHK voltage equations. Manipulating the concentrations of specific ions and comparing the change in the reversal potential with that predicted by these equations may also be done. Especially for the case of K^+ channels, there is a dichotomy between the experimental values for E_{rev} and that used by many models, in that in the former case the measured E_{rev} is rarely that predicted for a pure K^+ conductance, whereas in the latter case models often assume that all K^+ channels share the same $E_{rev} \;=\; E_K$. A more flexible approach is to allow the E_{rev} for nominally K^+ channels to be set to within a maximum of 20 millivolts or so above the Nernst E_K (typically this is -90 to -95mV), a range typically seen in the data. We have found that this additional free parameter allows for some useful fine tuning in the shape of the afterpotentials.

We may note as well that the value of E_K (and sometimes E_{Na}) in some models is not given explicitly, despite the fact that there are no reliable canonical values, and variations in these parameters can have a significant effect on cell behaviour.

8.2 Intrinsic Non-Linearity of Pore Conduction

As a particular ion moves farther from equilibrium (specifically the case for Ca^{2+}), the ohmic model becomes less accurate. One of the most widely used non-equilibrium models of pore conduction permeation is the constant field model, described by the Goldman-Hodgkin-Katz (GHK) current equation. In this equation (see Jack et al., 1983 and Hille, 1992), the non-linearity of the permeation term is explicit:

$$f(V, \Delta[X]) \;=\; \overline{p}_X \; \frac{Vz^2F^2}{RT} \; \frac{[X]_{in} - [X]_{out} \exp(-zFV/RT)}{1 - \exp(-zFV/RT)}$$

where, again assuming that the units of $f()$ are in nanoamperes, R is the gas constant, F is Faraday's constant, T is temperature in degrees Kelvin, $\overline{p}_X$ is the permeability (*not* the conductance) of the channel in cm^3/second, $[X]_{in}$ and $[X]_{out}$ are the intracellular and extracellular concentrations in millimolar and z is the valence of the permeant ion - here we assume that channel conduction is mediated by only one type of ion.

The non-linear behaviour of this term manifests itself as negative feedback for inward currents, particularly Ca^{2+} (e.g. Hess and Tsien, 1984), both because of the sublinear characteristic at typical values of $[Ca^{2+}]$ and because the driving force is reduced as the gradient of $[X]$ is reduced with current flow. We note, however, that the dynamic change of this characteristic due to typical concentration changes is not very large.

Neuron models which have used this formulation, in all cases for Ca^{2+} currents, include the Wathey92 Jaffe94 and Migliore95 models, models of thalamic relay neurons (Huguenard and McCormick, 1992) and cortical pyramidal cells (Lytton and Sejnowski, 1991). At membrane potentials far from the equilibrium point (e.g. $V_m <$ -20mV for Ca^{2+} channels) the GHK current equation becomes linear, and if the voltages in the model under consideration stay in this range it may be reasonable to substitute an ohmic equivalent (e.g. see De Schutter and Bower, 1994). This conversion also has to be considered when interpreting many of the reports on Ca^{2+} channels, where conduction values at some holding potential are reported instead of permeabilities.

8.3 Channel Gating *à la* Hodgkin and Huxley: Independent Voltage-Dependent Gating Particles

Hodgkin and Huxley (1952b) described channel gating as an interaction between different, independent two-state (open and closed) elements or "particles", all of which must be in the open state for channel conduction. The state dynamics of each particle are described with first order kinetics:

$$x_C \overset{\alpha_x(V),\beta_x(V)}{\rightleftharpoons} x_O \tag{2}$$

where x_C and x_O represent the closed and open states of gating particle x, respectively. $\alpha_x(V)$ and $\beta_x(V)$ are the forward and backward rate constants of the particle as a function of voltage, respectively. Taking x to be the probability of the open state, the associated differential equation is:

$$\frac{dx}{dt} = \frac{x - x_\infty(V)}{\tau_x(V)}$$

with the steady state value of x, $x_\infty(V)$, and the time constant, $\tau_x(V)$ given by $\alpha_x(V)$ and $\beta_x(V)$ (see below). A useful generalization of this kinetic scheme is to assume that the rate constants can be functions of other signals (e.g. $[Ca^{2+}]$); the general form of the gating term in this scheme is the product of the open probability of the channel's gating particles:

$$h(V,t,...) \;=\; \Pi x_i^{n_i}(V,t,...)$$

where x_i is the open probability of a given type of gating particle, and n_i is the number of particles of a given type associated with the channel. This system is a specific type of Markovian model (see Section 8.7), constrained by the independence condition; the general Markovian model allows arbitrary transitions between the states describing the channel kinetics.

The success of the Hodgkin and Huxley theory is in the utility of a kinetic scheme which is described by ensembles of independent two-state gating particles, each of which has transition rates which are functions of the membrane voltage. While Hodgkin and Huxley hypothesized that the steady state behaviour of each particle fit a Boltzman distribution, the underlying rate equations were fit to the data with various functions that included both linear and exponential voltage terms. Although taken as a canonical form by countless cell models, a consequence of the specific form of the equations is that there is not an obvious relationship between the equations' parameters and the standard kinetic description, i.e. in terms of the voltage dependence of the steady state x_∞ and time constant τ_x.

8.4 An Extended Hodgkin and Huxley Model

For gating particles that are dependent only on voltage, this theory can be recast in more explicit form by considering parameters of a single-barrier kinetic model for each particle (Jack et al., 1983, Borg-Graham, 1991). The advantages of this form are parameters which are both more directly related to the functional behaviour of the channel, and which have specific biophysical interpretations. Various neuron models have used this formalism (the BG87, Warman94, Migliore95, and Jaffe94 models; also Lytton and Sejnowski, 1991, Bush and Sejnowski, 1994 for cortical pyramidal cells, Quadroni and Knöpfel, 1994, for medial vestibular nuclei neurons, and Burgi and Grzywacz, 1994, for retina).

8.4.1 Comparison to the Original Hodgkin-Huxley Equations

A final advantage is that in its basic form, this formulation has five parameters for each particle ($V_{1/2}$, z, γ, K and τ_0; see below), whereas the Hodgkin-Huxley model has six parameters, in part because the dependence between $\alpha(V)$ and $\beta(V)$ is not explicit. Nevertheless, this formulation may be readily fitted to the original Hodgkin-Huxley equations of squid axon I_{Na} and I_K; the error is comparable to the error between the original equations and the data to which they were fit (cf. figures 4, 7, and 9 in Hodgkin and Huxley, 1952b).[7]

8.4.2 Parameters of the Single Barrier Gating Model

The formulation, which describes the first-order kinetics represented in Equation 2, is defined as follows - the following derivation is somewhat modified from the description given in Borg-Graham (1991).

We first derive the expressions of $\alpha'_x(V)$ and $\beta'_x(V)$, the forward and backward rate constants of the single barrier transition. For a given particle x, z (dimensionless) is the *effective* valence of the gating particle, where a positive value means that the particle tends to the open position with depolarization - i.e. it is an activation particle. Likewise, a negative value of the valence means that the particle tends to the open position with hyperpolarization - i.e. it is an inactivation particle.[8] The effective valence is the product of the actual valence of the particle (an integer) and the proportion of the membrane thickness that the particle moves through during state transitions; thus this parameter is not restricted to integers. γ (dimensionless, between 0 and 1) is the asymmetry of the gating particle voltage sensor within the membrane. K ($1/ms$) is the leading coefficient of both $\alpha'_x(V)$ and $\beta'_x(V)$. This term can be described in terms of Eyring rate theory, an explicit version of which may include an additional temperature term (Borg-Graham, 1991). We shall not consider this component explicitly here, and just take K as a constant. $V_{1/2}$ is the voltage for which $\alpha'_x(V)$ and $\beta'_x(V)$ are equal. The final equations for $\alpha'_x(V)$ and $\beta'_x(V)$ are then:

$$\alpha'_x(V) = K \exp\left(\frac{z\ \gamma\ (V - V_{1/2})\ F}{R\ T}\right)$$

$$\beta'_x(V) = K \exp\left(\frac{-z\ (1-\gamma)\ (V - V_{1/2})\ F}{R\ T}\right)$$

An additional parameter, τ_0, (not the same as the linear membrane time constant) represents a rate-limiting step in the state transition, for example "drag" on the particle conformation change.[9] This parameter is crucial for fitting the expressions to the original Hodgkin-Huxley equations. There are two equivalent ways of incorporating τ_0 into the kinetics. The more intuitive approach is to include τ_0 explicitly in the expression for the time constant $\tau_x(V)$ of the particle state differential equation:

$$\tau_x(V) = \frac{1}{\alpha'_x(V)\ +\ \beta'_x(V)}\ +\ \tau_0$$

We can also derive the appropriate forms for $\alpha_x(V)$ and $\beta_x(V)$ that characterize the kinetics of Equation 2:

$$\alpha_x(V) = \frac{\alpha'_x(V)}{\tau_0(\alpha'_x(V) + \beta'_x(V)) + 1}$$

$$\beta_x(V) = \frac{\beta'_x(V)}{\tau_0(\alpha'_x(V) + \beta'_x(V)) + 1}$$

Note that when τ_0 is 0, $\alpha_x(V)$ is equal to $\alpha'_x(V)$ and $\beta_x(V)$ is equal to $\beta'_x(V)$. Finally, the expression for $x_\infty(V)$ is:

[7] We have fitted this formulation to all Hodgkin-Huxley mechanisms in the channels used in the models of Section 7.1 - in every case model behaviours using the fitted versions were qualitatively the same as using the published versions.

[8] This definition for the sign convention of z is opposite to that found in Borg-Graham, 1991, for no profound reason. The convention used here is the same as that used in Jack et al., 1983 (eq. 8.33-34, p. 242), and depends only on the (arbitrary) definition of polarity of the gating particle with respect to the membrane inner and outer surfaces.

[9] The formulation in Borg-Graham (1991) used this parameter as a lower bound for $\tau_x(V)$. The form defined above not only avoids discontinuities in the characteristic but also seems more plausible. Similar considerations have been explored for other, more general, kinetic schemes, e.g. Patlak, 1991.

$$x_\infty(V) = \frac{\alpha'_x(V)}{\alpha'_x(V) \ + \ \beta'_x(V)} = \frac{\alpha_x(V)}{\alpha_x(V) \ + \ \beta_x(V)} \tag{3}$$

Two additional parameters, α_0 and β_0, may be considered in some cases, though they are not necessary in reproducing the original Hodgkin-Huxley equations. These parameters are forward and backward rate constants, respectively, of parallel state transitions which are voltage-independent, but nonetheless figure into the total kinetics. If considered, α_0 and β_0 alter the expressions for $\alpha_x(V)$, $\beta_x(V)$, and thus $\tau_x(V)$ and $x_\infty(V)$, which we will not consider here.

8.4.3 Relationships Between the Extended Hodgkin-Huxley Model Parameters and $x_\infty(V)$ and $\tau_x(V)$

As stated, an advantage of this formulation is a more clear connection between the parameters and the macroscopic characteristics $x_\infty(V)$ and $\tau_x(V)$. In particular, $V_{1/2}$ gives the midpoint and z sets the steepness of the $x_\infty(V)$ sigmoid. The symmetry parameter γ determines the skew of $\tau_x(V)$: $\gamma = 0.5$ gives a symmetrical bell-shaped curve for $\tau_x(V)$, which otherwise bends to one side or the other as γ approaches 0 or 1. z sets the width of $\tau_x(V)$, unless γ is equal to either 0 or 1, in which case $\tau_x(V)$ becomes sigmoidal and thus z sets the steepness as for $x_\infty(V)$.

With this scheme a particle with a voltage-independent rate constant can be represented by setting $1/K << \tau_0$, and both α_0 and β_0 to zero, thus making τ_0 the effective time constant. Likewise, both the time constant and steady-state become voltage-independent by setting $K = 0$ and choosing the appropriate α_0 and β_0. We should emphasize that the α_0 and β_0 parameters are included for flexibility; in all of the Hodgkin-Huxley type parameters that we shall discuss in this chapter, and in the discussion below, both parameters are taken as zero.

8.4.4 Determining the Number of Particles in Hodgkin-Huxley Models

The exponent n of a particular gating particle in the Hodgkin-Huxley description implies the number of that type of particle in the channel. The motivation of Hodgkin and Huxley for introducing this parameter was to account for sigmoidal characteristics of current activation under voltage clamp (the power for the inactivation particle h in the Hodgkin-Huxley I_{Na} model is one - however, their protocol did not directly measure the kinetics for the removal of inactivation). Some experimental papers report fitting integer powers of hypothetical gating particles according to the observed kinetics, but more typically steady-state activation or inactivation data is simply the observed macroscopic behaviour (that is, reflecting the steady-state of the ensemble of particles). Thus, for channel models gating particle powers can often be considered as another free parameter.

There are three immediate consequences of assuming more than one particle of a given type. First, while the transition from the closed to open state under voltage clamp of a single particle is exponential, as noted above (and key to Hodgkin and Huxleys' choice of parameters), powers greater than one result in a sigmoidal transition (arising from the time course of $(1 - \exp(-t))^n$ when n is greater than one). This trajectory implements a kind of delay in the closed to open state transition, which is often a major motivation for hypothesizing $n > 1$ in Hodgkin-Huxley models. Second, although the collective steady state behaviour of an ensemble of particles of a given type as a function of voltage is sigmoidal, the expression $(1/(1-\exp(V))^n$ goes to zero faster than $1/(1-\exp(V)$ (these functions in V are the basic form of Equation 3). Thus, if the parameters of the extended Hodgkin-Huxley model are fitted to the measured steady-state behaviour, assuming n greater than one can attenuate the zero-end of this characteristic. In some cases, we have found that using n greater than one has restricted this tail activation which otherwise could complicate the contribution of the channel in question at certain voltages. Finally, in this model when $n = 1$ the peak (when $0 < \gamma < 1$) or inflection point (when $\gamma = 0$ or 1) of $\tau_x(V)$ is roughly around $V_{1/2}$. Higher powers of n tend to shift these points in the direction of voltage for which $x_\infty(V)$ tends to 0. This shift may have a noticable functional effect between different values of n.

8.5 Activation versus De-Activation; Inactivation versus De-Inactivation

It is useful to briefly review the terminology of activation and inactivation. Traditionally, in the context of the Hodgkin-Huxley model, the difference between activation and inactivation is simply that they have an opposite dependence on membrane voltage. On the other hand in more general kinetic descriptions inactivation is often used to describe the transition into closed states after activated or open states. In

the Hodgkin-Huxley context, we can refer to a channel becoming open either by activation (assuming no concurrent inactivation) or by de-inactivation (assuming concurrent activation). Likewise, a channel can become closed by either by inactivation or by de-activation.

Finally, there are channels that become open with hyperpolarization, e.g. I_H. Assuming that they are persistent channels (no inactivation), it is more clear to say that these channels are gated by activation particles, even though this is inconsistent with the definitions given above for the voltage dependence of gating particles.

8.6 The Hodgkin-Huxley Model: Some Conclusions

The independence of gating particles in the Hodgkin-Huxley model has at least two advantages: presented in the proper form the kinetics of the model can be predicted in an intuitive way, especially when considering experimental data, and as a practical issue the numerical integration may be accomplished efficiently (Hines, 1984). On the other hand, this independence constrains the equivalent state space description (vis-a-vis the relative transition rates, Destexhe et al., 1994) of the more general Markovian model.

8.7 Channel Gating as Dynamical Systems *à la* Markov Models

The behaviour of a dynamical system is characterized by some trajectory in state space, where each "state" is defined fundamentally in terms of observed kinetics. For models of ion channels, including the Hodgkin-Huxley model, the general assumption is that each state corresponds to a specific conformation of the membrane protein, thus an individual channel can be in only one state at a time. The description of an ensemble of channels (e.g. as appropriate for a cell model) assigns a probablity at any given time for the occupancy of each state. The observable states of a channel are those that conduct current (the open states), but of course the non-open states (called closed or inactivated, depending on the particular model) are as important in understanding channel behaviour.

When the transitions between states in a dynamical system are stochastic with probabilities that are independent of the *history* of the system, the resulting model is a Markov model. This classification does not mean that the transitions can not be functions of time *per se*, however, most models of this sort do not use functions in which time is an explicit independent variable. State transitions may be functions of other quantities, certainly - for channel models the most common dependency is that of voltage.

Markov kinetic models are the standard description for detailed biophysical analysis of channel kinetics, but there have been relatively few applications in the neural modelling literature (however, see Bush and Sejnowski, 1991). One practical limitation for these models is that they are typically much more computationally expensive than two-state models such as the Hodgkin-Huxley model (for a hybrid of Markov and Hodgkin-Huxley , see below). The general methodology of Markov models as applied to channel mechanisms is beyond the scope of this chapter (see Colquhoun and Hawkes, 1995). Destexhe and colleagues (1994) have written a concise discussion on Markov models which is aimed in particular at cell level modelling of channels and synapses.

Although the Markovian framework puts no restrictions on the functions that define state transitions (other than the no-memory condition), the form presented above of the $\alpha_x(V)$ and $\beta_x(V)$ functions for the extended Hodgkin-Huxley model is convenient and very general. The voltage-dependent transitions Markov models that we shall use in the Working model for I_{Na} and I_{CT} (Sections 10.3 and 12.4.1) may be defined in such terms; however, we shall use the following squeezed exponential formula for the transition rate $\alpha_{ij}(V)$ from state i to state j:

$$\alpha_{ij}(V) \;=\; \left(\tau_{min} \;+\; \left((\tau_{max}-\tau_{min})^{-1} + \;\exp\left(\frac{(V-V_{1/2})}{k}\right)\right)^{-1}\right)^{-1} \tag{4}$$

where the inverse of τ_{min} (analogous to τ_0 in the extended Hodgkin-Huxley model) and τ_{max} put upper and lower bounds, respectively, on the rate constant $\alpha_{ij}(V)$. Note that there is an implicit coefficient of the exponential term of 1/ms (same units as either $1/\tau_{min}$ or $1/\tau_{max}$) in this equation.

8.7.1 Markov Mechanisms Can Decouple the Timecourse of Activation/Inactivation Signals and Functional Channel State Transitions

There are several cases in which there is an apparent delay between a modulating signal, S, e.g voltage or Ca^{2+}, and the functional state transition, say $A \rightarrow B$. For example the activation of the I_{AHP} channel is

dependent on a rise in $[Ca^{2+}]$, but the actual channel opening may lag by a few hundred milliseconds, by which time the $[Ca^{2+}]$ may have fallen below the activation threshold (Section 12.5). In a general Hodgkin-Huxley scheme of a collection of independent particles (where the modulating signal S is not necessarily voltage), the timecourse of S is directly coupled to the associated state transition, such that the subsequent removal of S would arrest a slow transition. The sigmoidal activation when $n > 1$ in this model effects a kind of delay, but the result is somewhat gradual, since the underlying time constant for the transition dependent on S is the same as that determining the delay. In the Markov description, a more independent delay may be accomodated by adding an additional state, say A', from where the transition to state B is defined by some constant slow rate. Thus, a change in S could move the channel from A to A', from which it would then move more slowly to B, assuming that the reverse transition $A' \rightarrow A$ was even slower and relatively independent of S.

We may note that the Moczydlowski and Latorre model (1983) described below has some degree of this sort of decoupling, in that the full closed to open transition is a sequence comprised of a Ca^{2+}-dependent, a Ca^{2+}-independent, and finally a Ca^{2+}-dependent step.

8.7.2 Linear Markov models based on the Hodgkin-Huxley model

The standard interpretation of the Hodgkin-Huxley gating model is that all particles associated with a channel must be in the open state for channel conduction. A generalization of this theme is to assume that for a channel with N Hodgkin-Huxley gating particles of the same type, the channel conducts when any M ($\leq N$) of the particles are in the open state (e.g. the model of retinal I_H of Barnes and Hille, 1989). We call this a linear Markov model since the Markov state diagram has no loops. Since all the particles are the same type, the computation of the channel gating is much more efficient than that for the general Markov case. Specifically, given N particles of type x, each with the same open probability p (since they are assumed to be identical and independent), then the contribution $h_x(V,t,...)$ of the ensemble of particles to the channel gating term $h(V,t,...)$ is given by a summation of binomial terms:

$$h_x(V,t,...) = \sum_{i=M}^{N} \left(\begin{array}{c} N \\ i \end{array} \right) p^i (1-p)^{(N-i)}$$

8.8 Ca^{2+}-Dependent Gating

In this section we review various data and models for the Ca^{2+}-dependence of K^+ channel activation.

8.8.1 The Barrett, Magleby and Pallotta 1982 Model

Using single-channel recordings of the Ca^{2+}-dependent K^+ channel (BK channel) in cultured rat muscle cells, Barrett et al. (1982) found an approximate third power relationship between channel open times and $[Ca^{2+}]$ that was strongly facilitated by depolarization. For example, at a membrane voltage of 10 millivolts, channels became open with a $[Ca^{2+}]$ threshold of about 1μM. The steady-state characteristic of this data was adapted in the Warman94 model for the kinetics of I_{CT}.

8.8.2 The Moczydlowski and Latorre 1983 Model

Moczydlowski and Latorre (1983) recorded from similar channels, reconstituted in planar lipid bilayers, and proposed a detailed Markovian kinetic scheme for the Ca^{2+} and voltage-dependent gating of these channels. Other work analysing the BK channel in rat muscle supports the Markov interpretation (McManus and Magleby, 1989).

The Moczydlowski and Latorre model has been applied in several neuron models (e.g. the Jaffe94 and Migliore95 models), in part, presumably, because this model is included in the NEURON package. We found it possible to apply the Moczydlowski and Latorre model to the Ca^{2+}-dependency of both I_{CT} and I_{AHP}, after appropriate adjustments of the model parameters for intracellular Ca^{2+} dynamics (Section 9.7). However, considering that the six parameters for the Moczydlowski and Latorre model do not have an obvious relationship with properties readily observed from whole cell currents, and that our particular fit required parameter values quite different from the original report, we chose to use a simpler Ca^{2+} dependence formulation (see below). Also, in the case of I_{AHP} the data does not indicate a voltage dependence (but see discussion in Section 12.5). We note as well that the parameters used in the cell models mentioned above are also quite different from the parameters in the original paper (and from each other), which puts

into question the utility of this description for neuron models without further data specific to neuronal Ca^{2+}-dependent K^+ channels. We may also note that the specific Markovian kinetic model chosen by these authors was not unique, but rather was the simplest (least number of states) given their data; this strategy is typical for Markovian analysis of single channel kinetics. A perhaps more robust general conclusion from the Moczydlowski and Latorre analysis was that channel kinetics were voltage as well as Ca^{2+}-dependent, and that the fully activated state required at minimum the binding of two Ca^{2+} ions.

8.8.3 A Simple Kinetic Model

A simple model for Ca^{2+}-dependent kinetics of a two-state gating particle can be described by the following reaction; a similar scheme was used in the BG87 and Migliore95 models (also Quadroni and Knöpfel, 1994, for medial vestibular nuclei neurons and Burgi and Grzywacz, 1994 for retina). Assume that w represents the open probability of a Ca^{2+}-dependent gating particle:

$$w + nCa^{++} \overset{\alpha,\beta}{\rightleftharpoons} w^*$$

where the $*$ superscript denotes the open state bound to n Ca^{2+} ions.[10] In the more general Markovian framework, w and w^* refer to two adjacent states out of the entire state space. The forward and backward rate constants are α and β, respectively. This scheme assumes that binding with Ca^{2+} ions is cooperative - either all binding sites are occupied or none are. We may also consider a τ_0 parameter as in the extended Hodgkin-Huxley model. If we assume that the binding of Ca^{2+} in this reaction does not appreciably change $[Ca^{2+}]$, then the steady state value for w^*, w_∞, and the time constant for the kinetics, τ_w, are given by:

$$w_\infty = \frac{\alpha[Ca^{2+}]^n}{\alpha[Ca^{2+}]^n + \beta} \tag{5}$$

$$\tau_w = \frac{1}{\alpha[Ca^{2+}]^n + \beta} + \tau_0 \tag{6}$$

Voltage dependence of this scheme can be added in a number of ways. For example in the Markov model of I_{CT} in the Working model the forward rate constant is defined by:

$$\alpha_w(V, [Ca^{2+}]) = \alpha_V(V) \times \alpha[Ca^{2+}]^n \tag{7}$$

where $\alpha_V(V)$ is the squeezed exponential function of voltage in Equation 4, such that the forward reaction speeds up with depolarization.

9 Ionic Concentration Dynamics

The ionic fluxes which underly neuronal activity necessarily change the concentrations of those ions on either side of the membrane. Whether or not these changes have any functional consequences depends on the relative size of the changes, and on any secondary effects (e.g. those not directly determining the driving force for the ionic current) of the concentrations. The necessary role of internal Ca^{2+} on both short and fast time scales in the control of various membrane properties and processes such as LTP is well established, and make this ion the most important candidate for considering the concentration dynamics in models.

For our purposes, at least two major K^+ currents have been clearly demonstrated to depend on the influx of Ca^{2+}: the large and fast I_{CT} and the small and much slower I_{AHP}. Thus for the Working model we develop a relatively simple model for $[Ca^{2+}]_{in}$ in order to account for the activation of these currents. Other Ca^{2+}-dependent currents that may be relevant to the reproduction of basic firing properties, but will not be included in the Working model, include the "slow" I_C, discussed in Section 12.4, the Ca^{2+}-dependence of I_M (Section 12.7), and the Ca^{2+}-dependent non-specific cation currents, discussed in Section 13.3.

Other modelling studies have considered the interaction between cell responses and changes in $[K^+]$ (e.g. Yamada et al., 1989 for bullfrog ganglion cells, and Pongracz et al., 1992 for HPCs, Section 7.1.4), and/or $[Cl^-]$ (e.g. Qian and Sejnowski, 1989 and 1990, for a non-specific dendritic spine model, Section 7.2).

In this section we shall discuss recent data on measurements of intracellular $[Ca^{2+}]$ during synaptic activity and current evoked spikes. We review the factors which set the resting level of $[Ca^{2+}]_{in}$ and the

[10] One can also imagine a similar but reverse reaction for the description of Ca^{2+}-dependent inactivation, for example as reported for Ca^{2+} channels (Section 11.2.3).

role of intracellular Ca^{2+} stores. We discuss membrane pumps both for Na^+ and, more relevant to the model, for Ca^{2+}. Models for intracellular Ca^{2+} buffers are described, and we then describe a fairly simple model which captures the basic characteristics of $[Ca^{2+}]$ dynamics, comparing this system with previous hippocampal models. We note that constructing an adequate model of $[Ca^{2+}]$ dynamics is very difficult since the quantitative data is somewhat inconsistent (see below) and the mechanisms for regulation of intracellular Ca^{2+} are poorly understood. Also, estimating Ca^{2+}-flux in a model is of course quite dependent on the model for the Ca^{2+} channel or channels.

9.1 The Data on Ca^{2+} Concentration Dynamics

As we shall see, estimates on the absolute change in $[Ca^{2+}]$ in response to either intracellular current or synaptic stimulus vary between different quantitative studies, as summarized in Table 3. The key figures that we must extract from the data are the incremental change of $[Ca^{2+}]$ per spike, which, since the sAHP amplitude increases incrementally with the number of spikes, is directly related to the Ca^{2+}-sensitivity of the current underlying the sAHP, I_{AHP} (Section 12.5), and the time constant for decay, which is related to the duration of the sAHP and thus I_{AHP}. These figures, combined with direct and indirect estimations of crucial I_{Ca} parameters, and a buffering parameter (Section 9.5.1), form the backbone of our model for $[Ca^{2+}]$. Note that the structure of the Ca^{2+} system that we shall use (Section 9.7), and its relationship to the Ca^{2+}-dependence of I_{CT}, implies that the large transient localized $[Ca^{2+}]_{in}$ relevant for I_{CT} will not be directly evident from, and thus not directly constrained by, $[Ca^{2+}]$ changes integrated over many microns of a cell process, as given by the available data.

We also note that the size of changes in proximal dendrite $[Ca^{2+}]$, as opposed to somatic $[Ca^{2+}]$, may be more relevant for determining parameters of the I_{AHP}, since the functional location of this current may be primarily the proximal apical dendrite (Sah and Bekkers, 1996; see Section 12.5). This factor will be neglected in the Working model, however, since all channels are located at the soma.

9.1.1 Ca^{2+} Influx Via Voltage-Gated Ca^{2+} and Synaptic Channels

First, it is important to recall the major sources of intracellular Ca^{2+} in general, that is via Ca^{2+} channels, synaptic Ca^{2+} entry, and release from Ca^{2+} stores. For example, Regehr and Tank (1992) describe synaptically evoked $[Ca^{2+}]$ changes in CA1 in the slice, distinguishing between those arising from voltage-gated Ca^{2+} channels versus NMDA channels (see also Miyakawa et al., 1992). Although a large fraction of the rise in $[Ca^{2+}]$ was blocked by intracellular application of QX-314 (indicating a dependence on I_{Na}-mediated depolarization), they also characterized a significant AP5 (NMDA-receptor blocker) sensitive component that was insensitive to Na^+ channel block. However, since we intend to model responses to intrinsic stimulation, we will focus only on Ca^{2+} influx via voltage-gated Ca^{2+} channels. Future development of the model will include evalation of Ca^{2+} release from Ca^{2+} stores.

9.1.2 $\Delta[Ca^{2+}]$ From Current-Evoked Spikes

Jaffe and colleagues (1992) studied the dynamics of $[Ca^{2+}]_{in}$ and its relationship with Na^+ entry in hippocampal neurons using Ca^{2+} and Na^+-sensitive dyes. They reported an increase of about 3nM in $[Ca^{2+}]_{in}$ 70μm from the soma with a single current evoked spike. A spike train of 29 spikes in response to a 500 millisecond current step evoked an steady increase in $[Ca^{2+}]_{in}$ both at the soma and 60μm away, with a total change of about 60nM and 100nM, corresponding to 2.1nm/spike and 3.5nM/spike, respectively. The correlation of Na^+ concentration changes in the dendrites with $[Ca^{2+}]_{in}$ changes indicated that dendritic Na^+ spikes were necessary for the major component of $[Ca^{2+}]$ changes in the tree. Little change in $[Ca^{2+}]$ was seen at locations greater than 250μm from the soma.

A similar study by Spruston et al. (1995), but using dual soma/dendritic recordings instead of Na^+-sensitive dye, also concluded that $[Ca^{2+}]$ changes in the dendritic tree were strongly correlated with dendritic action potentials. Single action potentials evoked an average 60nM increase in $[Ca^{2+}]$, roughly independent of location up to 400μm from the soma. Trains of action potentials, however, resulted in a peak $[Ca^{2+}]$ that fell roughly exponentially moving away from the soma, with a space constant of 200μm. This fall-off was mirrored by the progressive attenuation of dendritic spike trains. The particular $[Ca^{2+}]$ profile during sustained activity was spatially heterogenous, in that adjacent dendritic branches could have quite different profiles.

In experiments with neocortical pyramidal cells, Schiller et al. (1995) reported qualitatively similar results to Spruston et al. (1995), with respect to the maximum changes of $[Ca^{2+}]$ per spike. In this case, the

involvement of dendritic Na^+ spikes was inferred by the marked reduction of dendritic $[Ca^{2+}]$ changes when somatic spike voltage clamp waveforms were imposed under TTX. The primary difference between the results for cortical pyramidal cells and HPCs is in the pattern of $[Ca^{2+}]$: in Schiller et al. as a first approximation $[Ca^{2+}]$ increased with electrotonic distance from the soma, whereas in HPCs there is either little dependence on location (Spruston et al., 1995) or peak concentrations within 100μm from the soma (Jaffe et al., 1992). Possibly these differences could be most simply explained by differences in the dendritic distribution of voltage-gated Ca^{2+} channels of the each cell type.

The paper by Christie et al. (1995) described the contribution of specific Ca^{2+} channel types in HPCs on $[Ca^{2+}]$, as a function of location, by measuring the effect of specific Ca^{2+} channel blockers on spike-evoked $[Ca^{2+}]$. Transients were measured in response to trains of 15 spikes. Under control conditions the peak concentrations ranged from 170nM at the soma (11nM/spike) to 235nM in the proximal 50μm of the apical dendrite (16nM/spike), with intermediate values up to 200μm along the apical dendrite. The time constant of decay of $[Ca^{2+}]$ in the figures from this paper show values ranging from about 2 seconds at the soma down to about 500 milliseconds 200μm from the soma. This study inferred that high-threshold Ca^{2+} channels (N-, P-, Q-, and L-type, see Section 11.1) were concentrated at the soma, with the low-threshold T-types distributed on the apical dendrite.

9.2 Determinants of the Resting $[Ca^{2+}]_{in}$

The resting level for $[Ca^{2+}]_{in}$ is generally estimated at around 50nM, and in all models that we have examined this value is taken as a constant. An implicit justification for this may be that the resting value reflects an equilibrium state of the various buffering, extrusion and internal Ca^{2+} store mechanisms that regulate $[Ca^{2+}]_{in}$, under the assumption that there is no current through voltage-dependent Ca^{2+} channels at rest.

However, a recent report by Magee et al. (1996) showed that dihydropyridine blocked a hyperpolarization-induced reduction in $[Ca^{2+}]_{in}$, suggesting that Ca^{2+} channels may be a major factor influencing the resting $[Ca^{2+}]_{in}$. They propose that under physiological conditions, the L-type Ca^{2+} channel (normally high-voltage activated, Section 11.1), which is blocked by dihydropyridines, can start activating at potentials as low as -70mV, and thus contribute to the resting $[Ca^{2+}]_{in}$. The paper pointed out that this would provide a direct link between past voltage activity in the cell and the resting $[Ca^{2+}]_{in}$.

In the Working model simulations are run with a starting value of 50nM in all the Ca^{2+} compartments. However, the "true" resting value for $[Ca^{2+}]_{in}$ when the system is allowed to settle over about 20 seconds is slightly higher (about 65nM), due to a small activation of I_{CaT}, as mentioned earlier.

9.3 Considering Intracellular Ca^{2+} Stores

The model of Schiegg et al. (1995) focused on how $[Ca^{2+}]_{in}$ dynamics may be affected by Ca^{2+}-release from intracellular Ca^{2+} stores. Specifically, they proposed that such release was necessary to account for a one to two second elevation of $[Ca^{2+}]_{in}$ that is crucial for the induction of LTP (Malenka et al., 1992). In the structure of their model the Ca^{2+} store had apparently little effect on overall cellular $[Ca^{2+}]_{in}$ profile, since the store was only in a single spine head compartment, and the $[Ca^{2+}]_{in}$ "tail" in the spine head due to release from the store was less than 10% of the peak $[Ca^{2+}]_{in}$ in this compartment. Although we shall not consider this further in this chapter, it may be of interest to examine the effect of similar models of Ca^{2+} stores on $[Ca^{2+}]_{in}$ dynamics in the soma and dendrites.

9.4 Membrane Pumps

Important components for the maintenance of ion gradients include electrogenic membrane-bound pumps that transport Ca^{2+}, K^+ and Na^+ against their respective concentration gradients (Läuger, 1991).

9.4.1 The Sodium Pump

Sodium and potassium gradients are maintained by a pump driven by Na,K-ATPase that is typically referred to as the "sodium pump" (Rose and Ransom, 1997; for a recent review see Glynn 1993). The sodium pump extrudes three Na^+ ions for every two K^+ ions that are brought inside the cell, thus generating a net outward current.

Thompson and Prince (1986) showed that after prolonged depolarizations induced by focal application of glutamate (which results in high intracellular Na^+ accumulation), the current generated by this pump can be large enough (on the order of a few hundred pA) to significantly hyperpolarize the cell. Thus

in principle the sodium pump contributes to the electrical stability of the cell both by maintaining ionic gradients and by direct electrical action. The functional importance of the Na,K-ATPase pump has been suggested, for example, with respect to abnormal firing characteristics in epileptic hippocampus (Haglund and Schwartzkroin, 1990, Fukuda and Prince, 1992, Anderson et al., 1994) and bipolar illness (el-Mallakh and Wyatt, 1995).

A literature search failed to locate neuron models with explicit descriptions of the sodium pump; modelling this mechanism to date appears to be limited to isolated membrane systems, myocytes or oocytes (e.g. Sagar and Rakowski, 1994). In the Working model we neglect the sodium pump since the focus is on current-evoked responses, and we assume that changes in $[Na^+]_i$ are small under these conditions.

9.4.2 Ca^{2+} Pumps, and Models of Ca^{2+} Removal

Any model of $[Ca^{2+}]$ must take into account not only the influx of Ca^{2+}, but also some mechanism for the removal of Ca^{2+}. The simplest method is to include a steady-state term in the differential equation(s) describing $[Ca^{2+}]$. In the general case this value is associated with a second parameter corresponding to the time constant for concentration decay. The BG87, Traub91, Traub94 and Warman94 models used this type of description (see also Huguenard and McCormick, 1992, thalamic relay neurons).

More explicit models of Ca^{2+} removal includes mechanisms such as membrane-bound pumps. The spine model by Zador et al. (1990) included two pumps with Michaelis-Menton kinetics: one high-affinity, low-capacity, corresponding to a CaATPase-driven mechanism, and the other low-affinity, high-capacity, corresponding to a Ca^{2+}/Na^+ exchange mechanism (see also Yamada et al., 1989). These pumps were treated as a separate currents in the $[Ca^{2+}]$ differential equation. The parameters of this model were adapted in the model of Schiegg et al. (1995). The Jaffe94 model included a similar mechanism, but with a single pump. The major constraints for the pump parameters in this model was a $[Ca^{2+}]_{in}$ decay time constant of about 600 milliseconds in the proximal apical dendrites, and the parameters for the buffer (see below).

The Migliore95 model incorporated a pump which bound to intra and extracellular Ca^{2+} with various rate constants - these reactions were solved simultaneously with another binding reaction between $[Ca^{2+}]_{in}$ and a buffer.

9.4.3 Pump Model for the Working Model

For the removal of intracellular Ca^{2+} in the Working model, we shall adapt the Michaelis-Menton mechanism used by the Jaffe94 model:

$$J_{Ca^{2+}} = V_{max}\frac{[Ca^{2+}]_{in}}{K_d + [Ca^{2+}]_{in}} - J_{leak}$$

where $J_{Ca^{2+}}$ is the removal rate of Ca^{2+} per unit area, V_{max} is the maximum flux rate per unit area, K_d is the half-maximal $[Ca^{2+}]_{in}$, and J_{leak} compensates for the resting pump rate. The parameters for the Working model are:

$$V_{Max} = 6 \times 10^{-11} mM ms^{-1} cm^{-2}$$
$$K_d = 0.01 mM$$

with J_{leak} adjusted so that there is no net pump current at rest, assuming no resting activation of Ca^{2+} channels (however, there is evidence for such resting activation - as mentioned in Section 9.2 - and in the Working model there is a very slight activation of I_{CaT} at the usual holding potential of -65mV). This pump is associated with the membrane assigned to the second juxtamembrane compartment described in Section 9.7 - this is essentially equivalent to the entire surface area of an anatomical compartment. We ignore any electrogenic component of the Ca^{2+} pump.

9.5 Buffer Models

Endogenous intracellular Ca^{2+} buffers have a strong effect on the free $[Ca^{2+}]_{in}$. Cell models that consider Ca^{2+} dynamics have incorporated buffer mechanisms of varying complexities, including solving the dynamical equations for the buffer-Ca^{2+} reaction during the course of the simulation (e.g. the Migliore95 model, and the models of Zador et al. 1990 and Schiegg et al. 1995; also see Yamada et al., 1989).

Neither the Traub91 and Traub94 models, which treated $[Ca^{2+}]_{in}$ as a dimensionless variable, nor the BG87 and Warman94 models, which were in principle quantitative with respect to $[Ca^{2+}]_{in}$, include buffer mechanisms. None of these four models attempted to replicate the data for $[Ca^{2+}]_{in}$; the key functional parameters that "replaced" a buffering mechanism are found in the Ca^{2+} sensitivities of their Ca^{2+}-dependent K^+ channels.

9.5.1 Instantaneous Buffer Model

A simple way to treat intracellular buffering of Ca^{2+} is to assume a non-saturated buffer (i.e. $[Bu] >> [Ca^{2+}]_{in}$, where $[Bu]$ is the concentration of buffer binding sites) with instantaneous kinetics (e.g. the Jaffe94 model; also Stockbridge and Moore, 1984, model of frog neuromuscular junction).

The key parameter, β_{Bu}, in this mechanism equals the ratio of the concentration of bound Ca^{2+} and free Ca^{2+}:

$$\beta_{Bu} = \frac{[Ca^{2+}]^{bound}}{[Ca^{2+}]^{free}}$$

Thus, this mechanism implies that the predicted *measured* $[Ca^{2+}]$ is equal to the total $[Ca^{2+}]$ divided by $(\beta_{Bu} + 1)$. For non-diffusional models of $[Ca^{2+}]$, e.g. where there is one Ca^{2+} compartment per electrical compartment (see below in Section 9.6), this is the only role of the instantaneous buffer. For multiple compartment systems, the effective diffusion constant D' applied to the difference in total $[Ca^{2+}]$ between compartments must also be adjusted to take into account the instantaneous buffer, by setting D' equal to $D/(\beta_{Bu}+1)$, where D is the diffusion constant for the free ion. A variation on this scheme would be to assume that β_{Bu} is a function of each compartment; in this case the diffusion equation between compartments would reference the original D, with the concentration difference between any two compartments determined by the difference of the total concentrations, weighted by the appropriate β_{Bu}s.

What are reasonable values for β_{Bu}? We can start with an estimate of total buffer that is primarily calmodulin, with a concentration of 30 μM (Schiegg et al., 1995). Calmodulin binds four Ca^{2+} ions independently; thus the effective buffer concentration, $[Bu]$, becomes 120μM. The dissociation constant of each calmodulin binding site is estimated at 1μM (Schiegg et al., 1995). Thus:

$$[Ca^{2+}]^{free} + [Bu]^{free} \rightleftharpoons [Ca^{2+}]^{bound}, \quad K_d = 1\mu M$$

and, assuming that the change in $[Bu]$ from the binding reaction is negligble:

$$K_d = \frac{[Ca^{2+}]^{free}\ [Bu]}{[Ca^{2+}]^{bound}}$$

$$\beta_{Bu} = \frac{[Ca^{2+}]^{bound}}{[Ca^{2+}]^{free}} = \frac{[Bu]}{K_d}$$

$$\beta_{Bu} = \frac{120\mu M}{1\mu M} = 120$$

We note that the Jaffe94 model tested a range of 100 to 1000 for the values of β_{Bu}, with 1000 used for the simulations shown in the paper. These values can be compared to the range of 20 to 600 for β_{Bu} in a model of the frog neuromuscular junction (Stockbridge and Moore, 1984). In the Working model we use a somewhat low value of β_{Bu} equal to 20; this was necessary to generate reasonable (about 10nM) incremental changes of $[Ca^{2+}]_{in}$ per spike.

9.6 Models of Ca^{2+} Diffusion

At a minimum, models for Ca^{2+} concentration dynamics assign one compartment for integrating $[Ca^{2+}]$ per electrical compartment (e.g. the Traub91, Traub94 and Jaffe94 models). However, studying the implications of non-uniform local $[Ca^{2+}]_{in}$ as well as better approximations for diffusional equilibrium require more than a single compartment. The BG87 model used two juxtamembrane shells (one of which was subject to Ca^{2+} current influx), coupled with a constant concentration core compartment. Diffusional flow was considered between all three compartments; a similar model is discussed below in Section 9.7. Two uncoupled "partial" shells were used in the Warman94 model as an approximation of the BG87 model structure. In the Migliore95 model, each somatic/dendritic electrical compartment was divided into four concentric subshell diffusion

compartments, as supplied in NEURON. Finally, separate compartments for the spine neck and head were used by Zador et al. (1990); six diffusion compartments were assigned to the spine neck and head in Schiegg et al. (1995).

It remains to be seen if accounting for any *lateral* or longitudinal diffusion of Ca^{2+} along a dendritic process is important. For example, this could be especially relevant in understanding mechanisms for heterosynaptic plasticity. Preliminary indications that such diffusion is in fact not significant to account for overall changes in internal Ca^{2+} has been mentioned in some studies (e.g. Migliore et al., 1995), but systematic analysis of this question is still lacking.

9.7 The $[Ca^{2+}]_{in}$ System in the Working Model

The primary behaviour that we wish to capture in this model includes:

1. Profiles of locally averaged $[Ca^{2+}]_{in}$ in response to somatic current stimulation and at rest.
2. Differential and localized $[Ca^{2+}]_{in}$ profiles appropriate for the activation of I_{CT} and I_{AHP}.
3. Changes in $[Ca^{2+}]_{in}$ as seen by Ca^{2+} channels consistent with estimated currents from these channels.

9.7.1 A Multi-Compartment Ca^{2+} System with Instantaneous Buffer

We shall use a three compartment model to represent the internal Ca^{2+} dynamics in any anatomical (electrical) compartment (i.e. soma or dendritic segment) that includes Ca^{2+} channels, although in the version presented here only the soma has any channels. There is no Ca^{2+} diffusion between anatomical compartments. This model is designed to be intermediate in detail, based on quantitative estimates of the various parameters in a relatively simple geometry, that can be readily extended for more sophisticated schemes.

This model assumes that a juxtamembrane shell with thickness r_{shell} is split up into two diffusional compartments, with compartment 1 corresponding to a collection of "islands" or domains associated with co-localized Ca^{2+} channels and I_{CT}, that occupy some fraction α_1 of the cell element surface (Borg-Graham, 1987). The remaining fraction $1-\alpha_1$ of the juxtamembrane shell is assigned to compartment 2. If the surface area of the cell element is A_{total} (this definition approximates the actual area of the inside surface of the shell), then the volumes of compartments 1 and 2 (V_1 and V_2, respectively) are given by:

$$V_1 = \alpha_1 \times A_{total} \times r_{shell}$$

$$V_2 = (1 - \alpha_1) \times A_{total} \times r_{shell}$$

The volume of the inner compartment 3 is taken as the remainder of the cell element volume.

For simplicity, diffusional flow is considered only between compartments 1 and 2, and between compartments 2 and 3. A relatively simple way to assign the diffusional parameters describing Ca^{2+} flux between the islands assigned to compartment 1 and the surrounding shell compartment 2 is by using a free parameter $\alpha_{1:2}$, which is an interdigitation coefficient (in units of 1/distance). Thus the effective diffusional area $A_{1:2}$ between compartments 1 and 2 is given by:

$$A_{1:2} = \alpha_{1:2} \times A_{total} \times r_{shell}$$

In the present version of the Working model, $\alpha_{1:2}$ is set to 1. The diffusional area between compartments 2 and 3 is given by:

$$A_{2:3} = (1 - \alpha_1) \times A_{total}$$

Diffusional flux between the compartments is then given by the standard Fick's relationship, using a diffusion coefficient for Ca^{2+} of $8 \times 10^{-6} cm^2 sec^{-1}$ (25°C, Hille, 1992). As stated, instantaneous buffering with a $\beta_{Bu} = 20$ is assumed for all compartments.

The thickness r_{shell} of the juxta-membrane shell is 1μm. The value for α_1 is 0.001%: this represents a limiting value since smaller values give essentially the same peak transients of $[Ca^{2+}]$ in compartment 1. The profile of the concentration transient in this compartment is shown in Figure 7, and the change in concentration averaged over the entire soma compartment during a spike train is seen in Figure 15. The motivation for the two juxtamembrane compartments, which is solely concerned with the Ca^{2+}-dependence of I_{CT} and I_{AHP}, is discussed in Section 12.6.

Finally, as mentioned previously, the Ca^{2+} pump efflux is computed according to the surface area of compartment 2. Since α_1 is very small, this area represents practically the entire membrane of the anatomical (in this case somatic) compartment.

9.7.2 Consequences of the Soma/Short-Cable Model: Adjusting Ca^{2+} Channel Current Influx For $[Ca^{2+}]$ Integration

Placing all Ca^{2+} (or other type) channels at the soma in a soma/short-cable approximation may give a reasonable first estimation as to the *electrical* image (more so under current clamp) from the soma of channels that are in reality distributed throughout the dendritic tree. However, the concentration profile elicited by the "unnatural" concentration of Ca^{2+} channels could be overestimated, all other factors being equal (e.g. distribution of buffer and pump mechanisms). Thus, we introduce an additional parameter δ, which is a scaling coefficient, less than 1, for the Ca^{2+} influx from the integrated Ca^{2+} current. As a first approximation, δ is estimated by the ratio of the actual somatic conductance of a channel divided by the total conductance of the channel for the entire cell.

Here we will make the following approximation: we assume that in reality all Ca^{2+} channels have a constant membrane density over the soma and the proximal 200μm of apical dendrite (referring to the soma/short-cable geometry). The coefficient δ is then given by the ratio of somatic area divided by the sum of the total Ca^{2+} channel membrane area. If the soma diameter is 35μm and the dendrite diameter is 12μm, this sets δ to be about 1/3. Note that this value is probably a high estimate, since Ca^{2+} channels may be more spread out throughout the dendritic tree.

Non-Synaptic Channels of Hippocampal Pyramidal Cells

We shall now review the non-synaptic channels that have been characterized in HPCs, with the goal of building a link between the main experimental findings and model descriptions for the more prominent channels. The discussions will also mention some of the major pharmacological and neuromodulator susceptibilities for each channel type. These presentations are not exhaustive - more complete reviews of membrane currents and their functional roles include Rudy (1988), Adams and Galvan (1986), Storm (1990) and Brown et al. (1990), with the latter three focusing on hippocampus.

The sections on sodium and calcium channels will describe properties of the various types as a group, whereas potassium and the non-specific cation channels will be described individually by type. The channels that are included in the Working model are summarized in Table 4. The model parameters for these channels and their associated gating particles are listed in Tables 5 through 8.

10 HPC Sodium Channels

Probably the choice of kinetic description for the sodium current generating the spike is the most problematic component of a neuron model, essentially because these channels underly the fundamental instability of the membrane. Much progress has occured in the measurement of microscopic and macroscopic sodium currents, and in the theory of individual channel biophysics. However, the interpretation of this data for macroscopic models remains at an early stage.

The question remains as to what kinetic model is appropriate for a macroscopic model, e.g. the traditional Hodgkin-Huxley type or the more biophysically accurate Markovian description. Kinetic subtleties which may not be functionally important for other channels may have an important effect in the case of descriptions I_{Na}, simply because I_{Na} is by far the largest and fastest membrane current. Thus, conflicts arise when trying to simultaneously construct a model for I_{Na} that accounts for the more dramatic roles, but at the same time does not intrude *sotto voce* during other phases of firing behaviour.

The original parameters of Hodgkin-Huxley squid I_{Na} have been applied to recent models of mammalian neurons (e.g. the Jaffe94 model), which at best can be justified in that these parameters are well known and certainly will generate basic spiking behaviour. For more detailed replication of firing properties, however, these parameters are likely to be inappropriate, and I_{Na} channel data from more relevant preparations must be considered.

10.1 Electrophysiology of Sodium Channels in Mammalian Central Neurons

Over the past several years, there have been various reports documenting voltage clamp measurements of sodium currents and single channels from cortical and non-cortical mammalian cells (e.g. Sah et al., 1988b, French et al., 1990, Steinhäuser et al., 1990, Ogata and Tatebayashi, 1990, Cummins et al., 1994). Evidence for the functional role of dendritic I_{Na} was reported as early as Wong et al. (1979). Magee and Johnston (1995) measured single TTX-sensitive Na^+ channels in the apical dendrites of HPC CA1 neurons that had an activation threshold around -60mV. On the other hand, Masukawa et al. (1991) reported that a fast, inactivating TTX-sensitive inward current was consistently localized at the soma as compared to the dendrites in cultured hippocampal neurons.

10.1.1 Interpretations Based on the Sah et al. 1988b Data

One of the more influential papers is the one by Sah et al., (1988b), both because it was one of the first to do a quantitative voltage clamp study on I_{Na} in hippocampal (dissociated) neurons, and, indirectly, because of the reference to this paper by various cell models. However, the interpretations of Sah et al. have often been inconsistent with or strongly modified from the original paper.

For example, Brown et al. (1990) describe the voltage-dependency of I_{Na} by (implicitly) referencing data from a single cell shown in a figure from Sah et al. (Figure 10 of Sah et al., 1988b) whose characteristics are significantly different from the pooled analysis in Sah et al., in particular with respect to the slope and position of the steady-state activation and inactivation curves. That the properties suggested by the figure are more consistent with that expected from current clamp behavior of I_{Na} may have contributed to the discrepancy being overlooked by these and other authors.

The interpretation of the Sah et al. data by Traub et al. (1991, 1994) in turn has been used in models such as the Wathey92 and Migliore95 models, the HPC model of Pongracz et al. (1992) and, for example, in models of cortical pyramidal cells (Rhodes and Gray, 1994), and of thalamic reticular neurons (Destexhe et al., 1995). In their model of I_{Na}, Traub et al. increased the rate constants given in the Sah et al. data by a factor of about five to generate a spike upstroke dV/dt that was at least 100mV/ms. This model also included a rightward shift in inactivation kinetics (moving the steady-state curve to more depolarized levels) that was justified assuming a temperature of 32°C for the model, and considering the temperature of the experimental data (22°C). Although not discussed in the text, the inactivation characteristic was also much steeper than that shown in Sah et al.. Taken together, these changes result in a large overlap between activation and inactivation in the model. Also this shift would suggest that at the lower temperatures the spike would have a higher threshold, which is consistent with the report of Thompson et al. (1985, see Table 2). The Warman94 model also used modified Sah et al. (1988b) parameters, compensating for the higher temperature of the model simulations as compared to the data by a similar shift in kinetics as Traub et al., and speeding the time constants by a factor of three on the basis of an assumed Q_{10} of 2. Unlike Traub et al., the precise adaptation of the Sah et al. data in the Warman94 model was constrained by matching spike threshold and reduction of spike amplitude during spike trains to data and, significantly, avoiding intrinsic bursting by an over-excitable I_{Na}.

10.1.2 I_{Na} Modulation

$I_{Na}$is susceptible to a muscarinic downregulation of the peak current and a slowing of inactivation (Cantrell et al., 1996), acting via a protein kinase C pathway.

Cultured fetal hippocampal neurons in a mouse model of Down's syndrome (Galdzicki et al., 1993) have about 25% less sodium current (and a 20% slower action potential rise time) than control. It remains to be seen if this subtle difference in basic action potential properties can be linked to the cognitive deficit in Down's syndrome.

10.1.3 I_{Na} - Fast, Slow, Persistent Components?

A persistent, TTX-sensitive Na^+ current, I_{NaP}, has been characterized in HPCs (French and Gage, 1982, French et al., 1990). Other reports of slow or persistent I_{Na} currents include TTX-insensitive Na^+ currents (Hoehn et al., 1993, striatum and HPCs; Deisz, 1996, neocortex). In addition, MacVicar (1985) reported a subthreshold TTX-sensitive Na^+ current that contributed to the prepotentials described by Lanthorn et al. (1984).

As discussed in the recent review by Crill (1996), it is not altogether clear if in fact there is either a distinct channel underlying I_{NaP}, if I_{NaP} is a window current of the transient I_{Na} (see below), or finally if the persistent current arises from a non-inactivating state of normally transient I_{Na} channels (Alzheimer et al., 1993). Azouz et al. (1996) argued for a distinct I_{NaP} versus an I_{Na} window current since they found a different sensitivity of TTX between the active, Na^+-mediated ADP and the spike.

For the present discussion we will assume that whatever the actual source for the persistent Na^+ current, the data of French et al. (1990) set the size and range of activation for this component. We suggest that this report may be a more reliable quantitative reference than the reports of the fast I_{Na}, such as Sah et al. data, since the French et al. data was taken from both the intact slice and disassociated cell preparation (with comparable results), and the slow kinetics of the current makes for a more accurate measurement.

10.1.4 Stability and the "Window Current"

Steady state rectification of nominally transient currents, in the context of the Hodgkin-Huxley description, is due to an overlap of the activation and inactivation steady-state curves. This rectification, also known as the window current, is kinetically indistinguishable from an independent persistent, or non-inactivating current. In the case of I_{Na} (and possibly other transient channels), the window current may have an influence on the stability of the resting potential.

The data for a persistent Na^+ current sets an upper bound on any true window current of a transient I_{Na}, which, in the context of the Hodgkin-Huxley model, sets a limit as to the closest possible positions of the activation and inactivation curves. However, postulating a window current based on voltage clamp measurements of steady-state activation and inactivation curves is based on the assumption of the simple Hodgkin-Huxley model. Since evidence for this model has been increasingly put into doubt by detailed analysis of I_{Na} gating kinetics (Armstrong, 1981), this means that the interpretation of the Hodgkin-Huxley window current is problematic. As we shall see below (Section 10.2), most descriptions of I_{Na} in published cell models include a very large window current that is at variance with whole cell voltage clamp data (Sah et al., 1988b). Since in these models the window current has a profound effect on firing properties, it is necessary to consider kinetic schemes which follow the experimental data more faithfully. Apropos to this, a recent detailed model of Purkinje cells included a Hodgkin-Huxley form of the fast Na^+ current, and the potential error associated with the window current in their formulation was discussed (De Schutter and Bower, 1994).

The report on Na^+-dependent plateau potentials by Fraser and MacVicar (1996, Section 6.4.5) would seem to be evidence for a substantial I_{Na} window current, at least under cholinergic stimulation. On the other hand this phenomena was not blocked by TTX, and therefore probably does not arise from the classical Na^+ spike channel.

10.1.5 Na^+-only Spikes

The dynamic contribution of a putative Na^+ window current can be assessed in experiments in which all Ca^{2+} and K^+ currents are blocked (CsCl filled sharp electrode with extracellular TEA, 4-AP, and Mn^{2+}). In this situation single action potentials may be elicited by current pulses in HPCs which repolarize slowly back to the resting potential (Storm, unpublished data, shown in Borg-Graham, 1987a).[11] This behavior is further evidence against a large steady-state rectification. Long current steps under the same conditions can generate Na^+-only repetitive firing (*ibid.*), which adds additional constraints on the kinetics of recovery from inactivation. The two Hodgkin-Huxley type I_{Na} models in the BG87 model were developed specifically to reproduce this behaviour - in this model repetitive firing of Na^+-only spikes required a very delicate adjustment of the inactivation kinetics of the higher threshold current.

10.1.6 The Sub-threshold/Threshold Regime

Another important functional characteristic of I_{Na} kinetics concerns the sharpness of the threshold. For example, Storm (1987a) shows several protocols in which short pulses were adjusted to elicit just-threshold responses - in particular, the associated subthreshold responses were almost passive (though this is not always the case, for example see the quasi-active subthreshold "ADPs" of Jensen et al., 1994).

[11] In figure 12 of Storm, 1987a, this condition is approximated, showing that Na^+ spikes can eventually repolarize without active K^+ currents.

10.1.7 Relating I_{Na} Kinetics to Spike Properties and the PHP

The relationship between the resting potential, the initial and later spike thresholds during repetitive firing, and the depth of the interspike repolarizations (the PHP), also provide constraints on the activation and inactivation curves of the Hodgkin-Huxley model.

The assumption of a nominal value of the resting potential of -65mV and an initial spike threshold of -55mV puts a lower bound (corresponding to unchanging inactivation during the spike initiation phase) on the product of the inactivation curve at rest and the maximum conductance of the channel, since this value is directly related to the slope of the spike upstroke. Likewise, the spike threshold places the foot of the activation curve within a few millivolts of -55mV, and the change in voltage trajectory during the approach to threshold and beyond depends strongly on the steepness of the voltage dependency of activation.

The PHP constrains the parameters of the inactivation process during repetitive firing in that inactivation must be fairly well removed by the PHP, essentially because spike amplitude is well maintained throughout the train, at least at 37°C (Thompson et al., 1985). As mentioned earlier, a more sensitive measure of the I_{Na} magnitude would be the dV/dt of the later spikes, but this data is not readily available. In other words, spikes during a train require a substantial de-inactivation which, in the context of the preceeding spike, can result from a combination of incomplete inactivation and/or sufficient recovery from inactivation during the repolarizing phase. Thus the relationship between the PHP and the threshold is directly related to the kinetics of repetitive firing, and reflects limitations imposed on the firing by the interelationship of the repolarizing currents and the recovery kinetics of I_{Na}.

While the large PHP in non-pyramidal cells (or more generally, non-spiny hippocampal cells, Scharfman, 1993) may seem to relax the restrictions on the relative positions of inactivation/activation voltage dependencies, in fact in many of these cells the final approach to the sharp threshold, lasting tens of milliseconds, can be quite shallow. If we assume a Hodgkin-Huxley mechanism, then this loitering near threshold also puts a constraint on the steady-state voltage dependence of inactivation, in that if there is little overlap in the activation and inactivation steady-state curves, then this timecourse would tend to inactivate the I_{Na} channels before the spike. This supports the coupling of inactivation and activation, contrary to the Hodgkin-Huxley model (Armstrong, 1981, Patlak, 1991).

Finally, simulations (not shown) suggest that a model with stationary Boltzman-type kinetics that have a voltage-dependence which is not arbitrarily steep must show a non-zero depolarizing phase prior to threshold. On the other hand, the trajectories of some intra-burst spikes (which essentially have a zero PHP) suggest that spikes can arise abruptly from a *downward* moving voltage. At the moment we shall leave this as an unaddressed issue, other than to mention that this characteristic might be evidence for a non-somatic source of the fast spike during bursting, e.g. from the axon.

10.2 Comparison of I_{Na} Models from the Literature

We shall now discuss the various forms of I_{Na} models that have been proposed, both in the context of cell models, and in the context of single channel kinetic models.

10.2.1 Hodgkin-Huxley Type I_{Na} Models

We have mentioned several cell models that adapt the Hodgkin-Huxley squid axon formula for I_{Na} to match the data from more relevant preparations. In Figure 8 representative voltage clamp protocols are used to compare the kinetics and steady-state properties of some of these models with each other and the canonical Hodgkin-Huxley I_{Na} parameters. We also include the model of I_{Na} used by McCormick and Huguenard (1992) in their model of thalamic relay cells, which was adapted from I_{Na} measurements in cortical pyramidal cells (Huguenard et al., 1988). As described in the figure, the maximum conductance of each model was adjusted so that they would give approximately the same spike current. Although this results in a relatively crude quantitative comparison (since there was not a detailed fitting of this parameter), it is clear from the figure that the various I_{Na} models, although all adjusted to do more or less the same thing, have a wide range of kinetic and steady-state properties. The implications of these differences are seen in close examination of not only the individual spike properties of the various models, but also the variation in repetitive or bursting characteristics.

10.2.2 A Model with Multiple Hodgkin-Huxley Type I_{Na} Channels

As mentioned, another approach is to reconstruct the observed I_{Na} behavior with more than one Hodgkin-Huxley type model (Borg-Graham, 1987b), each with relatively non-overlapping activation and inactivation curves in order to limit Na^+ steady-state rectification. Note that this latter approach can be reduced to an equivalent single Markov model (Destexhe et al., 1994); an advantage with the separate channels is that it may be easier to do an initial map of desired kinetic characteristics to this form of an I_{Na} model than to determine an appropriate Markov form. On the other hand, as mentioned previously, there is no data to support these distinct channels.

10.2.3 Evaluating Published Markovian Kinetic Models

Markov-type models with complex state descriptions may offer a solution to the constraints that we have discussed for which the standard Hodgkin-Huxley approach cannot match (Kuo and Bean, 1994 from hippocampus; Vandenberg and Bezanilla, 1991 and Patlak, 1991 from squid axon).

However, simulations (not shown) of the model described by Kuo and Bean (1994), with modifications limited to a shifting of the voltage-dependent rate constants by 20mV in the hyperpolarizing direction (consistent with the authors' comment regarding the expected shift in voltage dependence for their whole-cell recordings) generated a spike with a shallow threshold, slow inactivation, and a significant steady state rectification starting around the resting potential and peaking on the order of 0.5 to 1nA. It may be expected that the kinetic details for suprathreshold voltages may not be well characterized by this report, since the model predictions were based on quantitative measurements at relatively hyperpolarized levels.

10.3 An *ad hoc* Markovian Model

In this section we propose a new Markovian model for I_{Na} in the Working model. The state diagram for the general framework of the model and the specific simple version used for simulations are shown in Figure 9, where the arrowheads correspond to the predominant transitions. The basic constraints for the model are the absolute spike thresholds taken from the relationships between spike threshold and PHPs, the generation of spikes of similar amplitude to the initial spike during spike trains, and the stability of resting potential. In particular, the version of the model that we demonstrate shows a sharp threshold over a 5 to 10 mV range, depending on the recent history of the channel, and the ability to recover from inactivation during repolarizations positive to earlier thresholds, without a large window current. This model is less constrained from the single channel data available to date, other than inactivation is voltage-independent and coupled to activation (Armstrong, 1981, Patlak, 1991, Kuo and Bean, 1994); it remains to be shown that the kinetic scheme described here can be reconciled with the experiments.

10.3.1 A Variable Threshold Without A Large Window Current

The most important idea of this model is that the available threshold depends on the history of firing, shifting down during the course of spike repolarization *without* giving a strong window current.

Crucially, inactivation occurs after the open state - this process is not decoupled from activation as in the Hodgkin-Huxley model. After reaching the open state (i.e. the spike) and inactivating, the channel passes through a series of closed states each of which offers a path to the open state at progressively more hyperpolarized thresholds. The effective removal of inactivation is determined by the voltage dependence of the path from the inactivated state to the chain of closed states. Steady state rectification is avoided by requiring that the transition *into* a given closed state occurs at a voltage range that is hyperpolarized relative to the closed to open transition for that state.

Thus the threshold of the closed to open transition ($C_1 \rightarrow O$) from the first closed state reached after inactivation determines the most depolarized threshold of the channel, and the necessary PHP for this firing transition is determined by the voltage dependence of the inactivated to first closed state transition ($I \rightarrow C_1$). Likewise, the threshold to the open state from the final, most hyperpolarized closed state ($C_N \rightarrow O$) determines the lowest threshold of the channel. The specific closed to open transition that is dominant for a subsequent spike depends on the strength of the repolarizing mechanisms (e.g. K^+ currents) and the stimulus current.

Figure 10 illustrates the voltage dependencies of the major state transitions in the simple four state version of the model, as set by the parameters listed in Table 6. Note that the two closed state to open state transitions correspond to the range of thresholds in the model, and the lack of overlap for the respective

rates into the closed states avoids significant steady-state activation. In contrast, measurements of steady-state activation and inactivation kinetics using standard voltage clamp protocols (activations measured as peak currents at various potentials from a holding potential of -100mV and inactivations measured as peak currents after a step to -20mV from various holding potentials) predict a large (and probably overestimated) overlap in the "Hodgkin-Huxley " interpretation.

10.3.2 Accounting for the Persistent Na^+ Current

This model can account in part for a persistent component of I_{Na} simply by adding a small voltage-independent rate term to the appropriate paths into the closed states (the α_0 term in Equation 4 and given in Table 6, analagous to the α_0 and β_0 terms described in Section 8.4.2). The effect of these terms is kinetically similar to the overlap of the inactivation and activation curves of the Hodgkin-Huxley model, e.g. a window current, with the important difference that the rectification is not limited for voltages higher than the threshold. The resulting rectification, the amplitude of which is related to the relative values of α_0 and τ_0 used for the transition pairs $C_1 \rightarrow C_2$ and $C_2 \rightarrow O$, and $I \rightarrow C_1$ and $C_1 \rightarrow O$, respectively, is shown in Figure 10, and can be compared with the properties of the persistent Na^+ current described by French et al. (1990), shown in Figure 8. The major difference is in the threshold of the persistent component of I_{Na}, around -55mV, which is determined in this scheme by the threshold of the $C_2 \rightarrow O$ transition. In the data of French et al., I_{NaP} turns on at about -70mV, thus implicating a small, but possibly significant, substhreshold activation of this current. This characteristic will be considered in future refinements of the I_{Na} Markov model used here.

10.3.3 Shortcomings of the I_{Na} Model

As can be seen, the range of thresholds and associated necessary PHPs of this model is determined by the different closed to open state paths. In the version illustrated here, there are two such paths, spanning a voltage range of about five millivolts. The parameters for these transitions are chosen so that the lowest threshold is about -55mV, and the highest threshold is about -50mV. The associated paths *into* the closed states have thresholds of about -60mV and -55mV, respectively; the higher value corresponds to the minimum PHP required to reset the channel. This value is clearly too low to account for the resetting of I_{Na} between the spikes during a burst if we assume that the somatic voltage directly determines the kinetics of the fast spikes during the burst. In the context of this kinetic scheme the solution is to add more closed states that may be entered from progressively higher membrane potentials, as shown in Figure 9.

Also, in its present form this model has a steep voltage dependence of steady-state inactivation and a very large overlap in the measured activation and inactivation characteristics, as shown in Figure 9, both of which are inconsistent with published data. It may be possible to adjust these characteristics with some additional hyperpolarized closed states.

11 HPC Calcium Channels

In this section we review the various Ca^{2+} channels and related phenomenology for HPCs. As we have mentioned in earlier sections, our description of Ca^{2+} channels have to consider not only the charge contribution of Ca^{2+} currents, but also their effect on $[Ca^{2+}]$.

In the literature Ca^{2+} currents are often described in terms of conductance, e.g. an equivalent conductance density per unit area of membrane in a given preparation. Some references reference a permeability model explicitly (Section 8.2); for the model description that we use here all conductances are converted to permeability units, assuming some value for the voltage at which the conductance value was estimated.

11.1 T-, N-, R-, P-, Q- and/or L-type: How Many Ca^{2+} Channels Are There in HPCs?

Several subtypes of Ca^{2+} channels have been characterized in neurons, with the T- (LVA, small conductance, rapidly inactivating), N-, R-, and P- or Q- (HVA, rapidly inactivating), and L- (HVA, large conductance, slowly inactivating) types, as well as non-specified types, variously identified in HPCs from different studies. The nomenclature of LVA (for low-voltage-activated) and HVA (for high-voltage-activated) is commonly used in the Ca^{2+} channel literature; an early review of the variety of neuronal calcium channels can be found in Hagiwara and Byerly (1981). With respect to HPCs, the existence of specific Ca^{2+} channel types in these

cells is somewhat controversial (see discussion in Brown et al., 1990), with different reports claiming from one to five channel types.

11.2 Electrophysiology of Calcium Channels

In general, under control conditions Ca^{2+} currents are too small to significantly effect the voltage waveform, so that the functional significance for these currents is primarily via their effect on $[Ca^{2+}]_{in}$. Under non-control conditions, however, we can consider at least two electrical signatures of Ca^{2+} currents.

First, when Na^{+} channels are blocked calcium channels in HPCs (as with other neurons) have the necessary voltage-dependent kinetics and are sufficiently concentrated to generate Ca^{2+} spikes (e.g. Schwartzkroin and Slawsky, 1977). The amplitude of these spikes is greatly enhanced by blocking K^{+} repolarizing channels. As we have mentioned earlier, although the involvement of Ca^{2+} spikes has been classically implicated for burst generation (e.g. Wong and Prince, 1978), this assumption is open to question. Rather, the severely non-physiological conditions necessary for the observation of Ca^{2+} spikes suggest that this phenomena is restricted to the experimenter's dish, and may be used at least to help constrain the parameters for a model of Ca^{2+} channels.

The second electrical signature of Ca^{2+} channels occurs under conditions closer to control. Concentrations of TEA sufficient to block the large outward current I_C (see Section 12.4) may reveal a small Ca^{2+}-mediated shoulder on the repolarizing phase of single Na^{+} spikes (e.g. Storm 1987b). We may note that it is not clear from the literature whether, under control conditions, a similar shoulder component of the repolarizing phase exists for later spikes in a train, when I_C is probably much smaller than during the intial spike. On the other hand, the kinetics of other repolarizing currents may shift during repetitive firing, so the comparison may not be appropriate.

11.2.1 I_{Ca} Modulation

Doerner et al. (1990) investigated second messenger pathways that modulate Ca^{2+} currents in HPCs via PKC. Ca^{2+} channels may be modulated by adenosine (Madison et al., 1987); the various types of these channels have different pharmacological profiles (Nowycky et al., 1985).

11.2.2 Characteristics of Calcium Spikes

Segal and Barker (1986) looked at putative Ca^{2+}-mediated responses in cultured rat hippocampal cells under TTX and TEA (25mM), including recordings with and without 4-AP. Ca^{2+} spikes elicited with current steps had a threshold of about -30mV, and peaked around 10 to 20mV. Under voltage clamp I_{Ca} activated with a time constant of about 20ms at -20mV, with an extrapolated reversal potential of 10mV, similar to what is predicted by the GHK model. This study also identified a Ca^{2+}-dependent K^{+} current as "I_C", but since I_C is blocked by TEA, and the kinetics of the reported current were slow, it is more likely that this current was I_{AHP}.

The levels of TEA used in this study would also be expected to block I_M and I_{DR} as well as I_C (Storm 1990), thus the estimation of the size of the Ca^{2+} current during spikes needs to take into account the involvement of I_A. In this regard, Segal and Barker showed Ca^{2+} spikes without 4-AP had a duration of about 50 to 100ms; under 1mM 4-AP (which blocks I_A) the spikes developed a long slowly-decaying plateau that started at about 0mV, decaying to about -10mV over about 200 ms before a much more rapid return to rest. In addition, a direct facilitation of the Ca^{2+} current by 4-AP was also determined. This study did not find evidence for more than one Ca^{2+} current, e.g. a low-threshold transient current or persistent current.

Recordings of Ca^{2+}-mediated activity under Na^{+} and K^{+} blockers may also be seen in the paper by Fraser and MacVicar (1996) - amplitudes of slow Ca^{2+} spike were similar to that of Na^{+} spikes prior to addition of blockers. The Ca^{2+} spikes under these conditions repolarized faster than those shown in Segal and Barker, however the 10mM TEA used in this paper may have not blocked repolarizing K^{+} currents as efficiently as the 25mM TEA used by Segal and Barker.

11.2.3 Kinetics of Activation and Inactivation of Ca^{2+} Currents

A persistent slow inward calcium current was described by Johnston et al. (1980) and by Brown and Griffith (1983b), with characteristics of an L-type Ca^{2+} current.

Kay and Wong (1987) described the activation of a Ca^{2+} current in isolated CA1 HPCs, fitting the current to Hodgkin-Huxley type m^2 kinetics. In a later study using the same protocol, Kay (1991) described

the voltage and Ca^{2+}-dependent inactivation of this current. He argued for a single type of Ca^{2+} current in HPCs since the three kinetic components of inactivation (roughly a fast τ of about 200ms, a slower τ of about 2 seconds, and a constant component) varied in concert under various conditions, and activation kinetics had but a single component.[12]

Kay argued that the T current is not functionally present in CA1 cells.[13] A complex, and unspecified, interaction between voltage and Ca^{2+} entry through individual channels (a "domain" model) was proposed for the inactivation process (a theoretical analysis of this type of process was described by Sherman et al., 1990, for mouse pancreatic β cells).

On the other hand, Fisher et al. (1990) proposed that there are three distinct types of Ca^{2+} channels (T-, L-, and N-type) in both CA1 and CA3 HPCs (and dentate gyrus granule cells), based on cell-attached recordings in the exposed slice preparation, a preparation somewhat between slice and acutely isolated cells. This conclusion was reached primarily because the single channel conductances fell into three groups and there was a strong correlation between the channel conductances and voltage-dependent kinetics. The proposed T-type channel had a conductance of about 8pS, activated above -40mV (half-maximal activation at -18mV) and inactivated within 50 milliseconds at holding potentials of -10mV or more. Inactivation was much slower at smaller depolarizations. The proposed N-type channel had a conductance of about 14pS, activated above -25mV (half-maximal activation at 0mV), with inactivation described as "variable". Finally, an approximately 25pS channel was identified as an L-type Ca^{2+} channel. It activated at potentials greater than -10mV, and did not show inactivation.

Recently, Avery and Johnston (1996) reported that the LVA Ca^{2+} current in acutely isolated CA3 HPCs derives from both a transient T-type channel and a sustained Ca^{2+} channel. This second component was tentively identified as an L-type channel, despite its activation at potentials more negative than that typically associated with HVA Ca^{2+} channels.

Fisher et al. also reported that T-, L-, and N-type calcium channels were in CA1 and CA3 HPC dendrites, as well as on the soma (see below). Magee and Johnston (1995) examined single channels in the apical dendrites of CA1 HPCs, and described L-, T- and R- (or possibly Q-) channel types, with a smaller density of N-type channels. On the other hand, as mentioned earlier, in CA1 HPCs Christie et al. (1995) reported that N-, P-, Q-, and L-type channels were concentrated at the soma, with T-type channels on the apical dendrite.

11.3 HPC Model Ca^{2+} Channels

Various HPC models have included from one to three types of Ca^{2+} channels, in every case with a Hodgkin-Huxley type kinetic description. Some models use an ohmic conduction scheme and others a constant-field model; the former group includes channels for which the driving force is dynamically calculated based on the Nernst potential from explicit $[Ca^{2+}]_{in}$ calculation, while others assume a constant E_{Ca}.

11.3.1 Models With A Single Type of Ca^{2+} Channel

Variations on the single Ca^{2+} channel description were used in the Traub91, Traub94 and Warman94 models, the differences being mainly in the inactivation kinetics. Although the BG87 model used two Ca^{2+} channels, a fast I_{Ca} and a slow I_{CaS}, the latter current (based on the report of Johnston et al., 1980) had little functional effect. In the Traub91 model steady-state inactivation as a function of voltage was set to 1 below the resting potential, and to a decreasing exponential function of voltage above resting potential, with a voltage-independent time constant of 200ms. The Traub94 model eliminated the inactivation term entirely. In the Warman94 model I_{Ca} steady-state inactivation was defined with a Boltzman expression of similar shape to the function used in the Traub91 model; the primary difference was that inactivation was quite rapid (bell-shaped function of voltage peaking at 8ms). A result of this characteristic is that Ca^{2+} influx in the Warman94 model is significantly reduced during subsequent spikes in a train (i.e. it is frequency dependent), in contrast with the rather constant increment in $[Ca^{2+}]_{in}$ per spike seen in imaging experiments during spike trains (see Section 9).

Because of the different inactivation characteristics, these models have very different Ca^{2+} spikes when all channels other than I_{Ca} are blocked. The Traub91 model generates a slow spike with a threshold at about -40mV, a peak at 80mV (E_{Ca} in the model), and a slow decay that halts at about 20mV because

[12] However, considering similar results from CA3 HPCs in slice, Zbicz and Weight (1986) interpreted multiple inactivation components as indicative of more than one Ca^{2+} current.

[13] Note that in the Jaffe94 and Migliore95 models I_{CaT} had a relatively minor contribution to the $[Ca^{2+}]_{in}$ profiles.

of a strong Ca^{2+} steady-state rectification. Since there is no I_{Ca} inactivation, under the same conditions the Traub94 model "locks up" at E_{Ca}. At the other extreme, the fast inactivation of I_{Ca} in the Warman94 model prevents any regenerative Ca^{2+}-only response. The description of I_{Ca} in the BG87 model reproduced the threshold and shape of the spikes shown in Segal and Barker (1986); this was not surprising since the Segal and Barker data was a major template in determining the I_{Ca} parameters for this model.

11.3.2 Models Incorporating Three Types of Ca^{2+} Channels

In contrast, the Jaffe94 and Migliore95 HPC models adopted the three Ca^{2+} channel position (T-, N-, and L-type), adapting the kinetics from both HPC and non-HPC data. The three Ca^{2+} channel types were included over the entire cell, with a uniform density. These models assume a total Ca^{2+} channel density of about $50pS/\mu m^2$, derived from an estimate of 5-20 channels per μm^2 and 10pS per channel, and adjusted to match $[Ca^{2+}]_{in}$ profiles. A T:N:L channel ratio of 1:10:10 was cited from the work of Fisher et al. (1990), with the density of the N and L channels set to $25pS/\mu m^2$and that of the T channels set to $2.5pS/\mu m^2$.

The driving force for the calcium channels was derived with the GHK rectification formula (Hagiwara and Byerly, 1981), modified to accomodate units of conductance (as above) instead of permeability. It should be noted that strictly speaking this translation of units is incorrect, since the permeability appropriate for the constant field model is quite different than the conductance of the ohmic model (Section 8).

These authors used a least-squares fitting of referenced Boltzman equation parameters, adjusted to m^2h or m^2 kinetics (T- and N-type channels for the former, L-type channels for the latter), to derive parameters for Hodgkin-Huxley type rate equations. No justification was given for the use of m^2 (as opposed to simply m).[14] The kinetic data referenced in the paper included voltage-independent time constants that were also used in the fitting to the Hodgkin-Huxley parameters. Because the inactivation kinetics reported by Fisher et al. (1990) were quite variable, inactivation parameters in this model were derived from non-hippocampal cells. The final result was a good fit to the steady-state data, but improbable time constant functions (in particular for inactivation), since the canonical Hodgkin-Huxley form has a poor fit to a time constant expression with a large voltage-independent term. In particular, the reference data for the τ's of inactivation for I_{CaT} and I_{CaN} were 10 and 50 ms, respectively: the fitted τ functions were bell-shaped, peaking at 8000 and 1600 ms, respectively. A consequence may be an overestimation of the Ca^{2+} influx, all other factors being equal.[15]

The experiments of Fisher et al. were done with 95mM Ba^{2+}in patch pipette in order to accentuate the single channel currents - thus, the voltage parameters of activation in the model were shifted -10mV to account for the charge-screening effect of the Ba^{2+}.

11.4 Major Properties for the Working Model Ca^{2+} Channels

For the Ca^{2+} channels in the Working model, we shall adapt the three channel models from the Jaffe94 and Migliore95 HPC models (T-, N-, and L-type), fitting the gating particles to the extended Hodgkin-Huxley scheme. To summarize, the major goals for our description of the Ca^{2+} currents are:

1. Generate Ca^{2+} spikes when Na^+ and K^+ channels are blocked.
2. Sufficient Ca^{2+} entry during single spikes for the activation of Ca^{2+}-dependent K^+channels.
3. Ca^{2+} entry consistent with measurements of $[Ca^{2+}]$ changes.
4. Current/voltage relationship consistent with the large concentration gradients seen by Ca^{2+} channels.

The associated goals for the description of internal Ca^{2+} dynamics were described in Section 9. Absolute permeabilities were adjusted in order to reproduce regenerative Ca^{2+}-only spikes (Segal and Barker, 1986).

12 HPC Potassium Channels

This section describes the variety of K^+ channels that have been identified in HPCs. These channels cover a wide range of kinetic scales, and thus have a variety of distinct roles in determining the overall cell response.

[14] Although m^2 kinetics is consistent with that proposed by Kay, he was fitting one, not three, channel models to the data.

[15] However, the slow inactivation of I_{CaT} mentioned earlier (Fisher et al., 1990) means that the fit may not be completely unreasonable.

12.1 The Slow Subthreshold K^+ Current: I_D

I_D is a transient K^+ current that has been implicated in the control of the onset of firing under certain conditions (Storm, 1988b), primarily those in which the cell has been at rest, or especially, below rest, for at least several seconds. In earlier reports of transient K^+ currents (e.g. Segal and Barker, 1984), it is possible that I_D was lumped together with I_A, since both are sensitive to 4-AP. However, Storm was able to dissect out I_D from I_A taking advantage of the fact that I_D is about $100\times$ more sensitive to 4-AP, and I_D is much slower than I_A.

The kinetics of I_D from Storm (1988b) show slow inactivation, ranging from 4.7 seconds at -110mV (measured in terms of recovery from inactivation) to about one second at -26mV (these values measured as current decays). Activation is apparently much faster, essentially instantaneous on the time base of seconds of Figure 2 in Storm (1988). Storm has suggested that the slow inactivation of I_D makes it particularly suitable for making the responsiveness of the neuron dependent on the past several seconds of activity. Taking into account the voltage dependence of inactivation, a maximum conductance of I_D on the order of 50nS can be inferred from this paper.

Lüthi et al. (1996) reported a slow K^+ current which may complicate the interpretation of I_D derived from Storm 1988b (Section 12.8; this current corresponds to a slow component of the 4-AP-sensitive current described by Storm, 1986). For our present purposes, since this current is about one tenth the size of I_D, we neglect it in the current Working model.

12.1.1 A Model of I_D

None of the models in Section 7.1 include an explicit I_D, although the kinetics of I_A in the BG87 model were adjusted to account for a 4-AP sensitive delay in initial firing. In the Warman94 model the role of I_D was also assumed to be mediated by I_A, although the kinetics of I_A were not adjusted accordingly. In the BG87 model the description of I_A resulted in a fairly delicate, non-robust mechanism; in the Working model accounting for the delay and the 4-AP sensitive component of spike repolarization with two channels (I_D and I_A, respectively) gives a much more robust result.

Our model for I_D uses fourth powers of both an activation and inactivation particle, primarily to restrict the voltage range of steady-state activation (window current) while still providing a good fit to the data in Storm (1988b) (see Section 8.4.4). The justification for this restriction was to avoid contribution of I_D to the resting state and thus simplify the model evaluation. The sigmoidal time course of activation resulting from setting $n = 4$ is not important for the model. However, it will be important to consider the possible contribution of I_D to resting potential mechanisms in future versions of the model.

Figure 16 illustrates the effect of I_D on repetitive firing with conditions similar to that used in Storm (1988b). Note that the inclusion of I_D has an effect mainly on the timing of the first spike. Apropos to this point, an interesting finding by Storm was the apparent relationship between I_D and accomodation. Under control conditions in HPCs, for low current stimulus strengths there is little accommodation, in particular the initial interspike interval during repetitive firing is close to the steady-state value. As the data in the paper by Storm (1988) shows, this is correlated with the long delay mediated by I_D, since this delay is only seen if the stimulus is sufficiently small (larger current steps appear to overwhelm the I_D rectification, giving the more classical immediate first spike in response to the current). When the cell is held at hyperpolarized holding potentials, which enhances I_D, the lack of accommodation is seen for a much larger range of current stimulus strengths. Conversely, when the cell is held at depolarized holding potentials, which inactivates I_D, accommodation is evident over the entire range of current strengths.

In the model, the time constant for inactivation is relatively fast at the peak of spike, so that a substantial portion of this current is inactivated by the first few spikes. It may be that the connection between I_D and accomodation is indirect, in that it is not I_D *per se* that influences the interspike interval, but rather that the delay to first spike mediated by I_D may tend to inactivate more classical accommodation mechanisms (specifically, I_{AHP} or I_M). In our simulations, we have found that a kinetic description for I_D which mediates a delay to first spike and is consistent with the estimate for the magnitude of I_D (Storm, 1988b) results in a rather feeble I_D between spikes, which contributes little in and of itself to the determination of the interspike interval.

12.2 The Delayed-Rectifier K^+ Current: I_{DR}

There is a variety of data in hippocampus concerning a slowly inactivating, TEA-sensitive, classical "Delayed Rectifier" K^+ current I_{DR}, analgous to the I_K described in the squid axon Hodgkin and Huxley, 1952a.

Although I_{DR} has been thought not to play a substantial part in the repolarization of the spike in cortical neurons, primarily due to the slower activation seen in some reports (see below), the observation (Storm, 1987a) that a TEA-sensitive component remains for repolarization after apparent block of I_A, I_C, and I_M suggests that I_{DR} is available for this role. Similarily, the limited degree of spike broadening reported in Storm (1988b) when both I_A and I_C are blocked pharmacologically suggest that I_{DR} must be large. In fact, during repetitive firing there is a down-regulation of both I_A and I_C, suggesting that I_{DR} might become more predominant during the repolarization of later spikes in a train. Finally, the analysis of Williamson and Alger (1990) suggest that I_{DR} may play a small role in the mAHP. In summary, although I_{DR} in HPCs certainly does not take the center stage for spike repolarization as it does in squid axon, it probably does make a significant contribution.

I_{DR} may also be present in dendrites - Masukawa and Hansen (1987) and Masukawa et al. (1991) reported a fast "outward delayed-rectifier" in patches from both the cell body and dendrites in cultured hippocampal neurons.

12.2.1 A Model of I_{DR}

Most of the previous HPC models use some variation of the Hodgkin-Huxley I_{DR}, with kinetics derived from, for example, either the original Hodgkin and Huxley (1952) data (e.g. the Jaffe94 model), Segal and Barker (1984, the BG87 model), Sah et al. (1988a, e.g. the Traub91, Traub94, and Warman94 models) or Ficker and Heinemann (1992, the Migliore95 model). The role of I_{DR} in the models varies from that of a primary repolarizing current (e.g. the Traub91 and Traub94 models) to being negligible (e.g. the Warman94 model). In the BG87 model, I_{DR} was strong enough to repolarize the spike if all other K^+ channels were blocked. Also, in this model I_{DR} was adjusted under control conditions to generate the mAHP; in the present version of the Working model the mAHP is mediated solely by I_M.

The voltage sensitivity of activation for the I_{DR} that we shall use in the Working model is based on measurements of the TEA-sensitive outward K^+ current in Storm (1988a), Segal and Barker (1984), Numann et al. (1987) and Sah et al. (1988a), all of which describe this current as activating at around -60 to -40 mV. The reported kinetics of activation, however, vary considerably, ranging from over 100ms (e.g. Segal and Barker, 1984) to one millisecond (Sah et al.) at depolarized levels. Furthermore, Sah et al. report relatively fast kinetics of activation/de-activation over a broad voltage range, described as a bell-shaped curve with a peak of seven milliseconds at about -60 mV (23°C). The time constant for inactivation has been reported as ranging from 450 milliseconds (Sah et al.) to over seconds (Segal and Barker).

Adjusting the kinetics of I_{DR} so that it can substantially repolarize the spike requires a reasonably fast turn on (within milliseconds) at depolarized levels. Since inactivation is slow this activation gives rise to a substantial mAHP-like component by I_{DR} unless de-activation is also fairly rapid (we assume that the majority of the mAHP is mediated by I_M; Section 12.7). For this reason, the activation kinetics for I_{DR} were chosen to match more closely the data of Sah et al. (1988a). Additionally, these workers fit a single exponential to the time course of activation, suggesting a single activation particle with respect to the Hodgkin-Huxley model framework (as compared to the four activation particles of the Hodgkin-Huxley squid I_{DR} model).

The reason for the large difference in kinetics for the putative I_{DR} (TEA-sensitive, non-Ca^{2+}-dependent current) in the literature remains to be determined. In the context of the model, it does not seem plausible to postulate a single mechanism whose kinetics could be sufficiently complex to account for the various findings. One obstacle is the lack of data implicating a specific role of I_{DR} independent of I_A and I_C (e.g. as might be observed when I_{DR} is blocked in isolation), in part because the concentrations of TEA needed to block I_{DR} in hippocampus (at least 20mM; Storm, 1988a, Sah et al., 1988a) also block I_C.

The final version of I_{DR} used in the model is the first repolarizing current to be activated during a spike (but not the largest), mainly because the single activation particle caused an immediate activation with depolarization (cf. I_A below).

12.3 The Fast Transient Repolarizing K^+ Current: I_A

A fast, transient, 4-AP-sensitive K^+ current, I_A is found in many neuronal types. In hippocampus there is conflicting data concerning the repolarization of the spike with agents that would be expected to block both I_C and I_A. For example, Figure 3 of Segal et al. (1984) shows recordings with 5mM Co^{2+} (to block Ca^{2+} currents, and thus I_C), with and without 5mM 4-AP. The addition of 4-AP acts primarily to decrease the latency of the first spike (suggesting action of a suppressed I_D) with "...[no] detectable changes in ...

[spike] duration.", although this cannot be easily ascertained by the scale of the figure. More importantly, the recordings both with and and without 4-AP show a prominent AHP that peaks about 15 mV below spike threshold, contrary to the recordings of Storm (1988b), and stronger than would be expected by contributions of I_M or I_{DR}. The depth of the AHP is more reminiscent of aspiny non-pyramidal hippocampal neurons (e.g. Scharfman, 1993): although the recordings in this study were made from "pyramidal-shaped" cultured cells, it is possible that some cells were non-pyramidal in origin.

I_A in cultured hippocampal cells was also described in Nakajima et al. (1985), showing that this current is antagonized by acetylcholine. I_A may also be modulated by the concentration gradient of K^+: lowering extracellular $[K^+]$ shifts the kinetics of I_A in the hyperpolarizing direction, and results in a Mg^{2+}-dependent *reduction* of I_A at potentials above -20mV (the voltage range at which the spike repolarizating role of I_A is initiated) (Eder et al., 1996). Since modulation of $[K^+]_o$ is associated with various pathological states (e.g. seizure-like events), this finding suggests counter-intuitive effects on the repolarization of the spike as mediated by I_A, in particular when $[K^+]_o$ is reduced, which would be expected to *increase* a K^+ current via an increase in the driving force. I_A is also susceptible to dendrotoxin at nanomolar concentrations, which may explain the mechanism of this toxin in the induction of epileptiform activity (Halliwell et al., 1986).

Voltage clamp data references for I_A include Halliwell et al. (1986) and Storm (1988b) for slice preparations, and Ficker and Heinemann (1992) for cultured cells. The voltage clamp data in Storm (1988b) sheds some light on the kinetics of I_A, for example showing that I_A inactivation has a time constant of about 20ms for voltage steps above -50mV. The steady-state inactivation was shallow, with a midpoint at about -50mV.

Under current clamp Storm (1987a) demonstrated that the action of 4-AP is seen immediately at the peak of the spike, and acts to broaden the spike by about ten to twenty percent until the peak of the fAHP.

Masukawa et al. (1991) reported an I_A-like channel in the dendrites of cultured hippocampal neurons. Andreasen and Lambert (1995) reported that 4-AP had quite strong effects on the firing patterns of CA1 HPC dendrites. For example, under concentrations (0.5mM) that uniformly broaden the somatic spike by ten or twenty percent (as above), 4-AP converted current-evoked fast dendritic spikes into incompletely repolarized fast spikes that subsequently led directly into complex, Ca^{2+}-mediated slow spikes. These results suggest that I_A may play a greater role in maintaining stability in the dendrites rather than the soma.

12.3.1 A Model of I_A

For our Working model the primary determinant for the functional properties of I_A is the report of Storm (1987a). In particular, the uniform broadening of the entire action potential when I_A is blocked implies that this current must activate quickly and strongly during the spike under control conditions.

Williamson and Alger (1990) note that 4-AP only broadens the early spikes in a spike train, somewhat consistent with the steady-state inactivation curve shown in Storm (1988b) but perhaps suggesting another component of inactivation (leading to stronger inactivation of I_A with prolonged depolarization).

The time course of activation of I_A is probably voltage-dependent, since this current must activate quickly at very depolarized levels but at the same time must not activate too quickly at substhreshold potentials, lest its effect be seen on the spike upstroke. A delay in activation can also be achieved by postulating more than one activation particle. Here, we define the kinetics of the activation particle with both characteristics. We note that the data in Storm (1988b) does not show an obvious delay in activation, but it may be that the time resolution of the presentation is inadequate to determine this. In the model, under control conditions I_A is the second repolarizing current to be activated, after I_{DR}.

The model that we use for I_A has several drawbacks. While the activation particle definition is quite reminiscent of the the Hodgkin-Huxley squid I_{DR} model (activation raised to the fourth power and voltage-dependent time constant, needed here to account for the apparent delay in activation under current clamp), it does not seem to match the kinetics in the HPC voltage clamp data. Second, the time course of I_A during the repolarization, as inferred from the blocking experiments (which show a broadening of the action potential under 4-AP all the way until the peak of repolarization), is suggestive of a current source, which implies a steady increase of conductance throughout the repolarization to compensate for the reduction in driving force. This behaviour is difficult to address with the Hodgkin-Huxley kinetics. One possibility is that a full Markov formulation is more consistent with the data.

12.4 The Fast Ca^{2+}-Dependent Repolarizing K^+ Currents: I_C and I_{CT}

A fast, TEA-sensitive component of the Ca^{2+}-activated K^+ current in hippocampus, referred to generally as I_C (also know as $I_{K(C)}$), was first described as distinct from a slow, non-TEA-sensitive component (I_{AHP},

see below) in hippocampus by Lancaster and Adams (1986). This current was found to be responsible for the fAHP during the repolarization of single spikes (Lancaster and Nicoll, 1987, Storm, 1987a).

However, there is substantial evidence that there is more than one type of channel underlying this current. Voltage clamp studies suggest that I_C may represent more than one current (reviewed in Storm, 1990), in particular a transient I_{CT} (also know as $I_{K(CT)}$) and a non-inactivating I_C (e.g. Zbicz and Weight, 1985).

The evidence demonstrating a partial dependence of the mAHP on Ca^{2+}-influx, as mentioned earlier, has been attributed to participation of I_C in the mAHP, especially when the cell was depolarized. This suggests that although I_C must inactivate quickly in order to account for the fAHP, residual I_C must be present for about one hundred milliseconds after a spike or spike train, during the mAHP. Likewise, Alger and Williamson (1988, see also Alger and Nicoll, 1980) reported a Ca^{2+}-dependent K^+ current, independent of the I_{AHP} (see below), that generated an after-hyperpolarization of about 150 milliseconds duration after epileptiform bursts.

Thus, the kinetics of the Ca^{2+}-dependent K^+ current must either be rather complex, and cover a relatively wide range, or in fact represent more than one current. For the Working model we shall focus on kinetics which mediate the fAHP, therefore we will refer to this current as I_{CT} (note that the Warman94 model refers to I_{CT}, not I_C). Most other cell models do not make this distinction, and just refer to I_C (e.g. although the description of this current in the BG87 model also was focussed on reproducing the fAHP, the current was called I_C).

The main references that we will use regarding the role of I_{CT} during the repolarization of the action potential, and the subsequent fAHP, are that of Lancaster and Nicoll (1987) and Storm (1987a). We may note that voltage clamp dissection of Ca^{2+}-dependent currents is even more difficult than other currents due to the difficulty of simultaneous voltage and $[Ca^{2+}]_{in}$ control (for one approach to this problem, see Ikemoto et al., 1989). Accordingly, the parameters for the model I_{CT} will be primarily determined by matching behaviour under current clamp.

I_C has been tentatively identified with the large conductance voltage and Ca^{2+} dependent BK channel recorded in patchs from hippocampal isolated and cultured cells (Sah, 1996). This channel has a threshold/half-activation point of $1/4\mu$M $[Ca^{2+}]$ at 0mV (Storm, 1990). On the other hand, the kinetics of the BK channel are probably too slow to account for the fAHP generating role of I_{CT} (Ikemoto et al., 1989).

The description of I_C in the BG87 model included four voltage-dependent fast activation particles, so that the abrupt phase of the fAHP was caused by the de-activation of these particles. A separate Ca^{2+} dependent activation particle was also part of the model. The kinetics of the fAHP was replicated in the Warman94 model by an activation particle with both voltage and Ca^{2+} dependence, based on the data of Barrett et al. (1982). Kinetics for I_C in the Traub91 and Traub94 models were adjusted from bullfrog sympathetic neuron data. As mentioned earlier, the description of I_C in the Jaffe94 and Migliore95 models were adapted from the Moczydlowski and Latorre model of the rat muscle BK channel.

The finding that dendritic fast spikes show a slight broadening under concentrations of TEA (1-2mM) that would be expected to block I_C (Andreasen and Lambert, 1995) allows the possibility that this current, or at least I_{CT}, is present in HPC dendrites.

12.4.1 A 3 State Markov Model for I_{CT} with Voltage and Ca^{2+} Dependent Transitions

Most reports on the kinetics of I_C describe it as a non-inactivating current, but this is at odds with the overall transient nature of the fAHP during repetitive firing (Section 6.4.1). This is further support for attributing a separate I_{CT} to the fAHP. For the slow inactivation during spike trains the I_C in the BG87 model and the I_{CT} in the Warman94 model included a distinct slow voltage-dependent inactivation particle.

Close examination of the behaviour of the fAHP suggests that inactivation occurs *after* activation: the preferential appearance of the fAHP on the *first* few spikes of a train, even though subsequent spikes traverse similar voltage ranges, argues against independent activation and inactivation voltage-dependent mechanisms. In particular, it is difficult to adjust the parameters of an independent voltage-dependent inactivation component such that the first spike causes much less inactivation (thus sparing the fAHP) than the second and subsequent spikes. For this reason we will adopt a simple three state Markov model to describe I_{CT} gating in the Working model, including a inactivated state that is reachable only through the open state. In this model, shown in Figure 9, the disappearance of the fAHP during repetitive firing is a result of a voltage dependent transition between the inactivated state and the closed state that is slow at depolarized potentials and speeds up with hyperpolarization. It may be that this transition accelerates with temperature, which could account for the apparent persistence of the fAHP during spike trains seen in Thompson et al., 1985,

as mentioned earlier.

The transition from the closed state to the open state is Ca^{2+} dependent (following the $[Ca^{2+}]$ in compartment 1 of the associated $[Ca^{2+}]_{in}$ integration system, being fast at $[Ca^{2+}]$ above 0.01mM) and voltage-dependent. It is not clear if this co-dependency is absolutely necessary for activation for the I_{CT} model since the large transient in the local $[Ca^{2+}]$ seen by the channel is strictly correlated with the spike peak, and further adjustment of the parameters defining the Ca^{2+}-mediated kinetics may allow the dropping of the voltage term. The fast shut off of I_{CT}, necessary in order to mediate the fAHP, is accomplished by a strong voltage dependence in the transition from the open state to the inactivated state.

12.5 The Slow Ca^{2+}-Dependent K^+ Current: I_{AHP}

The slow Ca^{2+}-dependent after-hyperpolarization (sAHP) is attributed to a Ca^{2+}-dependent and apparently voltage-independent I_{AHP} potassium current (Lancaster and Adams, 1986). The major functional role assigned to this current is that of regulating repetitive firing (Madison and Nicoll, 1984).

The sAHP is insensitive to TEA and charybdotoxin, unlike the fAHP, whereas in hippocampal interneurons cells the sAHP is sensitive to apamin (in HPCs apamin does not block the sAHP) (Storm, 1990). Both noradrenaline and cholinergic agonists, among other neurotransmitters, block I_{AHP}. Second messengers in addition to Ca^{2+} are involved in the regulation of I_{AHP}. Results from Pedarzani and Storm (1993, 1995a, 1996) indicate that PKA mediates the suppression of I_{AHP} by all the monoamine transmitters: noradrenaline, serotonine, histamine and dopamine; and there is a synergistic interaction between α and β receptor agonists. Zhang et al. (1996) showed that activation of muscarinic afferents blocks the I_{AHP} only if this occurs before the relevant rise in $[Ca^{2+}]_{in}$.

In single channel recordings from cultured rat E17 hippocampal neurons, Lancaster et al. (1991) identified a Ca^{2+}-dependent 19pS K^+ channel that they associate with I_{AHP}. In these recordings they noted a rise time of Ca^{2+} activation of approximately 70 milliseconds at -70mV. Noting the longer delay in the peak I_{AHP} of a few hundred milliseconds (consistent with the delay of the sAHP peak), they discount the possibility of Ca^{2+}-mediated Ca^{2+} release in hippocampus, and suggest that there must be some mechanism which restricts access of the channel to intracellular Ca^{2+}.

The I_{AHP} has been attributed to the SK class of channels, distinct from the BK channels mentioned earlier (Sah, 1996). Generally it is found that 100-400 nM $[Ca^{2+}]$ is necessary for the activation of the SK channel; this may be contrasted to the activation of hippocampal I_{AHP} by a rise from 30nM to 60nM $[Ca^{2+}]$ (Knöpfel et al., 1989).

Recently, a candidate channel for I_{AHP} has been cloned in mammalian brain (Köhler et al., 1996), which has the general attributes that would be expected from the macroscopic behavior of I_{AHP}. This paper suggested that the Ca^{2+}-dependence of the channel fit a Hill relationship with a coefficient of about four, in other words impling an involvement of 4 Ca^{2+} ions in channel gating, and a $K_{0.5}$ between 0.5 and 1.0 μM.

Despite the lack of direct supporting data the model of I_{AHP} in the BG87 model included explicit voltage-dependence via two types of voltage-dependent inactivation gating particles. The rationale for these particles was to account for the delay to peak of the sAHP and to avoid interaction between I_{AHP} and the shape and time course of either Na^+ or Ca^{2+} spikes. Although the latter motivation may be somewhat problematic, the former will be reconsidered below.

Lancaster and Adams (1986) found no voltage-dependence for I_{AHP} using either voltage clamp or hybrid clamp protocols. However, the maximum holding potential used was -47mV, thus it is conceivable that voltage-dependent inactivation, fast and relatively complete at spiking potentials, and removed slowly (hundreds of milliseconds) around rest, could account for the observed delay in the sAHP peak.

Steady-state activation based on the log of $[Ca^{2+}]_{in}$ was used for I_{AHP} in the Warman94 model, adapted from the work of Blatz and Magleby (1987), with a time constant for activation of 48 milliseconds.

12.5.1 A Model of I_{AHP}

In our Working model of I_{AHP}, we will use the simple Ca^{2+}-dependent gating model described in Section 8.8.3. This is similar to that used for the Ca^{2+}-dependence of both I_C and I_{AHP} in the BG87 model. On the other hand for this model of I_{AHP} we will neglect the voltage-dependent mechanisms used in the BG87 model. We shall assume cooperative binding of four Ca^{2+} ions in order the reproduce the distinct threshold in Ca^{2+} dependence that is necessary for this channel, assuming that activation of I_{AHP} depends on slow, accumulative changes in $[Ca^{2+}]_{in}$, and that the quiescent activation of I_{AHP} is negligible. The Ca^{2+} signal is taken from compartment 2 of the associated (somatic) $[Ca^{2+}]_{in}$ integration system.

In order to reconcile the small incremental change in $[Ca^{2+}]_{in}$ per spike (about 10nM) relative to the resting level (50nM), and to avoid a substantial resting activation of I_{AHP}, it was necessary to include two Ca^{2+}-dependent gating particles. This, plus the requirement of the binding of four Ca^{2+} ions for activation and the particular values used for α and β results in a distinct activation threshold around 50nM.

An important question is that of the mechanism underlying the long delay to peak of the sAHP, and thus I_{AHP}. We can consider at least two candidates, that is delay arising from either the intracellular diffusion of Ca^{2+} or from the intrinsic channel gating kinetics. Arguments for the latter cause include the strong temperature dependency of the sAHP peak (Thompson et al., 1985, Lancaster and Adams, 1986), and the relatively fast rise time of $[Ca^{2+}]$ signals in response to single spikes (e.g. Jaffe et al., 1992), which presumably reflect a global or average concentration over many microns. Accordingly, in the Working model I_{AHP} a value for τ_0 of 100 milliseconds the Ca^{2+}-binding kinetics contributes to a delay in the I_{AHP} peak after the rise in $[Ca^{2+}]_{in}$ in compartment 2 of the associated Ca^{2+} concentration integrator. A similar rate limiting term was used in the I_{AHP} in the Traub91 and Traub94 models.

On the other hand the value of 100 milliseconds does not account for the somewhat longer delays in the peak I_{AHP} reported in the literature (e.g. 400-700 milliseconds Lancaster and Adams, 1986). Using a longer value for τ_0 causes the I_{AHP} gating to "miss" the peak of the $[Ca^{2+}]_{in}$. It may be that either a voltage-dependent inactivation term should be retained, as in the BG87 model, or a Markov description that decouples the time course of the relevant $[Ca^{2+}]_{in}$ and the activation of I_{AHP} should be considered (ref. discussion in Section 8.7.1).

More importantly, recent data from Lancaster and Zucker (1994) show that photolytically released intracellular Ca^{2+} can trigger I_{AHP} with a delay on the order of 50 milliseconds, suggesting that the delay of the sAHP is due to factors extrinsic to the I_{AHP} channel. These workers suggested that delays due to diffusion, taking into account immobile buffers (see Section 9.5.1), would reach on the order of 400 milliseconds for distances of about 3μm. They suggest that the strong temperature dependence on the delay to sAHP peak is related to temperature dependence of the Ca^{2+} pump and buffer systems. Future refinements of the diffusion models described in Section 9 may support this scheme.

We note that choosing model parameters in order to avoid a resting contribution of I_{AHP} was done primarily for convenience, and it will be important to check if in fact the assumed 50nM level for resting $[Ca^{2+}]_{in}$ does not slightly activate I_{AHP}. If so, then the numerous modulatory influences on this current may also be expected to effect the neuron's resting state. In fact, as pointed out elsewhere, the true resting state of the Working model is reached after ten to twenty seconds, during which time a small Ca^{2+} influx from a small resting activation of the Ca^{2+} channels leads to a buildup of the resting $[Ca^{2+}]_{in}$, which in turn slightly activates I_{AHP}, hyperpolarizing the cell.

12.6 Is the Variance in Kinetics Between I_{CT} and I_{AHP} Due to Unique Pools of Ca^{2+}?

The difference in the kinetics of I_{CT} and I_{AHP} can be accounted for in part by a difference in the Ca^{2+} "pools" that each are exposed to. This can be inferred by the following reasoning.

The time course of the rise of $[Ca^{2+}]$ averaged over the entire volume of the soma or a section of dendrite is consistent with the buildup of the sAHP and thus by implication I_{AHP}. On the other hand, the I_{CT}-mediated fAHP is present at the first spike from the quiescent state. One way to account for this difference is for I_{CT} to be exposed to a Ca^{2+} pool with much faster rise time, such that the concentration in this pool rises significantly above the resting level with a single spike. This could be accomplished if I_{CT} channels were co-localized with one or more of the Ca^{2+} channel types, so that the I_{CT} channels would be triggered by very local and large increases of $[Ca^{2+}]$ that would occur adjacent to Ca^{2+} channels with every spike (Lancaster and Nicoll, 1987, the BG87 and Warman94 models).

This hypothesis is supported by the observation that a fast intracellular Ca^{2+} buffer (BAPTA) will block the repolarization by I_{CT}, whereas injection of a slower buffer (EGTA) blocks only the I_{AHP} component, as shown by Storm (1987b). Note that BAPTA does not prevent putative Ca^{2+}-mediated inactivation of Ca^{2+} channels (Kay, 1991, see Section 11.2.3), which suggests that I_{CT} channels may be close, but not immediately adjacent to Ca^{2+} channels.

The functional significance of microdomains of large and fast $[Ca^{2+}]$ changes in the vicinity of Ca^{2+} channels has been considered previously in the context of synaptic release, and recent studies confirm this phenenoma in the squid giant synapse (for references see Llinás et al., 1995). In addition, recent evidence for the functional colocalization of Ca^{2+} and Ca^{2+}-dependent K^+ channels have been reported in presynaptic membranes of hair cells and the neuromuscular junction (Roberts et al., 1990, Robitaille et al., 1993). Finally,

patch recordings of both somatic and dendritic membrane in cultured hippocampal cells (Masukawa et al., 1991) support the general idea of co-localized channels: they showed a high proportion of patches with both a "delayed-rectifier" type of outward current and either a non-inactivating or inactivating inward current. However, the evidence presented in this paper suggests that the inward currents are mediated by Na^+, rather than by Ca^{2+}.

The domain model, mentioned earlier, for Ca^{2+}-dependent inactivation of Ca^{2+} channels has been proposed based on the assumption of functionally relevant local high concentrations of Ca^{2+}. The model analyzed by Sherman et al. (1990), although investigated in the context of Ca^{2+} channel kinetics, is of the same structure as the model for I_{CT} Ca^{2+}-dependence described above.

12.7 The Muscarinic K^+ Current: I_M

Cholinergic agonists regulate a variety of channels, but the classical target (though not the most sensitive) is the non-inactivating K^+ current, I_M (Halliwell and Adams, 1982) - the "M" stands for "muscarinic". The major hallmark of I_M is the mAHP; the major functional role assigned to this current is for regulating repetitive firing (Benardo and Prince, 1982b, Madison and Nicoll, 1984).

I_M is activated over a narrow range, from about -60 to -40 mV (Halliwell and Adams, 1982). This threshold suggests that the contribution of I_M to the resting potential is minimal. Time constants of I_M relaxations under voltage clamp (and by implication, the time constant of activation) at 25°C are about 210ms at -45mV and 95ms at -55mV. Measurements by these workers at 30°C suggest a $Q10$ of about 5.

The voltage-dependent activation of I_M may also be inferred from the data of Williamson and Alger (1990). In one experiment, a mAHP-like potential was elicited under TTX and low Ca^{2+} by long current steps to various potentials. The amplitude of this potential increased somewhat linearly with the plateau potential, beginning when the step reached about -45mV. The amplitude of the mAHP-like potential increased for plateau potentials up to at least -32mV, but this may reflect a voltage-dependent increase in the rate of activation for I_M rather than a steady-state characteristic that is still rising at this voltage.

The reversal potential of I_M has been estimated at between -78mV (Halliwell and Adams, 1982) and -73mV (Williamson and Alger, 1990), suggesting that this is not a pure K^+ conductance.

As mentioned earlier, I_M in the models of Section 7.1 had different functional effects, including an important role in stablizing the resting potential, playing a role in accomodation, and terminating bursts. The Traub91 and Traub94 models did not include I_M, and the I_M used in the BG87 model was underestimated. On the other hand, I_M in the Warman94 model was adjusted to account for both the mAHP and the early regulation of repetitive firing. The question of whether or not I_M contributes to the resting potential is complicated by the many effects of muscarinic agonists, particularly the modulation of mechanisms that are active around rest.

12.7.1 A Model of I_M

The Working model description of I_M is based primarily on the voltage clamp data of Halliwell and Adams (1982) (and Brown and Griffith, 1983a), and the more functionally oriented analysis in Storm (1989) and Williamson and Alger (1990), such that I_M parameters were adjusted in order to account for the major properties of the mAHP.

In this description, I_M is completely shut at rest, The observation that there is a roughly constant increment per spike in the mAHP (Storm, 1989) can be accounted for in part if we use a second order in the activation term (that is, two activation particles), with a fast time constant at depolarized levels and a much slower value around threshold. The second power tends to equalize the incremental increase of I_M from spike to spike (the Warman94 model used a second order description of the I_M gating particle to implement a temporal delay in activation).

12.8 Anomalous Inward Rectification and Other K^+ Currents

Here we summarize the mechanism of anomalous inward rectification, and discuss additional K^+ currents that have been reported for HPCs. These currents will not be considered in the Working model, but are left for future work.

12.8.1 Anomalous Inward Rectification

Anomalous inward rectification is classically defined as an increase in a K^+ conductance with hyperpolarization (Katz, 1949, Hotson et al., 1979, Hille, 1992). The term "anomalous" is to highlight the difference from the classical delayed rectifier, or in general the fact that most K^+ conductances open with depolarization. However, as described below, anomalous inward rectifiers may also be mixed conductances.

There are two classes of inward rectifying currents. The first class consists of mixed cation inward rectifiers whose non-linearities are characterized in terms of voltage-dependent gating mechanisms (Section 13.1). The second class of inward rectifiers, which are pure K^+ currents, demonstrate an instantaneous voltage-dependence that shifts with the log of $[K^+]_o$, in other words relative to the difference between the membrane potential and E_K, and have an inflection in the IV curve around E_K. These channels may also show a time-dependent component of the rectification, as well as a $[K^+]_o$-dependency on the steepness of the steady-state IV characteristic. Rectification of these channels arises directly from the conduction properties of the channel ionophore, but they do so in a sense opposite to that which would be predicted by the constant field permeation model (Section 8.2). Hille (1995) discusses a multi-ion pore model with a monovalent intracellular blocking ion that seems to account for many of the pure K^+ inward rectifier properties.

As a side note, since under normal conditions the ion with the lowest equilibrium potential is K^+, there can be no channel mediated current (synaptic or otherwise) that can drive the membrane potential below E_K. This would suggest that K^+-mediated inward rectifiers are functionally relevant only for limiting below-E_K hyperpolarizations due to membrane pumps. With respect to HPCs, at present there is limited evidence for this type of channel under control conditions (but see Owen, 1987, Section 13.1, and discussion in Brown et al., 1990). A serotonin-activated inward-rectifier has been reported, however, and this current will be discussed next.

12.8.2 A Serotonin-activated Inward Rectifier

Serotonin (5-HT) has both an inhibitory and excitatory effects on HPCs causing an increase in one or more K^+ currents, which may include a true inward-rectifier, and causing a decrease in a resting K^+ conductance and the Ca^{2+}-dependent sAHP (Colino and Halliwell, 1987). The inward-rectifying characteristics of the serotonin-activated current include a dependence on the slope conductance with $[K^+]_o$ (Andrade and Nicoll, 1987). Rectification is relatively shallow, with approximately 3nS of activated conductance at -120mV compared to about 1nS at -30mv ($[K^+]_o$ of 3mM and 60μM 5-HT; Okuhara and Beck, 1994). This current may be preferentially expressed in the dendrites and axons while another serotonin-activated K^+ current, which has less obvious inward-rectifying properties, may be localized to the soma (Uneyma et al., 1993).

12.8.3 $I_{K,rest}$, $I_{T,slow}$, $I_{K(slow)}$

One candidate for the leak current is a K^+ current, $I_{K,rest}$ (see discussion by Storm, 1990), that is linear for tens of millivolts around rest, and persists with blockers of the major K^+ currents. There may also be a muscarinic-sensitive component to this current (Madison et al., 1987).

Ficker and Heinemann (1992) have described a slowly inactivating TEA-sensitive K^+ current, $I_{T,slow}$, in cultured hippocampal cells. This current is not unlike I_{DR} other than that $I_{T,slow}$ has a substantially higher threshold (between -40 and -30mV), and it is sensitive to 4-AP.

Lüthi et al. (1996) describe a $I_{K(slow)}$ which contributes particularly to the latency of the first action potential, along with I_D and perhaps I_A (see also Storm, 1986). This current had a reversal potential of about -93mV that shifted with changing $[K^+]_o$ as predicted by the Nernst equation given a pure K^+ current. The fully activated conductance was about 6nS (estimated from data presented in the paper). Several characteristics of $I_{K(slow)}$ are similar to I_D, a major difference being a slower inactivation.

13 Non-Specific Cation and Chloride Currents

We now mention a variety of other channels that have been reported in hippocampal pyramidal neurons. Other than I_H, these currents will not be demonstrated in the Working model. As before with the non-modelled K^+ currents, it remains to be seen how including these mechanisms will influence estimated parameters or functional consequences of the channel models described earlier.

13.1 The Hyperpolarization-Activated Sag Current: I_Q/I_H

Various descriptions of a hyperpolarization-activated, mixed cation inward current have been reported for hippocampal neurons. Although earlier reports (e.g. Halliwell and Adams 1982) called this current I_Q (for "queer", presumably in the same vein as "anomalous"), more recently this current has been identified as I_H due to the similarity to the I_H identified in several other cells (e.g. first in photoreceptors and heart cells, then in neurons, e.g. thalamic cells, McCormick and Pape, 1990; for a thorough review see Pape, 1996). This current, blocked by Cs^+, is mainly responsible for a depolarizing sag in response to long (one hundred milliseconds or more) hyperpolarizing current steps, and may contribute to resting properties. The biophysical details and, as suggested above, the name of this current have been somewhat inconsistent in the literature.

I_Q was characterized by Halliwell and Adams (1982) as a persistent current which was probably carried by both K^+ and Na^+ ions (they estimated the reversal potential for I_Q as around -55mV). In this report the activation of I_Q occured at minimum in the range between -120 and -80mV, and activation was well fitted to a single exponential with a time constant of that decreased monotonically with hyperpolarization (184ms at -82mV to 100ms at -130mV, 25°C; experiments at 30° suggested a $Q_{10} = 5$). The maximum conductance of this current can be estimated from the paper at about 4 to 5nS. Later papers also referred to either I_{AR} (for anomalous rectifier, Segal and Barker, 1984) or I_Q (Brown et al., 1990). Grove and Halliwell (1990) estimated E_{rev} for I_Q as -49±11mV. Colino and Halliwell (1993) showed that I_Q is potentiated by muscarinic agonists. A Cs^+-dependent component of the mAHP when the cell was hyperpolarized was demonstrated by Storm (1989), and later by Williamson and Alger (1990), suggesting a contribution of I_Q in the mAHP under these conditions.

I_H is enhanced by noradrenaline via beta receptors and cAMP (Pedarzani and Storm, 1995b, and by serotonin, histamine and dopamine, also by cAMP (Storm et al., 1996).

Maccaferri et al. (1993) describe an anomalous rectifer current, I_H, in rat CA1 cells that contributes significantly to the resting potential and is involved in after-hyperpolarizations: 2mM extracellular Cs^+ lowered the resting potential about 4mV lower than control, and blocked the mAHP. This paper reported a reversal potential for I_H of about -17mV, with a shallow activation starting at -50mV and saturating at -140mV, and a maximum conductance of around 2.6nS. The major difference between this and earlier reports of I_Q seems to be the more depolarized activation range of I_H (which gives it an important role under non-hyperpolarized conditions) and a significantly higher E_{rev}. Although these authors report a time constant of activation of about 180ms at -70mV, this seems to be too slow to account for the hyperpolarization-induced sag shown in the paper under current clamp, thus suggesting that the time constant becomes faster with hyperpolarization. Although the rectification by I_H seems to be due to voltage-dependent gating, the slope conductance was shown to increase with $[K^+]_o$, reminiscent of a true inward rectifier.

Perkins and Wong (1995) demonstrated intracellular blocking by QX-314 of what they refer to as I_Q; interestingly, examination of data shown in this paper suggest that average resting potentials were 5 to 10 millivolts *higher* when QX-314 was present in the whole-cell patch electrodes. In general the biophysical characteristics of this current differed slightly from that reported by Maccaferri et al.. Perkins and Wong showed a steeper activation that saturated at about -120mV, and estimations made from the data shown in this paper suggest a total conductance of about 10nS with an E_{rev} of about -40mV. Although the activation kinetics for current relaxations at -120mV were well fit to two exponentials, an approximate fit for modelling purposes may be made to a single exponential with a 60 millisecond time constant.

It may be that there is more than one current contributing to non-transmitter-activated inward-rectification in HPCs. In a short abstract, Owen (1987) described three types of inward rectifier currents: a current that he identified as I_Q, an inactivating fast current that he associated with the I_{fir} seen in other cell types, and a third low threshold current (-45mV, complete activation at -115mV), activating with a 100 millisecond time constant at -80mV, that he called I_{ltIR}. Grove and Halliwell (1990) demonstrated an additional inward rectifying current, other than I_Q, that is activated at hyperpolarizing potentials (below -80mV), with an E_{rev} close to E_K.

None of the models in Section 7.1 (other than a cursory non-functional description in the BG87 model) include I_Q.

13.1.1 A Model of I_H

For the description of I_H in the Working model we primarily refer to the data of Maccaferri et al. (1993). A single activation particle is used, and the effect at this stage of the model is mainly to generate a depolarizing sag in response to hyperpolarizing current steps (see Figures 5 and 12). Blocking this current in the model

hyperpolarizes the resting potential by only about 300μV, an effect about ten times less than that reported above. For future refinement it will be instructive to see if the linear-markov model of I_H in retina proposed by Barnes and Hille (1989) is relevant for hippocampus.

13.2 The Persistent Cl^- Current: $I_{Cl(V)}$

Madison et al. (1986b, rat HPCs in slice) and Brown et al. (1990, rat CA3 HPCs in cultured slice) describe a slowly activating (hundreds of milliseconds), persistent, voltage-dependent Cl^- current, $I_{Cl(V)}$. Estimates of the physiological value vary for the associated reversal potential, E_{Cl}, but is normally around the resting potential (-70mV). In the first report this current has a shallow steady state inactivation with a midpoint about -50mV, and thus may contribute to the resting potential under control conditions. In the second report, however, inactivation was complete below -60mV, so its contribution to the maintenance of the resting potential in this case is less obvious. In either case, $I_{Cl(V)}$ is blocked by either activation of PKC (demonstrated with phorbol esters) or 100 μM Cd^{2+}. The susceptibility to PKC activation implies that this current may have a modulatory role, particularly with respect to synaptic integration. A primarily dendritic location for $I_{Cl(V)}$ was inferred by difficulty of detection when K^+ channels blockers were not used.

The conductance of $I_{Cl(V)}$ of about 8nS at -70mV, as reported by Madison's group, would be expected to contribute on the order of 30% of the resting input impedance for sharp electrode recordings; for whole cell recordings this value could account for the *entire* input impedance (8nS corresponds to 125MΩ). This clearly presents a problem, for at least the following reasons: first, the voltage range for the current inactivation depends on the preparation (see above), thus this is not a "reliable" mechanism; second, recordings with KCl electrodes would considerably raise the reversal potential of this current, and thus have a strong depolarizing effect on the resting potential.

13.3 The Ca^{2+}-dependent Non-Specific Cation Currents: I_{ADP}, I_{CAN}, I_{ACPD}

Non-specific cation (CAN) currents have been described for HPCs, and may be a candidate for the crucial slow depolarizing mechanism underlying bursts (Crépel et al., 1994).

In cultured slice Caeser et al. (1993) describe a Ca^{2+}-dependent ADP that is carried by at least a mix of K^+ and Na^+ ions, observed after either cholinergic or metabotropic glutamate receptor (mGluR) mediated blockade of the sAHP. The magnitude (about 250pA at holding potentials between -65 and -50mV) and timing of the underlying I_{ADP} current (also referred to as I_{CAN}) suggest that the neurotransmitter agonists enhance this current, rather than the ADP being more or less "hidden" during the sAHP under control conditions. This interpretation, also reported by Colino and Halliwell (1993), suggests that the delay of the I_{AHP} peak is not due to an early interval of activated I_{ADP}. The decay of I_{ADP} under voltage clamp was significantly slower than the time course of simultaneous $[Ca^{2+}]_{in}$ measurements. This current apparently has an intrinsic voltage-dependency, activating a potentials higher than -90mV and becoming maximal at about -60mV. The reversal potential of this current has been estimated as about -20mV (Colino and Halliwell, 1993).

A similar (but voltage-independent) Ca^{2+}-dependent non-specific cation current, upregulated by activation of mGluRs, was reported by Crépel et al. (1994), who named it I_{ACPD} in reference to the mGluR agonist used in the experiment. This current, which was about 100pA at a holding potential of -60mV, had a reversal potential around -20mV. The contribution to the cell's conductance by the activation of I_{ACPD} by mGluRs may be partially offset by the reduction of K^+ currents by mGluRs (I_M and I_{AHP}, Charpak et al., 1990), and may generate a long-lasting depolarization in response to rises in $[Ca^{2+}]_{in}$.

14 Simulations of HPC Properties with the Working Model

We conclude this chapter with some additional simulations illustrating various characteristics of the Working model.

The role of the major repolarizing currents on shaping the spike is seen in Figure 11, where single evoked spikes are shown under various conditions. Note that the subthreshold time course and spike upstroke are identical under all conditions, showing that for the initiation of firing, modulation of either the Ca^{2+} currents (and by implication, I_{CT} and I_{AHP}) or I_A has no effect on these characteristics. The same holds for I_{DR} (simulations not shown).

The classical basic computational characteristic of a neuron is the transformation of stimulus intensity into the frequency of repetitive spikes. The response of the Working model to long current steps is shown in

Figure 12, which among other things illustrates the time dependence of the output due to various adaptation mechanisms (Figures 14 and 15). Increasing R_m to bring the linear properties of the model closer to that seen with whole cell patch recordings changes the response to long current steps quantitatively but not qualitatively, as seen in Figure 13. The f/I plot, as discussed in Section 6.6, encapsulates these characteristics in a more quantitative form. The validity of this measure in a functional context remains to be demonstrated, primarily since *in-vivo* input is never as stereotypically constant as the current steps used in experimental protocols. Nonetheless, comparing the model f/I plot with those reported in the literature is another test of the collective properties of the model mechanisms (Figure 17).

Acknowledgements

Part of this work was covered by HFSP grant RG69/93, and grants from the Fondation Fyssen, Fondation Phillipe, and a CNRS ATIPE Fellowship. I would like to acknowledge the very useful discussions, both past and present, with Johan Storm and John Lisman, and the intial impetus for this project from Tommy Poggio, Christof Koch, and Paul Adams. I would also like to acknowledge Yves Fregnac for his comments and support during the writing of this paper, and Nicolas Gazeres, Cyril Monier and Ragnhild Halvorsrud for very thorough feedback including the testing of model properties using Surf-Hippo, GENESIS, and NEURON.

References

[1] P. R. Adams and M. Galvan. Voltage-dependent currents of vertebrate neurons and their role in membrane excitability. In A. Delgado-Escueta, A. A. Ward, D. M. Woodbury, and R. Porter, editors, *Advances in Neurology, Vol. 4, Basic Mechanisms of the Epilepsies*, pages 137–170. Raven Press, 1986.

[2] H. Agmon-Snir. A novel theoretical approach to the analysis of dendritic transients. *Biophysical Journal*, 69:1633–1656, November 1995.

[3] H. Agmon-Snir and I. Segev. Signal delay and input synchronization in passive dendritic structures. *Journal of Neurophysiology*, 70:2066–2085, 1993.

[4] B. E. Alger. Hippocampus: Electrophysiological studies of epileptiform activity *in vitro*. In R. Dingledine, editor, *Brain Slices*, pages 157–199. Plenum Press, 1984.

[5] B. E. Alger, S. S. Dhanjal, R. Dingledine, J. Garthwaite, G. Henderson, G. L. King, P. Lipton, A. North, P. A. Schwartzkroin, T. A. Sears, M. Segal, T. S. Whittingham, and J. Williams. Brain slice methods. In R. Dingledine, editor, *Brain Slices*, pages 381–437. Plenum Press, 1984.

[6] B. E. Alger and R.A. Nicoll. Epileptiform burst afterhyperpolarization: calcium-dependent potassium potential in hippocampal CA1 pyramidal cells. *Science*, 210:1122–1124, December 1980.

[7] B. E. Alger and A. Williamson. A transient calcium-dependent potassium component of the epileptiform burst after-hyperpolarization in rat hippocampus. *Journal of Physiology*, 399:191–205, 1988.

[8] C. Alzheimer, P. C. Schwindt, and W. E. Crill. Modal gating of Na^+ channels as a mechanism of persistent Na^+ current in pyramidal neurons from rat and cat sensorimotor cortex. *Journal of Neuroscience*, 13(2):660–673, February 1993.

[9] P. Andersen, J. Storm, and H. V. Wheal. Thresholds of action potentials evoked by synapses on the dendrites of pyramidal cells in the rat hippocampus *in vitro*. *Journal of Physiology*, 383:509–526, 1986.

[10] W. R. Anderson, J. E. Franck, W. L. Stahl, and A. A. Maki. Na,K-ATPase is decreased in hippocampus of kainate-lesioned rats. *Epilepsy Research*, 17(3):221–231, March 1994.

[11] R. Andrade and R. A. Nicoll. Pharmacologically distinct actions of serotonin on single pyramidal neurones of the rat hippocampus recorded *in vitro*. *Journal of Physiology*, 394:99–124, 1987.

[12] M. Andreasen and J. D. C. Lambert. Regenerative properties of pyramidal cell dendrites in area CA1 of the rat hippocampus. *Journal of Physiology*, 483:421–441, 1995.

[13] C. M. Armstrong. Sodium channels and gating currents. *Physiol. Rev.*, 61:644–683, July 1981.

[14] R. B. Avery and D. Johnston. Multiple channel types contribute to the Low-Voltage-Activated calcium current in hippocampal CA3 pyramidal neurons. *Journal of Neuroscience*, 16(18):5567–5582, September 1996.

[15] R. Azouz, M. S. Jensen, and Y. Yaari. Ionic basis of spike after-depolarization and burst generation in adult rat hippocampal CA1 pyramidal cells. *Journal of Physiology*, 492:211–223, 1996.

[16] S. Barnes and B. Hille. Ionic channels of the inner segment of tiger salamander cone photoreceptors. *Journal of General Physiology*, 94:719–743, October 1989.

[17] J. N. Barrett, K. L. Magleby, and B. S. Pallotta. Properties of single calcium-activated potassium channels in cultured rat muscle. *Journal of Physiology*, 331:211–230, 1982.

[18] L. Benardo, L. Masukawa, and D. Prince. Electrophysiology of isolated hippocampal pyramidal dendrites. *Journal of Neuroscience*, 2(11):1614–1622, November 1982.

[19] O. Bernander, R. J. Douglas, K. A. C. Martin, and C. Koch. Synaptic background activity influences spatiotemporal integration in single pyramidal cells. *Proc. Natl. Acad. Sci. USA*, 88:11569–11573, 1991.

[20] L. S. Bernardo and D. A. Prince. Cholinergic excitation of mammalian hippocampal pyramidal cells. *Brain Research*, 249:315–331, 1982a.

[21] L. S. Bernardo and D. A. Prince. Ionic mechanisms of cholinergic excitation in mammalian hippocampal pyramidal cells. *Brain Research*, 249:333–344, 1982b.

[22] U. S. Bhalla, D. H. Bilitch, and J. M. Bower. Rallpacks: a set of benchmarks for neuronal simulators. *Trends In Neurosciences*, 15(11), 1992. Available from ftp://genesis.bbb.caltech.edu/pub/genesis.

[23] U. S. Bhalla and J. M. Bower. Exploring parameter space in detailed single neuron models: simulations of the mitral and granule cells of the olfactory bulb. *Journal of Neurophysiology*, 69(6), June 1993.

[24] D. K. Bilkey and P. A. Schwartzkroin. Variation in electrophysiology and morphology of hippocampal CA3 pyramidal cells. *Brain Research*, 514:77–83, 1990.

[25] A. L. Blatz and K. L. Magleby. Calcium-activated potassium channels. *Trends In Neurosciences*, pages 463–67, November 1987.

[26] L. Borg-Graham. Modelling the electrical behavior of cortical neurons – simulations of hippocampal pyramidal cells. In R. M. J. Cotterill, editor, *Computer Simulation in Brain Science*. Cambridge University Press, 1987a.

[27] L. Borg-Graham. Modelling the somatic electrical behavior of hippocampal pyramidal neurons. Master's thesis, Massachusetts Institute of Technology, 1987b. Also appears as MIT AI Laboratory Technical Report 1161 (1989).

[28] L. Borg-Graham. Simulations suggest information processing roles for the diverse currents in hippocampal neurons. In D. Z. Anderson, editor, *Neural Information Processing Systems*. American Institute of Physics, 1987c.

[29] L. Borg-Graham. Modelling the non-linear conductances of excitable membranes. In J. Chad and H. Wheal, editors, *Cellular Neurobiology: A Practical Approach*, chapter 13, pages 247–275. IRL/Oxford University Press, 1991.

[30] L. Borg-Graham. The SURF-HIPPO neuron simulation program. ftp://ftp.ai.mit.edu/pub/surf-hippo, 1995. v.2.5.

[31] L. Borg-Graham, C. Monier, and Y. Frégnac. Voltage-clamp measurements of visually-evoked conductances with whole-cell patch recordings in primary visual cortex. *Journal of Physiology [Paris]*, 90:185–188, 1996.

[32] J. M. Bower and D. Beeman. *The Book of GENESIS: Exploring Realistic Neural Models with the GEneral NEural SImulation System.* TELOS/Springer-Verlag, 1994.

[33] J. M. Bower and C. Koch. Experimentalists and modelers: can we all just get along? *Trends In Neurosciences*, 15(11):458–461, 1992.

[34] D. Brown and W. Griffith. Calcium activated outward current in voltage clamped hippocampal neurones of the guinea pig. *Journal of Physiology*, 337:287–301, 1983a.

[35] D. Brown and W. Griffith. Persistent slow inward calcium current in voltage clamped hippocampal neurones of the guinea pig. *Journal of Physiology*, 337:303–320, 1983b.

[36] D. A. Brown, B. H. Gähwiler, W. H. Griffith, and J. V. Halliwell. Membrane currents in hippocampal neurons. In J. Storm-Mathisen, J. Zimmer, and O.P. Ottersen, editors, *Progress in Brain Research*, volume 83, pages 141–160. Elsevier Science Publishers B. V. (Biomedical Division), 1990.

[37] T. H. Brown, R. A. Fricke, and D. H. Perkel. Passive electrical constants in three classes of hippocampal neurons. *Journal of Neurophysiology*, 46(4):812–827, October 1981.

[38] T. H. Brown, A. M. Zador, Z. F. Mainen, and B. J. Claiborne. Hebbian computations in hippocampal dendrites and spines. In T. McKenna, J. Davis, and S.F. Zornetzer, editors, *Single Neuron Computation*. Academic Press, 1992.

[39] P. S. Buckmaster, B. W. Strowbridge, and P. A. Schwartzkroin. A comparison of rat hippocampal mossy cells and CA3c pyramidal cells. *Journal of Neurophysiology*, 70(4), October 1993.

[40] P.-Y. Burgi and N. M. Gryzwacz. Model based on extracellular potassium for spontaneous synchronous activity in developing retina. *Neural Computation*, 6:983–1004, 1994.

[41] P. C. Bush and T. J. Sejnowski. Simulations of a reconstructed cerebellar purkinje cell based on simplified channel kinetics. *Neural Computation*, 3:321–332, 1991.

[42] P. C. Bush and T. J. Sejnowski. Effects of inhibition and dendritic saturation in simulated neocortical pyramidal cells. *Journal of Neurophysiology*, 71(6):2183–2193, 1994.

[43] M. Caeser, D. A. Brown, B. H. Gähwiler, and T. Knöpfel. Characterization of a calcium-dependent current generating a slow afterdepolarization of CA3 pyramidal cells in rat hippocampal slice cultures. *European Journal of Neuroscience*, 5:560–569, 1993.

[44] L. W. Campbell, S. Hao, O. Thibault, E. M. Blalock, and P. W. Landfield. Aging changes in voltage-gated calcium currents in hippocampal CA1 neurons. *Journal of Neuroscience*, 16:6286–6295, 1996.

[45] A. R. Cantrell, J. Y. Ma, T. Scheuer, and W. A. Catterall. Muscarinic modulation of sodium current by activation of protein kinase C in rat hippocampal neurons. *Neuron*, 16:1019–1026, 1996.

[46] N. T. Carnevale, K. Y. Tsai, and B. J. Claiborne. Qualitative electrotonic comparison of three classes of hippocampal neurons in the rat. In J. Bower, editor, *Neurobiology of Computation*. Kluwer Academic Publishers, 1995. Vol. 4.

[47] S. Charpak, B. H. Gähwiler, K. Q. Do, and T. Knöpfel. Potassium conductances in hippocampal neurons blocked by excitatory amino-acid transmitters. *Nature*, 347, October 1990.

[48] B. R. Christie, L. S. Eliot, K. Ito, H. Miyakawa, and D. Johnston. Different Ca^{2+} channels in soma and dendrites of hippocampal pyramidal neurons mediate spike-induced Ca^{2+} influx. *Journal of Neurophysiology*, 73(6):2553–2557, June 1995.

[49] J. Church. A change from HCO_3^--CO_2- to HEPES-buffered medium modifies membrane properties of rat CA1 pyramdical neurones *in vitro*. *Journal of Physiology*, 455:51–71, 1992.

[50] B. J. Claiborne, A. M. Zador, Z. F. Mainen, and T. H. Brown. Computational models of hippocampal neurons. In T. McKenna, J. Davis, and S.F. Zornetzer, editors, *Single Neuron Computation*. Academic Press, 1992.

[51] A. Colino and J. V. Halliwell. Differential modulation of three separate K-conductances in hippocampal CA1 neurons by serotonin. *Nature*, 328:73–77, July 1987.

[52] A. Colino and J. V. Halliwell. Carbachol potentiates Q current and activates a calcium-dependent non-specific conductance in rat hippocampus *in-vitro*. *European Journal of Neuroscience*, 5:1198–1209, 1993.

[53] D. Colquhoun and A. G. Hawkes. The principles of the stochastic interpretation of ion-channel mechanisms. In B. Sakmann and E. Neher, editors, *Single-Channel Recording, 2nd edition*, chapter 18, pages 397–482. Plenum Press, New York, 1995.

[54] B. W. Connors and M. J. Gutnick. Intrinsic firing patterns of diverse neocortical neurons. *Trends in Neuroscience*, 13(3):99–104, 1990.

[55] J. Cooley and F. Dodge. Digital computer solutions for excitation and propagation of the nerve impulse. *Biophysics Journal*, 6, 1966.

[56] V. Crépel, L. Aniksztejn, Y. Ben-Ari, and C. Hammond. Glutamate metabotropic receptors increase a Ca^{2+}-activated nonspecific cationic current in CA1 hippocampal neurons. *Journal of Neurophysiology*, 72(4):1561–1569, October 1994.

[57] W. E. Crill. Persistent sodium current in mammalian central neruons. In *Annual Review of Physiology*, pages 349–362. Annual Reviews Incorporated, 1996. Vol. 58.

[58] T. R. Cummins, Y. Xia, and G. G. Haddad. Functional properties of rat and human neocortical voltage-sensitive sodium currents. *Journal of Neurophysiology*, 71(3), March 1994.

[59] E. De Schutter and J. M. Bower. An active membrane model of the cerebellar purkinje cell I. Simulation of current clamps in slice. *Journal of Neurophysiology*, 71(3):375–400, January 1994.

[60] E. D. De Schutter. A consumer guide to neuronal modeling software. *Trends In Neurosciences*, 15(11), 1992.

[61] R. A. Deisz. A tetrodotoxin-insensitive sodium current initiates burst firing of neocortical neurons. *Neuroscience*, 70(2):341–351, 1996.

[62] A. Destexhe, Contreras, M. D. Steriade, T. Sejnowski, and J. Huguenard. In vivo, in vitro and computational analysis of dendritic calcium currents in thalamic reticular neurons. *Journal of Neuroscience*, 1995.

[63] A. Destexhe, Z. F. Mainen, and T. Sejnowski. Synthesis of models for excitable membranes, synaptic transmission and neuromodulation using a common kinetic formalism. *Journal of Computational Neuroscience*, 1:195–230, 1994.

[64] J. Deuchars and A. M. Thomson. CA1 pyramid-pyramid connections in rat hippocampus *in-vitro*: dual intracellular recordings with biocytin filling. *Neuroscience*, 74(4):1009–1018, 1996.

[65] D. Doerner, M. Abdel-Latif, T. B. Rogers, and B. E. Alger. Protein kinase C-dependent and -independent effects of phorbol esters on hippocampal calcium channel current. *Journal of Neuroscience*, 10(5):1699–1706, May 1990.

[66] C. Eder, R. Klee, and U. Heinemann. Modulation of A-currents by $[K^+]_o$ in acutely isolated pyramidal neurones of juvenile rat entorhinal cortex and hippocampus. *Neuroreport*, 7:1565–1568, 1996.

[67] R. S. el-Mallakh and R. J. Wyatt. The Na,K-ATPase hypothesis for bipolar illness. *Biological Psychiatry*, 37(4):235–244, February 1995.

[68] J. D. Evans, G. C. Kember, and G. Major. Techniques for obtaining analytical solutions to the multicylinder somatic shunt cable model for passive neurones. *Biophysical Journal*, 63:350–365, 1992.

[69] E. Ficker and U. Heinemann. Slow and fast transient potassium currents in cultured rat hippocampal cells. *Journal of Physiology*, 445:431–445, 1992.

[70] A. Figenschou, G.-Y. Hu, and J. F. Storm. Cholinergic modulation of the action potential in rat hippocampal neurons. *European Journal of Neuroscience*, 8:211–219, 1996.

[71] R. E. Fisher, R. Gray, and D. Johnston. Properties and distribution of single voltage-gated calcium channels in adult hippocampal neurons. *Journal of Neurophysiology*, 64(1), July 1990.

[72] W. R. Foster, L. H. Ungar, and J. S. Schwaber. Significance of conductances in Hodgkin-Huxley models. *Journal of Neurophysiology*, 70(6), December 1993.

[73] D. D. Fraser and B. A. MacVicar. Cholinergic-dependent plateau potential in hippocampal CA1 pyramidal neurons. *Journal of Neuroscience*, 16(13):4113–4128, 1996.

[74] C. French and P. Gage. A threshold sodium current in pyramidal cells in rat hippocampus. *Neuroscience Letters*, 56:289–293, 1985.

[75] C. French, P. Sah, K. J. Buckett, and P. Gage. A voltage-dependent persistent sodium current in mammalian hippocampal neurons. *Journal of General Physiology*, 95:1139–1157, 1990.

[76] A. Fukuda and D. A. Prince. Postnatal development of electrogenic sodium pump activity in rat hippocampal pyramidal neurons. *Developmental Brain Research*, 65:101–114, 1992.

[77] Z. Galdzicki, E. Coan, and S. I. Rapoport. Cultured hippocampal neurons from trisomy 16 mouse, a model for Down's syndrome, have an abnormal action potential due to a reduced inward sodium current. *Brain Research*, 604:69–78, 1993.

[78] I. M. Glynn. All hands to the sodium pump. *Journal of Physiology*, 462:1–30, 1993.

[79] S. A. N. Goldstein and T. J. Colatsky. Ion channels: Too complex for rational drug design? *Neuron*, 16:913–919, 1996.

[80] E. A. Grove and J. V. Halliwell. Two inward rectifier currents revealed in CA1 neurones of the rat hippocampus *in vitro*. *Journal of Physiology*, 424:46P, 1990.

[81] H. L. Haas, J. G. R. Jefferys, N. T. Slater, and D. O. Carpenter. Modulation of low calcium induced field bursts in the hippocampus by monoamines and cholinomimetics. *European Journal of Physiology*, 400:28–33, 1984.

[82] S. Hagiwara and L. Byerly. Calcium channel. In *Annual Review of Neuroscience*. Annual Reviews Incorporated, 1981. Vol. 4.

[83] M. M. Haglund and P. A. Schwartzkroin. Role of Na-K pump potassium regulation and IPSPs in seizures and spreading depression in immature rabbit hippocampal slices. *Journal of Neurophysiology*, 63(2):225–239, February 1990.

[84] J. Halliwell and P. Adams. Voltage clamp analysis of muscarinic excitation in hippocampal neurons. *Brain Research*, 250:71–92, 1982.

[85] J. V. Halliwell, I. B. Othman, A. Pelchen-Matthews, and J. O. Dolly. Central action of dendrotoxin: selective reduction of a transient K conductance in hippocampus and binding to localized receptors. *Proceedings of the National Academy of Sciences*, 83:493–497, January 1986.

[86] K. M. Harris, F. E. Jensen, and B. Tsao. Three-dimensional structure of dendritic spines and synapses in rat hippocampus (CA1) at postnatal day 15 and adult ages: implications for the maturation of synaptic physiology and long-term potentiation. *Journal of Neuroscience*, 12:2685–2705, 1992.

[87] P. Hess and R. Tsien. Mechanism of ion permeation through calcium channels. *Nature*, 3, May 1984.

[88] B. Hille. *Ionic Channels of Excitable Membranes*. Sinauer Associates, Sunderland, Massachusetts, 1992. Second edition.

[89] M. Hines. Efficient computation of branched nerve equations. *Int. J. Bio-Medical Computing*, 15:69–76, 1984.

[90] M. Hines. NEURON — a program for simulation of nerve equations. In F. Eeckman, editor, *Neural Systems: Analysis and Modeling*. Kluwer Academic Publishers, 1992. Vol. 2, http://www.nnc.yale.edu/HTML/YALE/NNC/neuron/neuron.html.

[91] M. Hines and N. T. Carnevale. Computer simulation methods for neurons. In M. Arbib, editor, *The Handbook of Brain Theory and Neural Networks*. MIT Press, 1994.

[92] A. L. Hodgkin. Chance and design in electrophysiology: an informal account of certain experiments on nerve carried out between 1934 and 1952. *Journal of Physiology*, 263:1–21, 1976.

[93] A. L. Hodgkin and A. F. Huxley. Currents carried by sodium and potassium ions through the membrane of the giant axon of *Loligo*. *Journal of Physiology*, 116:449–72, 1952a.

[94] A. L. Hodgkin and A. F. Huxley. A quantitative description of membrane current and its application to conduction and excitation in nerve. *Journal of Physiology*, 117:500–44, 1952b.

[95] K. Hoehn, T. W. J. Watson, and B. A. MacVicar. A novel tetrodotoxin-insensitive, slow sodium current in striatal and hippocampal neurons. *Neuron*, 10:543–552, March 1993.

[96] W. R. Holmes and W. B. Levy. Insights into associative long-term potentiation from computational models of NMDA receptor-mediated calcium influx and intracellular calcium concentration changes. *Journal of Neurophysiology*, 63(5):1148–1168, May 1990.

[97] W. R. Holmes and W. Rall. Electrotonic length estimates in neurons with dendritic tapering or somatic shunt. *Journal of Neurophysiology*, 68(4), October 1992a.

[98] W. R. Holmes and W. Rall. Electrotonic models of neuronal dendrites and single neuron computation. In T. McKenna, J. Davis, and S.F. Zornetzer, editors, *Single Neuron Computation*. Academic Press, 1992b.

[99] W. R. Holmes and W. Rall. Estimating the electrotonic structure of neurons with compartmental models. *Journal of Neurophysiology*, 68(4), October 1992c.

[100] W. R. Holmes, I. Segev, and W. Rall. Interpretation of time constant and electrotonic length estimates in multicylinder or branched neuronal structures. *Journal of Neurophysiology*, 68(4), October 1992.

[101] J. R. Hotson, D. Prince, and P. Schwartzkroin. Anomalous inward rectification in hippocampal neurons. *Journal of Neurophysiology*, 42:889–895, May 1979.

[102] J. R. Hotson and D. A. Prince. A calcium-activated hyperpolarization follows repetitive firing in hippocampal neurons. *Journal of Neurophysiology*, 43(2):409–419, 1980.

[103] J. R. Huguenard, O. P. Hamill, and D. A. Prince. Developmental changes in Na^+ conductances in rat neocortical neurons: appearance of a slowly inactivating component. *Journal of Neurophysiology*, 59(3), March 1988.

[104] J. R. Huguenard and D. A. McCormick. Simulation of the currents involved rhythmic oscillations in thalamic relay neurons. *Journal of Neurophysiology*, 68(4), 1992. October.

[105] Y. Ikemoto, K. Ono, A. Yoshida, and N. Akaike. Delayed activation of large-conductance Ca^{2+}-activated K channels in hippocampal neurons of the rat. *Biophysical Journal*, 56:207–212, July 1989.

[106] J. J. B. Jack, D. Noble, and R. W. Tsien. *Electric Current Flow In Excitable Cells*. Clarendon Press, Oxford, 1983.

[107] D. B. Jaffe, D. Johnston, N. Lasser-Ross, J. E. Lisman, H. Miyakawa, and W. N. Ross. The spread of Na^+ spikes determines the pattern of dendritic Ca^{++} entry into hippocampal neurons. *Nature*, 357, May 1992.

[108] D. B. Jaffe, W. N. Ross, J. E. Lisman, N. Lasser-Ross, H. Miyakawa, and D. Johnston. A model for dendritic Ca^{2+} accumulation in hippocampal pyramidal neurons based on fluorescence imaging measurements. *Journal of Neurophysiology*, 71(3), March 1994.

[109] M. S. Jensen, R. Azouz, and Y. Yaari. Variant firing patterns in rat hippocampal pyramidal cells modulated by extracellular potassium. *Journal of Neurophysiology*, 71(3):831–839, March 1994.

[110] M. S. Jensen, R. Azouz, and Y. Yaari. Spike after-depolarization and burst generation in adult rat hippocampal CA1 pyramidal cells. *Journal of Physiology*, 492:199–210, 1996.

[111] O. Jensen, M. A. Idiart, and J. E. Lisman. Physiologically realistic formation of autoassociative memory in networks with theta/gamma oscillations: role of fast NMDA channels. *Learning and Memory*, 3:243–256, 1996b.

[112] A. R. Johnston, C. Black, J. Fraser, and N. MacLeod. Scrapie infection alters the membrane and synaptic properties of mouse hippocampal CA1 pyramidal neurones. *Journal of Physiology*, 500(1):1–15, 1997.

[113] D. Johnston and T. Brown. Interpretation of voltage-clamp measurements in hippocampal neurons. *Journal of Neurophysiology*, 50(2), August 1983.

[114] D. Johnston, J. Hablitz, and W. Wilson. Voltage clamp discloses slow inward current in hippocampal burst-firing neurones. *Nature*, 286, 1980.

[115] D. Johnston, J. C. Magee, C. M. Colbert, and B. R. Christie. Active properties of neuronal dendrites. In *Annual Review of Neuroscience*, pages 165–186. Annual Reviews Incorporated, 1996. Vol. 19.

[116] S. W. Jones. On the resting potential of isolated frog sympathetic neurons. *Neuron*, 3:153–161, August 1989.

[117] L. K. Kaczmarek and I. B. Levitan, editors. *Neuromodulation: The Biochemical Control of Neuronal Excitability*. Oxford University Press, 1987.

[118] E. R. Kandel and W. A. Spencer. Electrophysiology of hippocampal neurons: IV. fast pre-potentials. *Journal of Neurophysiology*, 24:272–285, 1961.

[119] B. Katz. Les constantes electriques de la membrane du muscle. *Arch. Sci. Physiol.*, 3:285–299, 1949.

[120] A. R. Kay. Inactivation kinetics of calcium current of acutely dissociated CA1 pyramidal cells of the mature guinea-pig hippocampus. *Journal of Physiology*, 437:27–48, 1991.

[121] A. R. Kay and R. K. S. Wong. Calcium current activation kinetics in isolated pyramidal neurones of the CA1 region of the mature guinea-pig hippocampus. *Journal of Physiology*, 392:603–616, 1987.

[122] H. Kettenmann and R. Grantyn, editors. *Practical Electrophysiological Methods*. Wiley-Liss, 1992.

[123] T. Knöpfel, D. A. Brown, I. Vranesic, and B. H. Gähwiler. Depression of Ca^{2+} activated potassium conductance by muscarine and isoproternenol without alteration of depolarization-induced transient rise in cytosolic free Ca^{2+} in hippocampal CA3 pyramidal cells. *European Journal of Neuroscience*, 2(92), 1989. Suppl.

[124] C. Koch, T. Poggio, and V. Torre. Nonlinear interactions in a dendritic tree: Localization, timing, and role in information processing. *Proc. Natl. Acad. Sci.*, 80:2799–2802, 1983.

[125] M. Köhler, B. Hirschberg, C. T. Bond, J. M. Kinzie, N. V. Marrion, J. Maylie, and J. P. Adelman. Small-conductance, calcium-activated potassium channels from mammalian brain. *Science*, 273:1709–1714, 1996.

[126] A. Konnerth, H. D. Lux, and U. Heinemann. Ionic properties of burst generation in hippocampal pyramidal cells. In U. Heinemann, M. Klee, E. Neher, and W. Singer, editors, *Calcium Electrogenesis and Neuronal Functioning*, pages 368–374. Berlin: Springer Verlag, 1986.

[127] C. C. Kuo and P. B. Bean. Na^+ channels must deactivate to recover from inactivation. *Neuron*, 12:819–829, 1994.

[128] B. Lancaster and P. Adams. Calcium dependent current generating the afterhyperpolarization of hippocampal neurons. *Journal of Neurophysiology*, 1986.

[129] B. Lancaster and R. A. Nicoll. Properties of two calcium-activated hyperpolarizations in rat hippocampal neurones. *Journal of Physiology*, 389:187–203, 1987.

[130] B. Lancaster, R. A. Nicoll, and D. J. Perkel. Calcium activates two types of potassium channels in rat hippocampal neurons in culture. *Journal of Neuroscience*, 11(23), 1991.

[131] B. Lancaster and R. S. Zucker. Photolytic manipulation of Ca^{2+} and the time course of slow, Ca^{2+}-activated K^+ current in rat hippocampal neurones. *Journal of Physiology*, 475(2):229–239, 1994.

[132] P. W. Landfield and T. A. Pitler. Prolongation of calcium-dependent afterhyperpolarizations in hippocampal neurons in aged rats. *Science*, 226:1089–1091, November 1984.

[133] T. Lanthorn, J. Storm, and P. Anderson. Current to frequency transduction in CA1 hippocampal pyramidal cells: Slow prepotentials dominate the primary range firing. *Experimental Brain Research*, 53:431–443, 1984.

[134] P. Läuger. *Electrogenic Ion Pumps*. Sinauer Associates, Sunderland, Massachusetts, 1991.

[135] R. Lipowsky, T. Gillessen, and C. Alzheimer. Dendritic Na^+ channels amplify EPSPs in hippocampal CA1 pyramidal cells. *Journal of Neurophysiology*, 76(4):2181–2191, October 1996.

[136] J. Lisman. Bursts as a unit of neural information: making unreliable synapses reliable. *Trends In Neurosciences*, 20(1):38–43, 1996.

[137] R. Llinás, M. Sugimori, and R. B. Silver. Time resolved calcium microdomains and synaptic transmission. *J. Physiol. Paris*, 89:77–81, 1995.

[138] A. Lüthi, B. H. Gähwiler, and U. Gerber. A slowly inactivating potassium current in CA3 pyramidal cells of rat hippocampus *in-vitro*. *Journal of Neuroscience*, 16(2):586–594, 1996.

[139] W. W. Lytton and T. J. Sejnowski. Simulations of cortical pyramidal neurons synchronized by inhibitory interneurons. *Journal of Neuroscience*, 66(3), September 1991.

[140] G. Maccaferri, M. Mangoni, A. Lazzari, and D. DiFrancesco. Properties of the hyperpolarization-activated current in rat hippocampal CA1 cells. *Journal of Neurophysiology*, 69(6):2129–2136, June 1993.

[141] B. A. MacVicar. Depolarizing prepotential are Na^+ dependent in CA1 pyramidal neurons. *Brain Research*, 333:378–381, 1985.

[142] D. V. Madison, A. P. Fox, and R. W. Tsien. Adenosine reduces an inactivating component of calcium current in hippocampal CA3 neurons. *Biophysical Journal*, 51(30a), 1987.

[143] D. V. Madison, B. Lancaster, and R. A. Nicoll. Voltage clamp analysis of cholinergic action in the hippocampus. *Journal of Neuroscience*, 7(3):733–741, March 1987.

[144] D. V. Madison, R. C. Malenka, and R. A. Nicoll. Phorbol esters block a voltage-sensitive chloride current in hippocampal pyramidal cells. *Nature*, 321:695–697, June 1986.

[145] D. V. Madison and R. A. Nicoll. Control of repetitive discharge of rat CA1 pyramidal neurones in vitro. *J. Physiol.*, 354:319–331, 1984.

[146] J. C. Magee, R. B. Avery, B. R. Christie, and D. Josnston. Dihydropyridine-sensitive, voltage-gated Ca^{2+} channels contribute to the resting intracellular Ca^{2+} concentration of hippocampal CA1 pyramidal neurons. *Journal of Neurophysiology*, 76(5):3460–3470, November 1996.

[147] J. C. Magee and D. Johnston. Characterization of single voltage-gated Na^+ and Ca^{2+} channels in apical dendrites of rat CA1 pyramidal neurons. *Journal of Physiology*, 487(1):67–90, 1995.

[148] J. Magistretti, M. Mantegazza, E. Guatteo, and E. Wanke. Action potentials recorded with patch-clamp amplifiers: are they genuine? *Trends In Neurosciences*, 19(12):530–534, 1996.

[149] Z. F. Mainen, N. T. Carnevale, A. M. Zador, B. J. Claiborne, and T. H. Brown. Electrotonic architecure of hippocampal CA1 pyramidal neurons based on three-dimensional reconstructions. *Journal of Neurophysiology*, 76(3):1904–1923, 1996.

[150] Z. F. Mainen, J. Joerges, J. R. Huguenard, and T. J. Sejnowski. A model of spike initiation in neocortical pyramidal neurons. *Neuron*, 15:1427–1439, December 1995.

[151] Z. F. Mainen and T. J. Sejnowski. Influence of dendritic structure on firing patterns in model neocortical neurons. *Nature*, 382:363–366, July 1996.

[152] G. Major, A. U. Larkman, P. Jonas, B. Sakmann, and J. J. B. Jack. Detailed passive cable models of whole-cell recorded CA3 pyramidal neurons in rat hippocampal slices. *Journal of Neuroscience*, 14(8):4613–4638, 1994.

[153] R. C. Malenka, B. Lancaster, and R. S. Zucker. Temporal limits on the rise in postsynaptic calcium required for the induction of long-term potentiation. *Neuron*, 9:121–128, 1992.

[154] A. Marty and E. Neher. Tight-seal whole-cell recording. In B. Sakmann and E. Neher, editors, *Single-Channel Recording, 2nd edition*, chapter 2, pages 31–51. Plenum Press, New York, 1995.

[155] M. Mascagni and A. S. Sherman. Numerical methods for neuronal modeling. In C. Koch and I. Segev, editors, *Methods in Neuronal Modeling*, volume 2, chapter 13. MIT Press/Bradford Books, 1998.

[156] L. Masukawa and D. Prince. Synaptic control of excitability in isolated dendrites of hippocampal neurons. *Journal of Neuroscience*, 4(1):217–227, January 1984.

[157] L. M. Masukawa, L. S. Benardo, and D. A. Prince. Variations in electrophysiological properties of hippocampal neurons in different subfields. *Brain Research*, 242:341–344, 1982.

[158] L. M. Masukawa and A. Hansen. Regional distribution of voltage-dependent single channel conductances in cultured hippocampal neurons from the rat. In *Neuroscience Abstracts*, page 1442. Society for Neuroscience, 1987.

[159] L. M. Masukawa, A. J. Hansen, and G. Shepard. Distribution of single-channel conductances in cultured rat hippocampal neurons. *Cellular and Molecular Neurobiology*, 11(2), 1991.

[160] D. A. McCormick and H. C. Pape. Properties of a hyperpolarization-activated cation current and its role in rhythmic oscillation in thalamic relay neurones. *Journal of Physiology*, 431:291–318, 1990.

[161] T. McKenna, J. Davis, and S. F. Zornetzer, editors. *Single Neuron Computation*. Academic Press, 1992.

[162] O. B. McManus and K. L. Magleby. Kinetic time constants independent of previous single-channel activity suggest markov gating for a large-conductance Ca-activated K channel. *Journal of General Physiology*, 94:1037–1070, December 1989.

[163] C. L. Meier and F. E. Dudek. Spontaneous and stimulation-induced synchronized burst afterdischarges in the isolated CA1 of kainate-treated rats. *Journal of Neurophysiology*, 76(4):2231–2239, October 1996.

[164] B. Mel. Information processing in dendritic trees. *Neural Computation*, 6:1031–1085, 1994.

[165] M. Migliore, E. P. Cook, D. B. Jaffe, D. A. Turner, and D. Johnston. Computer simulations of morphologically reconstructed CA3 hippocampal neurons. *Journal of Neurophysiology*, 73(3), March 1995.

[166] H. Miyakawa, W. N. Ross, D. Jaffe, J. C. Callaway, N. Lasser-Ross, J. E. Lisman, and D. Johnston. Synaptically activated increases in Ca^{2+} concentration in hippocampal CA1 pyramidal cells are primarily due to voltage-gated Ca^{2+} channels. *Neuron*, 9:1163–1173, December 1992.

[167] E. Moczydlowski and R. Latorre. Gating kinetics of Ca^{2+}-activated K^+ channels from rat muscle incorporated into planar lipid bilayers. *Journal of General Physiology*, 82, October 1983.

[168] J. Moore, N. Stockbridge, and M. Westerfield. On the site of impulse initiation in a neurone. *Journal of Physiology*, 336:301–311, 1983.

[169] W. Müller and H. D. Lux. Analysis of voltage-dependent membrane currents in spatially extended neurons from point-clamp data. *Journal of Neurophysiology*, 69(1):241–247, January 1993.

[170] Y. Nakajima, S. Nakajima, R. J. Leonard, and K. Yamaguchi. Acetylcholine raises excitability by inhibiting the fast transient potassium current in cultured hippocampal neurons. *Proc. Natl. Acad. Sci. USA*, 83:3022–3026, May 1986.

[171] M. Nowycky, A. Fox, and R. Tsien. Three types of neuronal calcium channel with different calcium agonist sensitivity. *Nature*, 316, January 1985.

[172] R. E. Numann, W. J. Wadman, and R. K. S. Wong. Outward currents in single hippocampal cells obtained from the adult guinea-pig. *Journal of Physiology*, 393:331–353, 1987.

[173] N. Ogata and H. Tatebayashi. Sodium current kinetics in freshly isolated neostriatal neurones of the adult guinea pig. *European Journal of Physiology*, 416:594–603, 1990.

[174] D. Y. Okuhara and S. G. Beck. 5-HT_{1A} receptor linked to inward-rectifying potassium current in hippocampal CA3 pyramidal cells. *Journal of Neurophysiology*, 71(6):2161–2167, June 1994.

[175] D. G. Owen. Three types of inward rectifier currents in cultured hippocampal neurones. *Neuroscience Letters*, 29:S18, 1987. Supplement.

[176] B. S. Pallotta and P. K. Wagoner. Voltage-dependent potassium channels since Hodgkin and Huxley. *Physiological Reviews*, 72(4(Suppl.)):S49–S67, October 1992.

[177] H. C. Pape. Queer current and pacemaker: the hyperpolarization-activated cation current in neurons. In *Annual Review of Physiology*, pages 299–327. Annual Reviews Incorporated, 1996. Vol. 58.

[178] J. Patlak. Molecular kinetics of voltage-dependent Na^+ channels. *Physiological Reviews*, 71(4), October 1991.

[179] P. Pedarzani and J. Storm. PKA mediates the effects of monomamine transmitters on the K^+ current underlying the slow spike frequency adaptation in hippocampal neurons. *Neuron*, 11:1–20, December 1993.

[180] P. Pedarzani and J. Storm. Dopamine modulates the slow Ca^{2+}-activated current I_{AHP} via cyclic AMP-dependent protein kinase in hippocampal neurons. *Journal of Neurophysiology*, 74(6), 1995a.

[181] P. Pedarzani and J. Storm. Protein kinase A-independent modulation of ion channels in the brain by cyclic AMP. *Proc. Natl. Acad. Sci. USA*, 92:11716–11720, 1995b.

[182] P. Pedarzani and J. F. Storm. Interaction between α- and β-adrenergic receptor agonists modulating the slow Ca^{2+}-activated K^+ current I_{AHP} in hippocampal neurons. *European Journal of Neuroscience*, 8:2098–2110, 1996.

[183] K. L. Perkins and R. K. S. Wong. Intracellular QX-314 blocks the hyperpolarization-activated inward current I_q in hippocampal CA1 pyramidal cells. *Journal of Neurophysiology*, 73(2):911–915, February 1995.

[184] F. Pongracz, N. P. Poolos, J. D. Kocsis, and G. M. Shepherd. A model of NMDA receptor-mediated activity in dendrites of hippocampal CA1 pyramidal neurons. *Journal of Neurophysiology*, 68(6):2248–59, December 1992.

[185] G. K. Pyapali and D. A. Turner. Denervation-induced dendritic alterations in CA1 pyramidal cells following kainic acid hippocampal lesions in rats. *Brain Research*, 652:279–290, 1994.

[186] N. Qian and T. J. Sejnowski. An electro-diffusion model for branching dendrites, spines and axons. *Biological Cybernetics*, 62:1–15, 1989.

[187] N. Qian and T. J. Sejnowski. When is an inhibitory synapse effective? *Proceedings of the National Academy of Science*, 87:8145–8149, October 1990.

[188] R. Quadroni and T. Knöpfel. Compartmental models of Type A and Type B guinea pig medial vestibular neurons. *Journal of Neurophysiology*, 72(4):1911–1924, October 1994.

[189] W. Rall. Cable theory for dendritic neurons. In C. Koch and I. Segev, editors, *Methods in Neuronal Modeling*, chapter 2. MIT Press/Bradford Books, 1989.

[190] W. Rall, R. E. Burke, W. R. Holmes, J. J. B. Jack, S. J. Redman, and I. Segev. Matching dendritic neuron models to experimental data. *Physiological Reviews*, 72(4(Suppl.)), October 1992.

[191] M. Rapp, Y. Yarom, and I. Segev. Modeling back propagating action potential in weakly excitable dendrites of neocortical pyramidal cells. *Proc. Natl. Acad. Sci. USA*, 93:11985–11990, October 1996.

[192] W. G. Regehr and D. W. Tank. Calcium concentration dynamics produced by synaptic activation of CA1 hippocampal pyramidal cells. *Journal of Neuroscience*, 12(11):4202–4223, 1992.

[193] K. H. Reid, H. L. Edmonds, A. Schurr, M. T. Tseng, and C. A. West. Pitfalls in the use of brain slices. *Progress in Neurobiology*, 31(1):1–18, 1988.

[194] P. A. Rhodes and C. M. Gray. Simulations of intrinsically bursting neocortical pyramidal neurons. *Neural Computation*, 6:1086–1110, 1994.

[195] W. M. Roberts, R. A. Jacobs, and A. J. Hudspeth. Colocalization of ion channels involved in frequency selectivity and synaptic transmission at presynaptic active zones of hair cells. *Journal of Neuroscience*, 10(11):3664–3684, November 1990.

[196] R. Robitaille, M. L. Garcia, G. J. Kaczorowski, and M. P. Charlton. Functional colocalization of calcium and calcium-gated potassium channels in control of transmitter release. *Neuron*, 11:645–655, October 1993.

[197] S. N. Roper, A. Obenaus, and F. E. Dudek. Increased propensity for nonsynaptic epileptiform activity in immature rat hippocampus and dentate gyrus. *Journal of Neurophysiology*, 70(2):857–862, August 1993.

[198] C. R. Rose and B. R. Ransom. Regulation of intracellular sodium in cultured rat hippocampal neurones. *Journal of Physiology*, 499(3):573–587, 1997.

[199] B. Rudy. Diversity and ubiquity of K channels. *Neuroscience*, 25(3):729–749, 1988.

[200] A. Sagar and R. F. Rakowski. Access channel model for the voltage dependence of the forward-running Na^+/K^+ pump. *Journal of General Physiology*, 103(5):869–893, May 1994.

[201] P. Sah. Ca^{2+}-activated K^+ currents in neurones: types, physiological roles and modulation. *Trends in Neurosciences*, 19(4), 1996.

[202] P. Sah and J. M. Bekkers. Apical dendritic location of slow afterhyperpolarization current in hippocampal pyramidal neurons: implications for the integration of long-term potentiation. *Journal of Neuroscience*, 16(15):4537–4542, 1996.

[203] P. Sah, A. J. Gibb, and C. French. Potassium current activated by depolarization of dissociated neurons from adult guinea pig hippocampus. *Journal of General Physiology*, 92:263–278, 1988a.

[204] P. Sah, A. J. Gibb, and P. W. Gage. The sodium current underlying action potentials in guinea pig hippocampal CA1 neurons. *Journal of General Physiology*, 91, March 1988b.

[205] B. Sakmann and E. Neher, editors. *Single-Channel Recording*. Plenum Press, New York, 2 edition, 1995.

[206] H. E. Scharfman. Spiny neurons of area CA3c in rat hippocampal slices have similar electrophysiological characteristics and synaptic responses despite morphological variation. *Hippocampus*, 3(1), January 1993.

[207] A. Schiegg, W. Gerstner, R. Ritz, and J. Leo van Hammen. Intracellular Ca^{2+} stores can account for the time course of LTP induction: a model of Ca^{2+} dynamics in dendritic spines. *Journal of Neurophysiology*, 74(3), September 1995.

[208] J. Schiller, F. Helmchen, and B. Sakmann. Spatial profile of dendritic calcium transients evoked by action potentials in rat neocortical pyramidal neurones. *Journal of Physiology*, 487(3):583–600, 1995.

[209] P. Schwartzkroin. Further characteristics of hippocampal CA1 cells in vitro. *Brain Research*, 128:53–68, 1977.

[210] P. A. Schwartzkroin and M. Slawsky. Probable calcium spikes in hippocampal neurons. *Brain Research*, 135:157–161, 1977.

[211] M. Segal and J. Barker. Rat hippocampal neurons in culture: Potassium conductances. *Journal of Neurophysiology*, 51(6), June 1984.

[212] M. Segal and J. Barker. Rat hippocampal neurons in culture: Calcium and calcium–dependent potassium conductances. *Journal of Neurophysiology*, 55(4):751–766, April 1986.

[213] M. Segal, M. Rogawski, and J. Barker. A transient potassium conductance regulates the excitability of cultured hippocampal and spinal neurons. *Journal of Neuroscience*, 4(2):604–609, February 1984.

[214] I. Segev. Single neuron models: oversimple, complex and reduced. *Trends In Neurosciences*, 15(11):414–421, 1992.

[215] I. Segev, J. W. Fleshman, and R. E. Burke. Compartmental models of complex neurons. In C. Koch and I. Segev, editors, *Methods in Neuronal Modeling*, chapter 3. MIT Press/Bradford Books, 1989.

[216] I. Segev, M. Rapp, Y. Manor, and Y. Yarom. Analog and digital processing in single nerve cells: dendritic integration and axonal propagation. In T. McKenna, J. Davis, and S.F. Zornetzer, editors, *Single Neuron Computation*. Academic Press, 1992.

[217] A. Sherman, J. Keizer, and J. Rinzel. Domain model for Ca^{2+}-inactivation of Ca^{2+} channels at low channel density. *Biophysical Journal*, 58:985–995, October 1990.

[218] R. Sherman-Gold, editor. *The Axon Guide*. Axon Instruments, 1993.

[219] R. R. Sokal and F. J. Rohlf. *Biometry: The principles and practice of statistics in biological research*. W. H. Freeman and Company, 1981.

[220] I. Spigelman, L. Zhang, and P. L. Carlen. Patch-clamp study of postnatal development of CA1 neurons in rat hippocampal slices: membrane excitability and K^+ currents. *Journal of Neurophysiology*, 68(1):55–69, July 1992.

[221] N. Spruston, D. B. Jaffe, S. H. Williams, and D. Johnston. Voltage- and space-clamp errors associated with the measurement of electrotonically remote synaptic events. *Journal of Neurophysiology*, 70(2):781–802, August 1993.

[222] N. Spruston and D. Johnston. Perforated patch-clamp analysis of the passive membrane properties of three classes of hippocampal neurons. *Journal of Neurophysiology*, 67(3):508–529, March 1992.

[223] N. Spruston, Y. Schiller, G. Stuart, and B. Sakmann. Activity-dependent action potential invasion and calcium influx into hippocampal CA1 dendrites. *Science*, 268, 1995.

[224] K. J. Staley, T. S. Otis, and I. Mody. Membrane properties of dentate gyrus granule cells: comparison of sharp microelectrode and whole-cell recordings. *Journal of Neurophysiology*, 67(5), May 1992.

[225] S. F. Stasheff, M. Hines, and W. A. Wilson. Axon terminal hyperexcitability associated with eplieptogenesis in vitro. I. Origin of ectopic spikes. *Journal of Neurophysiology*, 70(3), September 1993.

[226] C. Steinhäuser, M. Tennigkeit, H. Matthies, and J. Gündel. Properties of the fast sodium channels in pyramidal neurones isolated from the CA1 and CA3 areas of the hippocampus of postnatal rats. *Pflügers Arch. - European Journal of Physiology*, 415:756–761, 1990.

[227] N. Stockbridge and J. W. Moore. Dynamics of intracellular calcium and its possible relationship to phasic transmitter release and facilitation at the frog neuromuscular junction. *Journal of Neuroscience*, 4(3):803–811, March 1984.

[228] E. W. Stockley, H. M. Cole, A. D. Brown, and H. V. Wheal. A system for quantitative morphological measurement and electrotonic modelling of neuron: three-dimensional reconstruction. *Journal of Neuroscience Methods*, 47:39–51, 1993.

[229] J. F. Storm. A-current and ca-dependent transient outward current control the initial repetitive firing in hippocampal neurons. *Biophysical Journal*, 49:369a, 1986.

[230] J. F. Storm. Action potential repolarization and a fast after-hyperpolarization in rat hippocampal pyramidal cells. *Journal of Physiology*, 385:733–759, 1987a.

[231] J. F. Storm. Intracellular injection of a Ca^{2+} chelator inhibits spike repolarization in hippocampal neurons. *Brain Research*, 435:387–392, 1987b.

[232] J. F. Storm. Four voltage-dependent potassium currents in adult hippocampal pyramidal cells (HPCs). *Biophysical Journal*, 53:148a, 1988a.

[233] J. F. Storm. Temporal integration by a slowly inactivating K^+ current in hippocampal neurons. *Nature*, 336, November 1988b.

[234] J. F. Storm. An after-hyperpolarization of medium duration in rat hippocampal pyramidal cells. *Journal of Phsysiology*, 409:171–190, 1989.

[235] J. F. Storm. Potassium currents in hippocampal pyramidal cells. In J. Storm-Mathisen, J. Zimmer, and O.P. Ottersen, editors, *Progress in Brain Research*, volume 83, pages 161–187. Elsevier Science Publishers B. V. (Biomedical Division), 1990.

[236] J. F. Storm, L. Borg-Graham, and P. R. Adams. A passive component of the afterdepolarization (ADP) in rat hippocampal pyramidal cells. *Biophysical Journal*, 51:65a, 1987.

[237] J. F. Storm, T. Winther, and P. Pedarzani. h-current modulation by norepinephrine, serotonin, dopamine, histamine and cyclic-amp analogues in rat hippocampal neurons. *Neuroscience Abstracts*, page 1444, 1996.

[238] G. J. Stuart and B. Sakmann. Active propagation of somatic action potentials into neocortical pyramidal cell dendrites. *Nature*, 367, 1994.

[239] O. Thibault and P. W. Landfield. Increase in single L-type calcium channels in hippocampal neurons during aging. *Science*, 272, 1996.

[240] S. M. Thompson and B. H. Gähwiler. Organotypic hippocampal slice cultures. In H. Kettenmann and R. Grantyn, editors, *Practical Electrophysiological Methods*, chapter 2.7, pages 58–61. Wiley-Liss, 1992.

[241] S. M. Thompson, L. M. Masukawa, and D. A. Prince. Temperature dependence of intrinsic membrane properties and synaptic potentials in hippocampal CA1 neurons *in vitro*. *Journal of Neuroscience*, 5(3):817–824, March 1985.

[242] S. M. Thompson and D. A. Prince. Activation of electrogenic sodium pump in hippocampal CA1 neurons following glutamate-induced depolarization. *Journal of Neurophysiology*, 56(2):507–522, August 1986.

[243] I. Tinoco Jr., K. Sauer, and J. C. Wang. *Physical Chemistry: Principles and Applications in Biological Sciences*. Prentice-Hall, 1978.

[244] R. Traub. Simulation of intrinsic bursting in CA3 hippocampal neurons. *Neuroscience*, 7(5):1233–1242, 1982.

[245] R. Traub and R. Llinas. Hippocampal pyramidal cells: Significance of dendritic ionic conductances for neuronal function and epileptogenesis. *Journal of Neurophysiology*, 42(2), March 1979.

[246] R. D. Traub, J. G. R. Jefferys, R. Miles, M. A. Whittington, and K. Tóth. A branching dendritic model of a rodent CA3 pyramidal neurone. *Journal of Physiology*, 481(1), 1994.

[247] R. D. Traub and R. Miles. *Neuronal networks of the hippocampus*. Cambridge University Press, 1991.

[248] R. D. Traub, M. A. Whittington, S. B. Colling, G. Buzsáki, and J. G. R. Jefferys. Analysis of gamma rhythms in the rat hippocampus in vitro and in vivo. *Journal of Physiology*, 1996. In press.

[249] R. D. Traub, R. K. S. Wong, R. Miles, and H. Michelson. A model of a CA3 hippocampal pyramidal neuron incorporating voltage-clamp data on intrinsic conductances. *Journal of Neurophysiology*, 66(2), August 1991.

[250] K. Y. Tsai, N. T. Carnevale, B. J. Claiborne, and T. H. Brown. Efficient mapping from neuroanatomical to electrotonic space. *Network*, 5:21–46, 1994.

[251] D. Turner. Conductance transients onto dendritic spines in a segmental cable model of hippocampal neurons. *Biophysics Journal*, 46:85–96, July 1984a.

[252] D. Turner. Segmental cable evaluation of somatic transients in hippocampal neurons (CA1, CA3, and dentate). *Biophysics Journal*, 46:73–84, July 1984b.

[253] D. Turner and P. A. Schwartzkroin. Steady-state electrotonic analysis of intracellularly stained hippocampal neurons. *Journal of Neurophysiology*, 44(1):184–199, July 1980.

[254] D. Turner and P. A. Schwartzkroin. Passive electrotonic structure and dendritic properties of hippocampal neurons. In R. Dingledine, editor, *Brain Slices*, chapter 4. Plenum Press, 1984.

[255] D. A. Turner, X.-G. Li, G. K. Pyapali, A. Ylinen, and G. Buzsaki. Morphometric and electrical properties of reconstructed hippocampal CA3 neurons recorded in vivo. *Journal of Comparative Neurology*, 356:580–594, 1995.

[256] R. W. Turner, D. E. R. Meyers, T. L. Richardson, and J. L. Barker. The site for initiation of action potential discharge over the somatodendritic axis of rat hippocampal CA1 pyramidal neurons. *Journal of Neuroscience*, 11(7):2270–2280, 1991.

[257] H. Uneyma, S. Ueno, and N. Akaike. Serotonin-operated potassium current in CA1 neurons dissociated from rat hippocampus. *Journal of Neurophysiology*, 69(4):1044–1052, April 1993.

[258] C. A. Vandenberg and F. Bezanilla. A sodium channel gating model based on single-channel, macroscopic ionic, and gating currents in the squid giant axon. *Biophysical Journal*, 60:1511–1533, 1991.

[259] E. Warman, D. Durand, and G. Yuen. Reconstruction of hippocampal CA1 pyramidal cell electrophysiology by computer simulation. *Journal of Neurophysiology*, 71(6):2033–2045, June 1994.

[260] J. C. Wathey. ntscable - Neuron anatomy file conversion program. Modified version available from ftp://ftp.ai.mit.edu/pub/surf-hippo, 1989.

[261] J. C. Wathey, W. W. Lytton, J. M. Jester, and T. J. Sejnowski. Computer simulations of EPSP-spike (E-S) potentiation in hippocampal CA1 pyramidal cells. *Journal of Neuroscience*, 12(2):607–618, February 1992.

[262] R. E. Westenbroek, D. K. Merrick, and W. A. Catterall. Differential subcellular localization of the R_I and R_{II} Na^+ channel subtypes in central neurons. *Neuron*, 3:695–704, 1989.

[263] A. Williamson and B. E. Alger. Characterization of an early afterhyperpolarization after a brief train of action potentials in rat hippocampal neurons in vitro. *Journal of Neurophysiology*, 63(1):72–81, January 1990.

[264] R. K. S. Wong and D. A. Prince. Participation of calcium spikes during intrinsic burst firing in hippocampal neurons. *Brain Research*, 159:385–390, 1978.

[265] R. K. S. Wong and D. A. Prince. Afterpotential generation in hippocampal pyramidal cells. *Journal of Neurophysiology*, 45(1):86–97, January 1981.

[266] R. K. S. Wong, D. A. Prince, and A. I. Basbaum. Intradendritic recordings from hippocampal neurons. *Proceedings of the National Academy of Science*, 76(2):986–990, February 1979.

[267] R. K. S. Wong, R. D. Traub, and R. Miles. Cellular basis of neuronal synchrony in epilepsy. In A. V. Delgado-Esueta, A. A. Ward, Jr., D. M. Woodbury, and R. J. Porter, editors, *Basic mechanisms of the epilepsies. Molecular and cellular approaches. Advances in Neurology*, volume 44, pages 583–592. New York: Raven, 1986.

[268] W. M. Yamada, C. Koch, and P. R. Adams. Multiple channels and calcium dynamics. In C. Koch and I. Segev, editors, *Methods in Neuronal Modeling*, chapter 4. MIT Press/Bradford Books, 1989.

[269] G. L. F. Yuen and D. Durand. Reconstruction of hippocampal granule cell electrophysiology by computer simulation. *Neuroscience*, 41(2/3):411–423, 1991.

[270] A. Zador, C. Koch, and T. H. Brown. Biophysical model of a hebbian synapse. *Proceedings of the National Academy of Sciences*, 87:6718–6722, September 1990.

[271] A. M. Zador. *Biophysics of computation in single hippocampal neurons.* PhD thesis, Yale University, 1993.

[272] A. M. Zador, H. Agmon-Snir, and I. Segev. The morphoelectrotonic transform: a graphical approach to dendritic function. *The Journal of Neuroscience*, 15(3):1669–1682, 1995.

[273] K. Zbicz and F. Weight. Transient voltage and calcium dependent outward currents in hippocampal CA3 pyramidal neurons. *Journal of Neurophysiology*, 53(4), April 1985.

[274] K. Zbicz and F. Weight. Voltage-clamp analysis of inward calcium current in hippocampal CA3 pyramidal neurons. *Neuroscience Abstracts*, 11:520, 1986.

[275] L. Zhang, D. Han, and P. L. Carlen. Temporal specificity of muscarinic synaptic modulation of the Ca^{2+}-dependent K^+ current (I_{sAHP}) in rat hippocampal neurones. *Journal of Physiology*, 496(2):395–405, 1996.

[276] L. Zhang, J. L. Weiner, T. A. Valiante, A. A. Velumian, P. L. Watson, S. S. Jahromi, S. Schertzer, P. Pennefather, and P. L. Carlen. Whole-cell recording of the Ca^{2+}-dependent slow afterhyperpolarization in hippocampal neurones: effects of internally applied anions. *Pflügers Arch. - European Journal of Physiology*, 426:247–253, 1994.

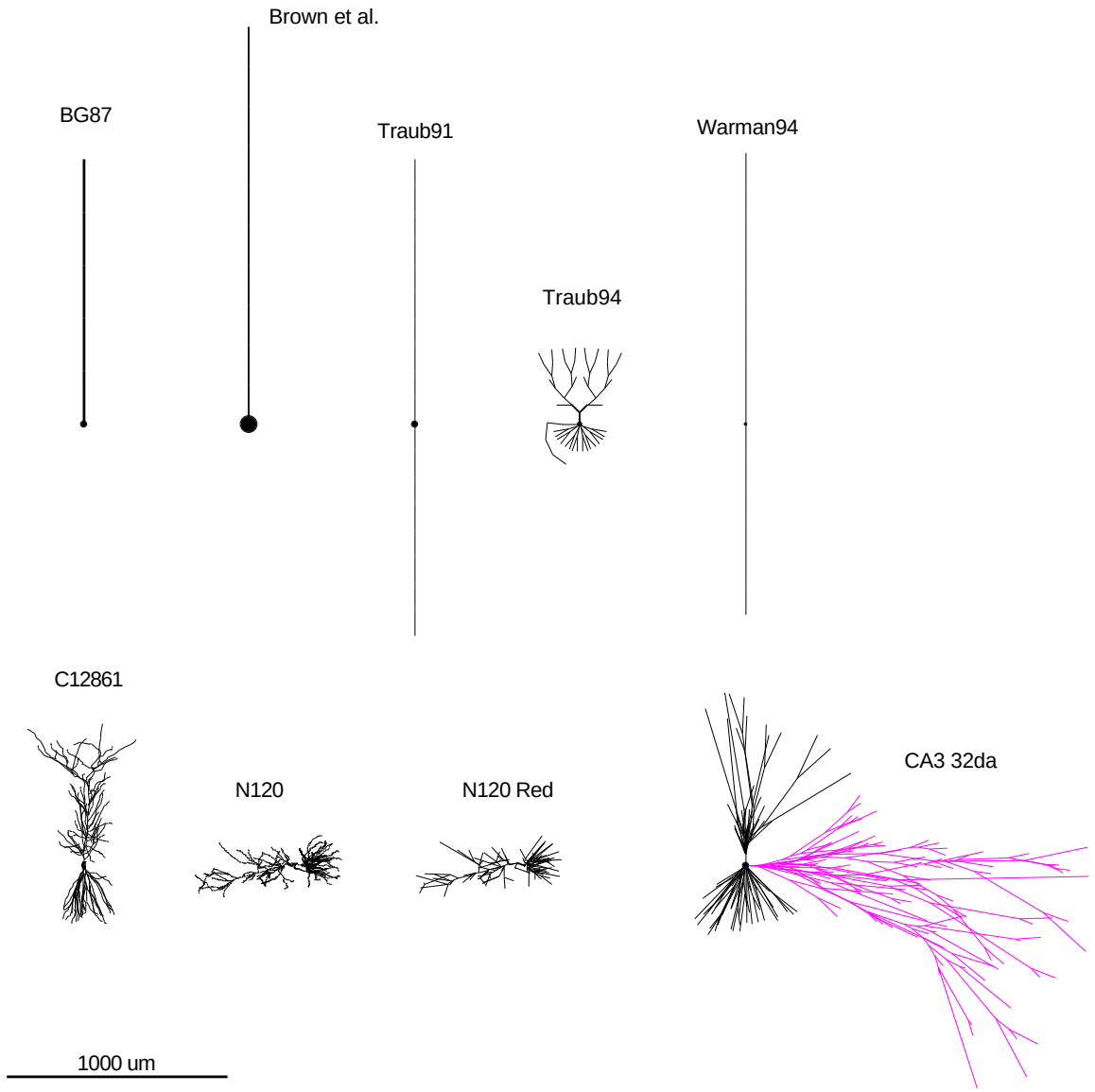

Figure 1: CA1 and CA3 pyramidal cell model anatomies illustrating a range from simplified abstractions to those derived from fully-detailed anatomical data. Models are drawn to scale as represented by the Surf-Hippo neuron simulator. Diameters of non-vertically or horizontally oriented processes are distorted in this figure because of the printing resolution, such that they are drawn as if the diameter was 5μm. Abstracted model anatomies include the BG87 (used in the Working model, six compartments), Traub91 (19 compartments), Traub94 (66 compartments), and Warman94 (16 compartments) models (Section 7.1). The process curving left and down from the soma in the Traub94 anatomy is the axon. The Brown et al. anatomy is a reverse-engineered soma/short-cable model derived from parameters given in Brown et al., 1981, as described in Section 5.3.2. The remaining representations are taken directly or derived from anatomical files. C12861 (941 compartments) is a CA1 cell (supplied by David Amaral, in the ntscable program distribution, Wathey, 1989). A 400 compartment version of this cell, with an axon, was used for the Wathey92 model (Section 7.1). The N120 cell (3205 compartments) is also from CA1, and was supplied by Dennis Turner (appears in Pyapali and Turner, 1994, Figure 3A - although this paper describes dendritic alterations subsequent to kainic acid lesions, this particular cell is from a normal animal). The N120 Red cell (193 compartments) is derived from N120 (see Section 4.2 and Figure 3). The CA3 32da anatomy (367 compartments) was supplied by Guy Major; the original cell is drawn in Figure 9 of Major et al., 1994. The anatomy file did not include 3D locations, so in this rendering an *ad hoc* procedure was applied to branch points to give a reasonable overall shape. Also, the axon was traced in this cell, and is the structure branching off to the right.

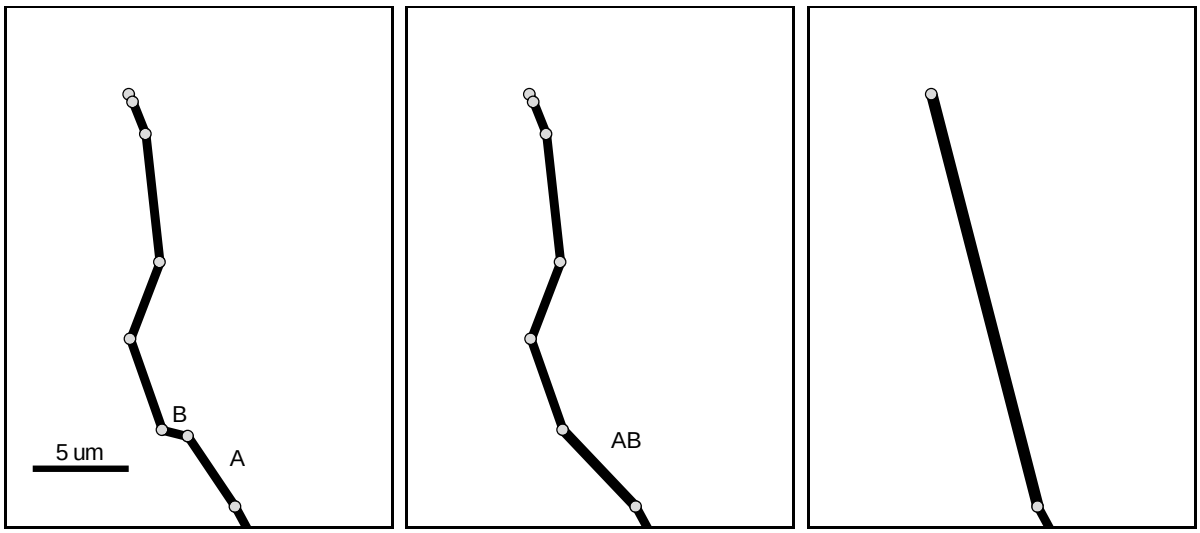

Figure 2:
Demonstration of the consolidation of dendritic compartments. The algorithm described in the text works on successive pairs of dendritic segments, working distally. In the panel on the left, segments A and B are chosen to be consolidated into segment AB, shown in the middle panel. The proximal and distal endpoints of AB correspond to the proximal endpoint of A and the distal endpoint of B, respectively. The panel on the right shows the final result after continuing this procedure down the dendrite, assuming that the electrotonic length of a segment resulting from the consolidation of all the original segments is less than some *a priori* criteria. Notice that the diameter of the final replacement segment is slightly larger than that of the original segments, reflecting the conservation of membrane area in the algorithm and the shorter final path length of the branch.

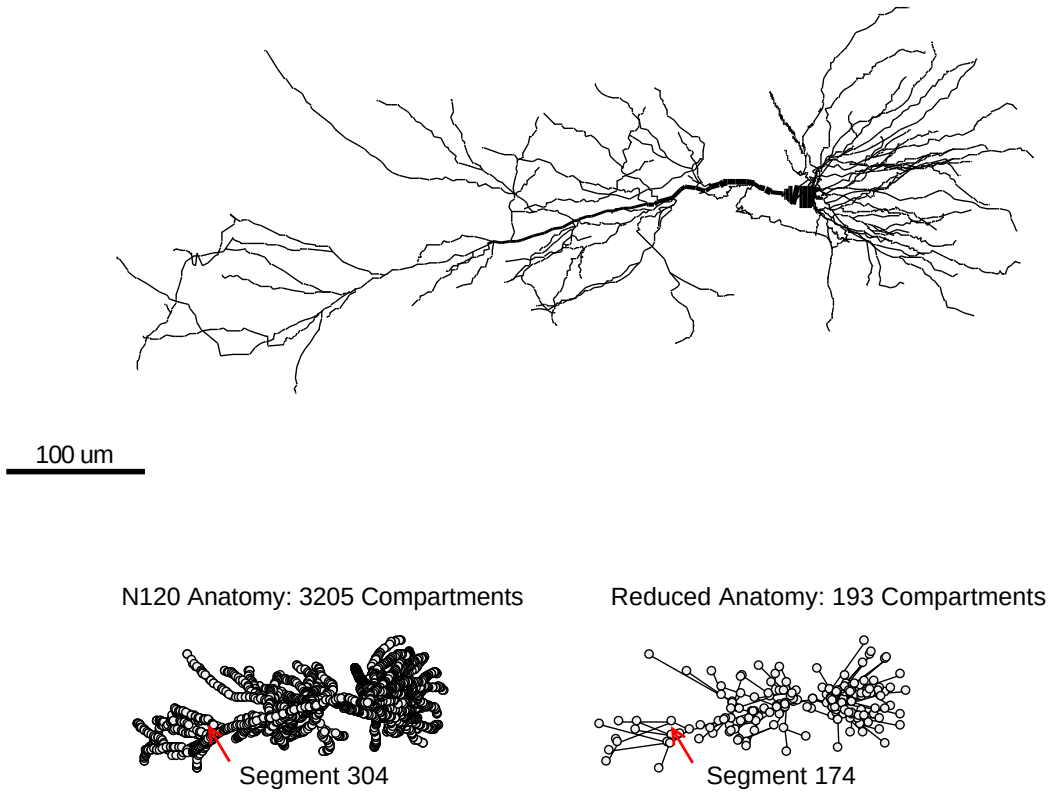

Figure 3: Top: Larger view of the cell model derived from original anatomy file of CA1 N120 cell (Pyapali and Turner, 1994, Figure 3A). Somatic "notches" result from approximating the soma with a series of right cylinders. Bottom: Comparison of compartment density for original anatomy model and reduced model (the N120 Red model in Figure 1) derived by the algorithm described in Section 4.2. Current sources and voltages associated with segments 304 and 174 are referenced in simulations shown in Figure 4. Scale bar applies to cell model at top.

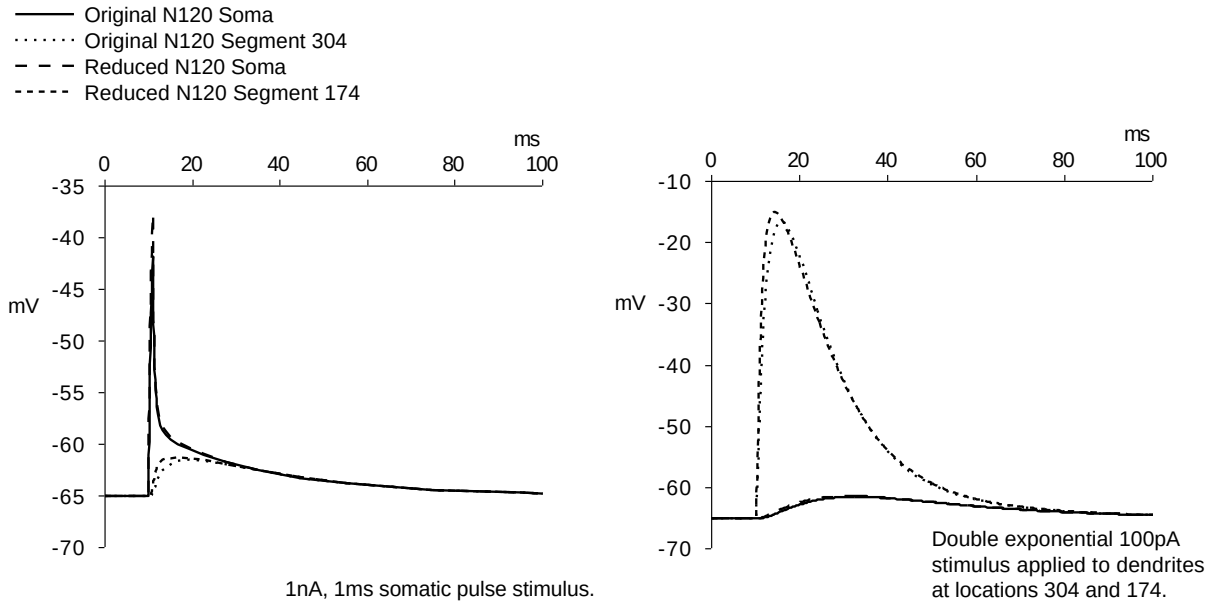

Figure 4: Responses to dendritic and somatic stimulation for the original N120 anatomy and the reduced N120 anatomy described in Section 4.2, demonstrating the close equivalence of these passive models. Dendrite segments 304 and 174 correspond to locations shown in Figure 3. Left: Somatic and dendritic response to 1nA 1millisecond current pulses applied at the somas. Right: Somatic and dendritic response to double exponential current waveforms (difference of 1 millisecond τ and 10 millisecond τ exponentials, with waveform amplitude of 100pA) applied at dendrite locations 304 and 174. The linear parameters for both cells are $R_m = 40\text{k}\Omega\text{cm}^2$, $R_i = 200\Omega\text{cm}$, and $C_m = 0.7\mu\text{F/cm}^2$. R_{in} of the original N120 cell is 191 MΩ, and of the reduced N120 cell is 199 MΩ.

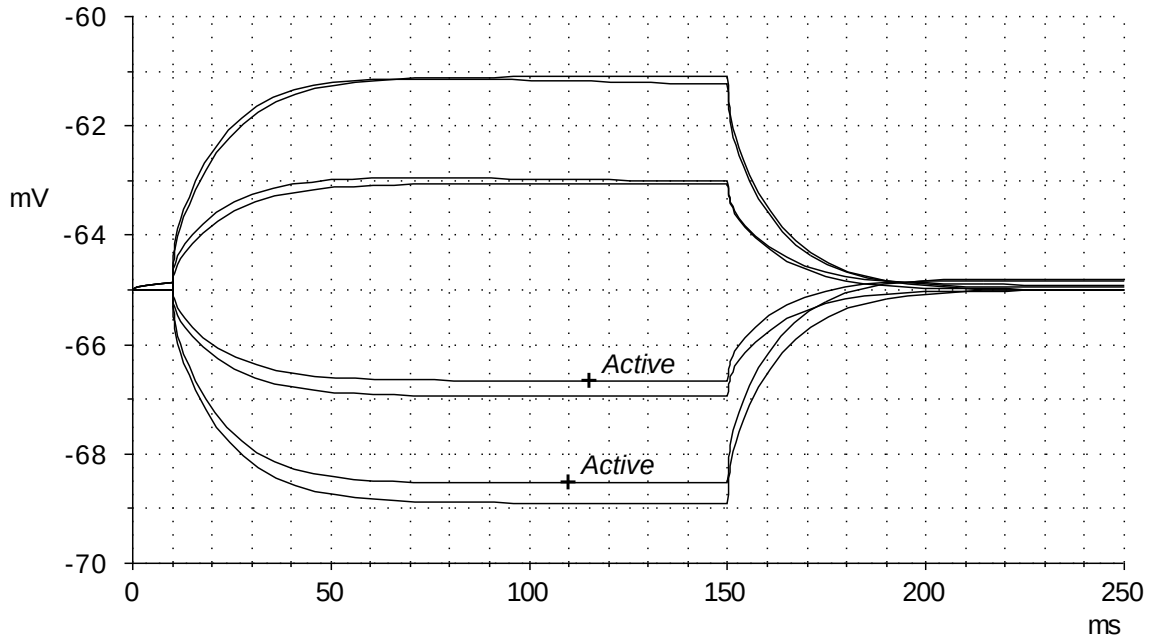

Figure 5: Response of the Working model to small current steps ($\pm$0.05 and 0.1nA), both with all the channels active and blocked. The value for τ_0 in the passive case is 14.4 milliseconds, and in the active case the τ_0 for the response to a 0.1nA step is 14.1 milliseconds; the passive R_{in} is 39MΩ. Note the small inward rectification in the two hyperpolarizing active responses, due mainly to I_H. The depolarizing transient in the active case at the beginning of the trace is due to the fact that the simulation starts with an imposed resting potential of -65mV; after settling of the small activated currents around rest the final resting potential is -65.7mV.

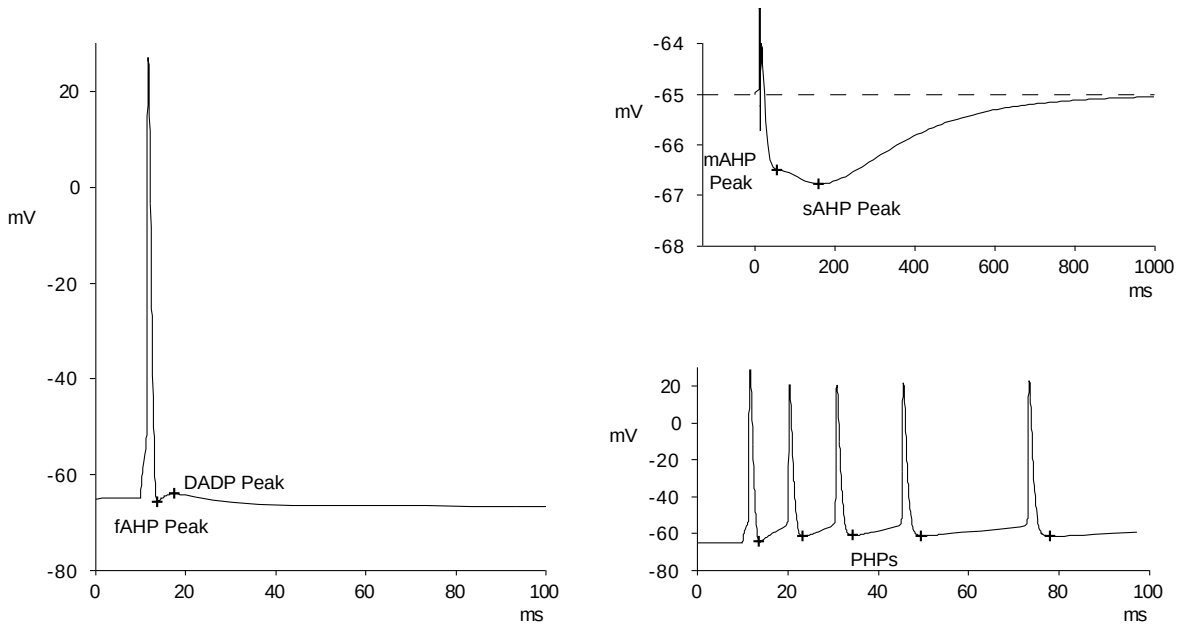

Figure 6: Single spike and spike train responses of the Working model under control conditions illustrating the various landmarks of firing. These include the fast after-hyperpolarization (fAHP), the after-depolarization (ADP), which in this case is a depolarizing ADP (thus DADP), the medium after-hyperpolarization (mAHP) and the slow after-hyperpolarization (sAHP) after a single spike, and the pre-hyperpolarization peak between spikes during repetitive firing (PHP). Note the change of scale in the single spike responses illustrated in the left and upper right panels. In this model, the mAHP moves directly into the sAHP; real cells may show a much more distinct transition. The spike train is in response to a 1.0nA current step; single spikes are in response to 2.5 millisecond 1.0nA pulses. The dashed line in the upper right figure shows the resting potential.

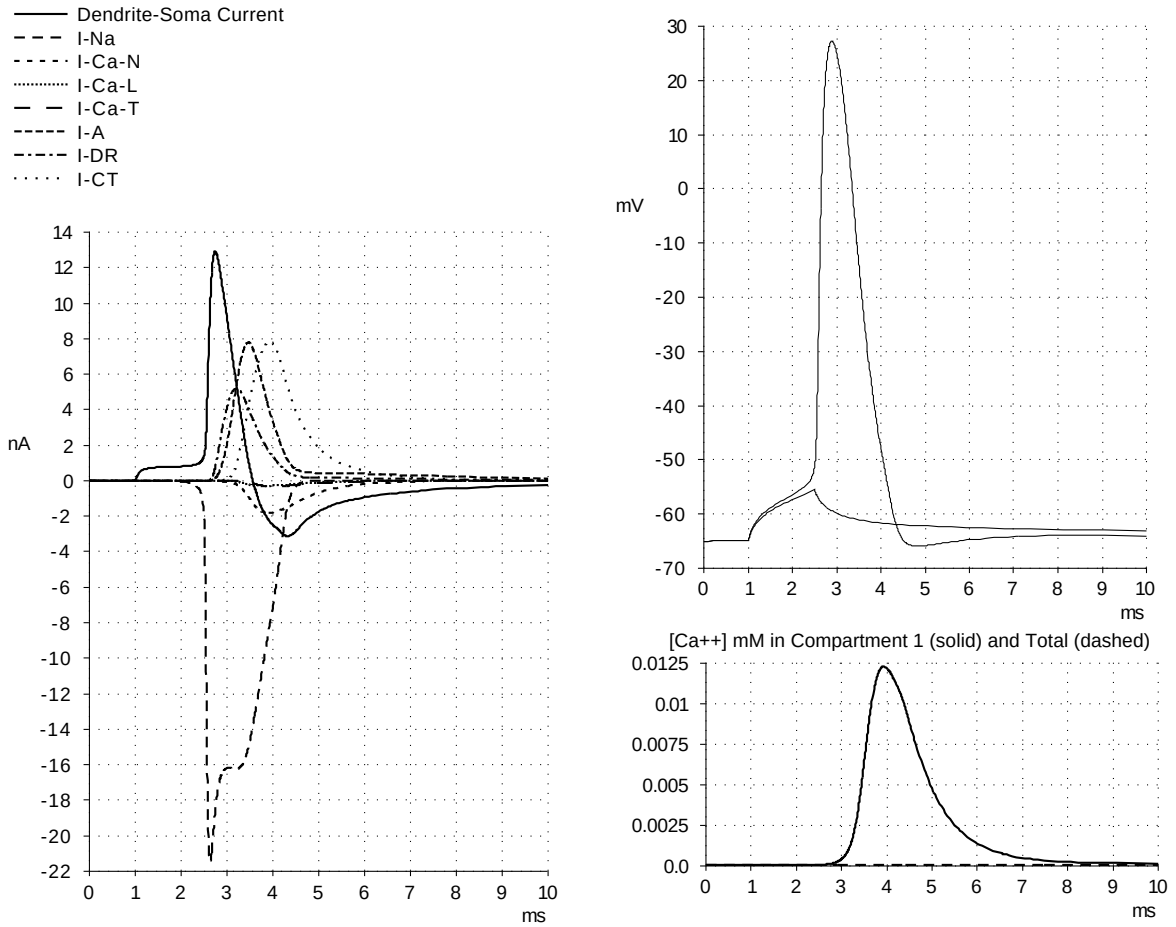

Figure 7: Single spike of the Working model under control conditions, in response to 1.5 millisecond 1.0nA pulse, the major currents active during the spike, and the transient change in $[Ca^{2+}]_{in}$ for the small Ca^{2+} compartment assigned to the Ca^{2+} channels and I_{CT}. Also shown is the subthreshold response to a 1.5 millisecond 0.9nA pulse, showing the sharp threshold in this model. In this version of the model the kinetics of the inward currents are very transient for single spikes, thus the DADP, whose peak occurs between the times of 8 and 9 milliseconds, is mediated almost completely by the capacitive redistribution current from the dendrite cable. Note, however, that the DADP under these conditions is rather short, and that for other HPC cells with more prominent ADPs the role of active currents is more likely. Also, note that the concentration "spike" in compartment 1 is much larger and more transient than the concentration change averaged over the entire soma (compare with Figure 15).

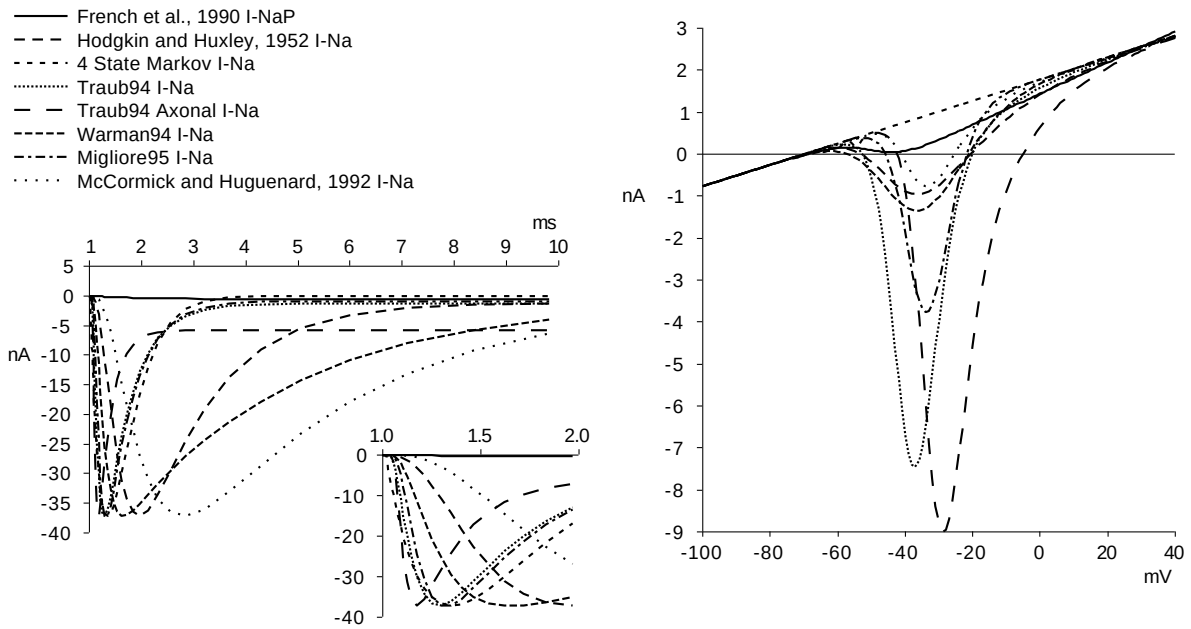

Figure 8: Representative ideal voltage clamp currents and steady-state rectification for various models of I_{Na} and I_{NaP}, corresponding to experiments in which all other voltage-dependent channels are blocked. Thus, for each trace the associated I_{Na} or I_{NaP} is the only activated non-linear current. All I_{NaP} or I_{Na} of a given type is at the soma, and the dendrite is passive. Cell geometry is the BG87 soma/short-cable model, with an input impedance of 39MΩ, and a reversal potential of the leak conductance of -70mV. For this comparison, the maximum conductances for each I_{Na} model was adjusted by normalizing the peak current of each under the voltage clamp protocol shown here to that of the 4 State Markov model. The maximimum conductance of the latter model was adjusted to reproduce the spike characteristics discussed in the text. Thus, each adjusted I_{Na} model would give spike currents of similar (though not exactly the same) magnitude. Also, the 4 State Markov I_{Na} shown here lacks the small steady-state rectification term discussed in the text; the steady-state of the full model is shown in Figure 10. The parameters for the I_{NaP} model are those described by French et al.(1990), with a maximum conductance of 1.2nS (corresponding to measurements in the hippocampal slice preparation). The reversal potentials for the currents are: I_{NaP}, 30mV; Hodgkin and Huxley (1952b) I_{Na}, 55mV; 4 State Markov I_{Na}, 65mV; both Traub94 I_{Na}s, 55mV; Warman94 I_{Na}, 65mV; Migliore95 I_{Na}, 50mV; McCormick and Huguenard (1992) I_{Na}, 45mV. Left (main and inset): Voltage clamp currents in response to clamp voltage step to -20mV, from a holding potential of -70mV. Right: Steady-state rectification of I_{Na}, or window current, compared with I_{NaP}, demonstrated by steady-state I-V characteristics.

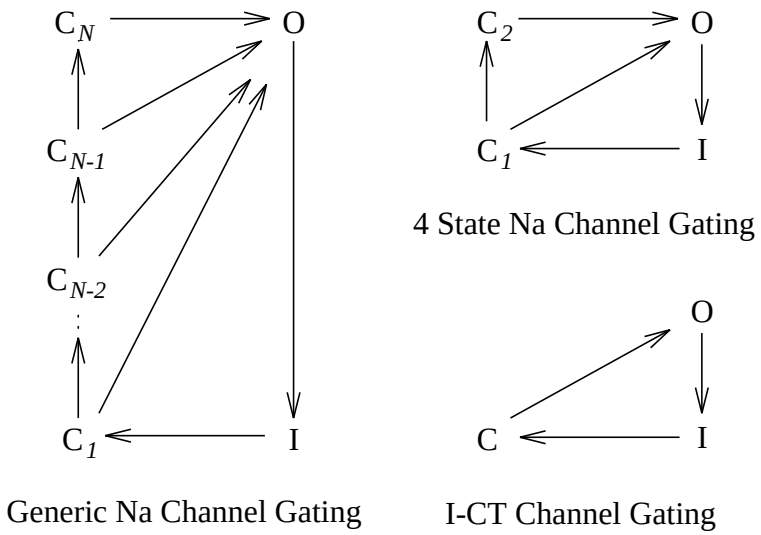

Figure 9: Left: General state diagram for a hypothetical Markov gating model used for I_{Na} in the Working model. From the single inactivated state I, the N closed states C_i are reached with increasing hyperpolarization. The $C_i \rightarrow O$ transitions implement in effect distinct thresholds, occuring at progressively lower potentials with increasing i. Likewise, the $I \rightarrow C_1$ and $C_i \rightarrow C_{i+1}$ transitions occur at voltages hyperpolarized to the associated $C_1 \rightarrow O$ and $C_{i+1} \rightarrow O$ transitions, respectively, somewhat like a rachet mechanism. The $O \rightarrow I$ transition is voltage-independent. Top Right: The 4 state version of the general framework, used in the current version of I_{Na}. Bottom Right: A three state Markov model for I_{CT} gating. The $C \rightarrow O$ transition is Ca^{2+}- and voltage-dependent. The $O \rightarrow I$ transition is strongly voltage-dependent, accounting for the fast turn off of I_{CT} during spike repolarization, giving rise to the fAHP. The much slower $I \rightarrow C$ transition is also voltage-dependent, such that removal of inactivation is slow while the cell is depolarized. In all these schemes the arrows denote the dominant transitions during spike depolarization/repolarization.

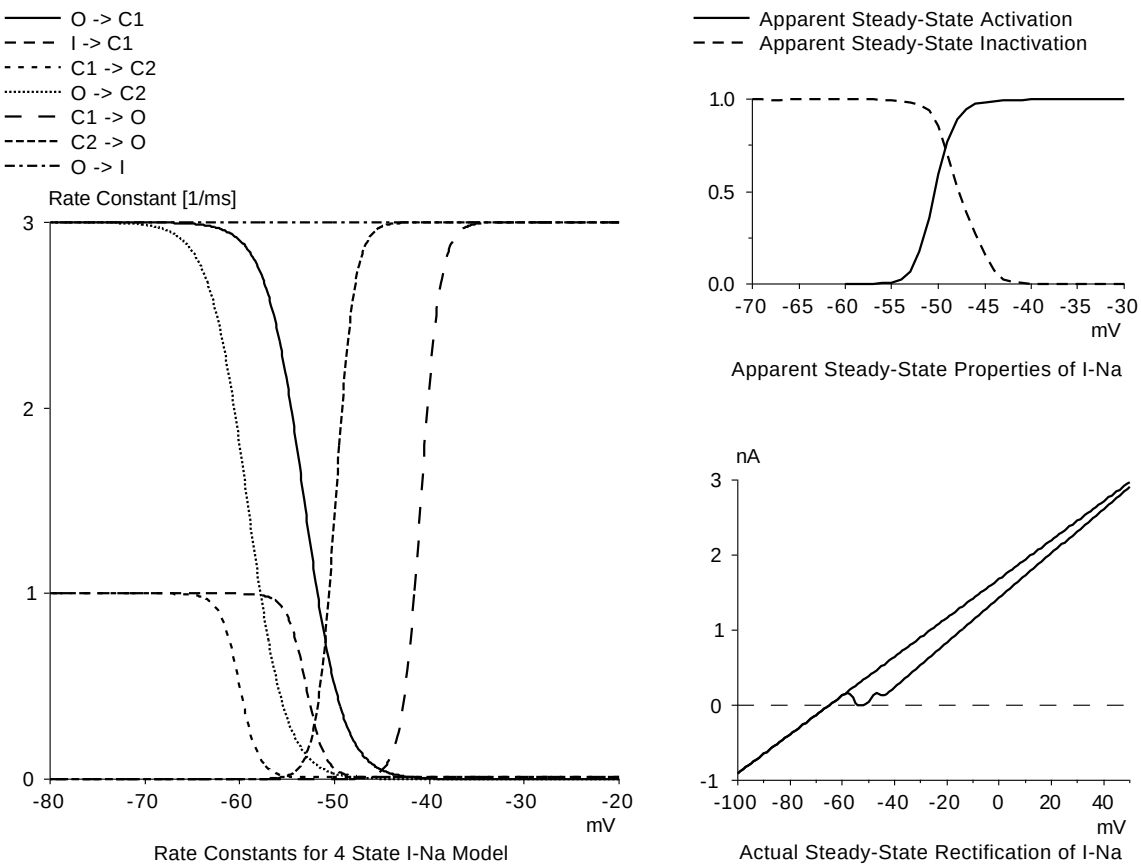

Figure 10: Rate functions for the major state transitions in a 4 state Markov I_{Na} model and voltage clamp simulations. The parameters for the rate functions plotted in the left panel are given in Table 6, according to Equation 4. Note that the "steady-state" activation and inactivation curves derived with standard voltage clamp protocols (upper right panel), predict a substantial overlap, and thus a large window current. However, the actual steady state rectification is minimal (lower right panel), and compares well with the measurements of the persistent Na^+ current I_{NaP} (French et al., 1990), as illustrated in Figure 8.

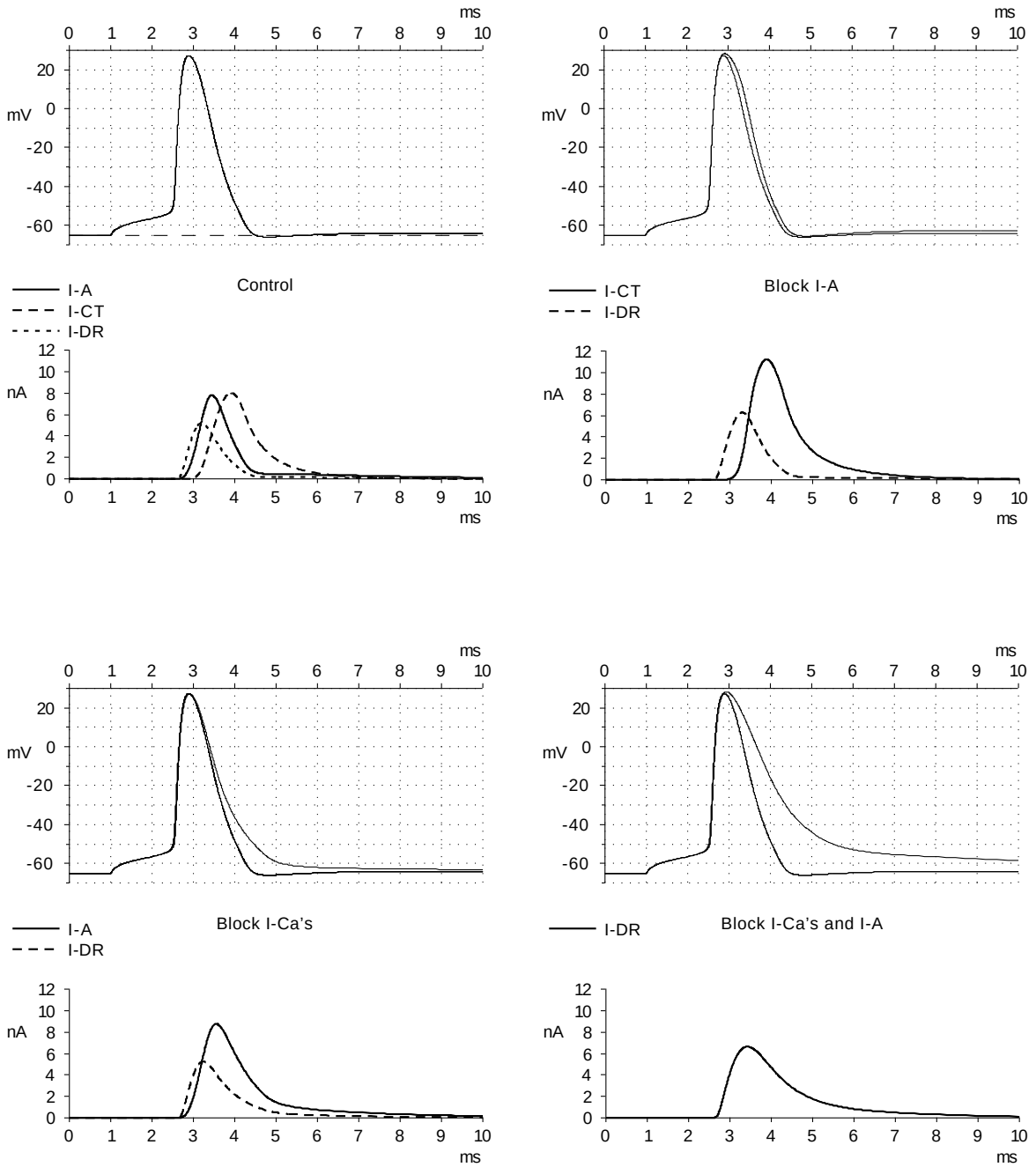

Figure 11: Simulations of the Working model of single spikes and the major K^+ currents evoked with just-threshold short current pulses (1.0nA, 1.5ms), comparing control spike with spikes after the blocking of various channels (cf. Figures 2 and 10 in Storm, 1987a). In the simulations, I_{CT} is effectively blocked when the Ca^{2+} currents are blocked. Note that various combinations of I_{DR}, I_A, and I_{CT} can combine to repolarize the spike, with each combination having a distinct spike signature.

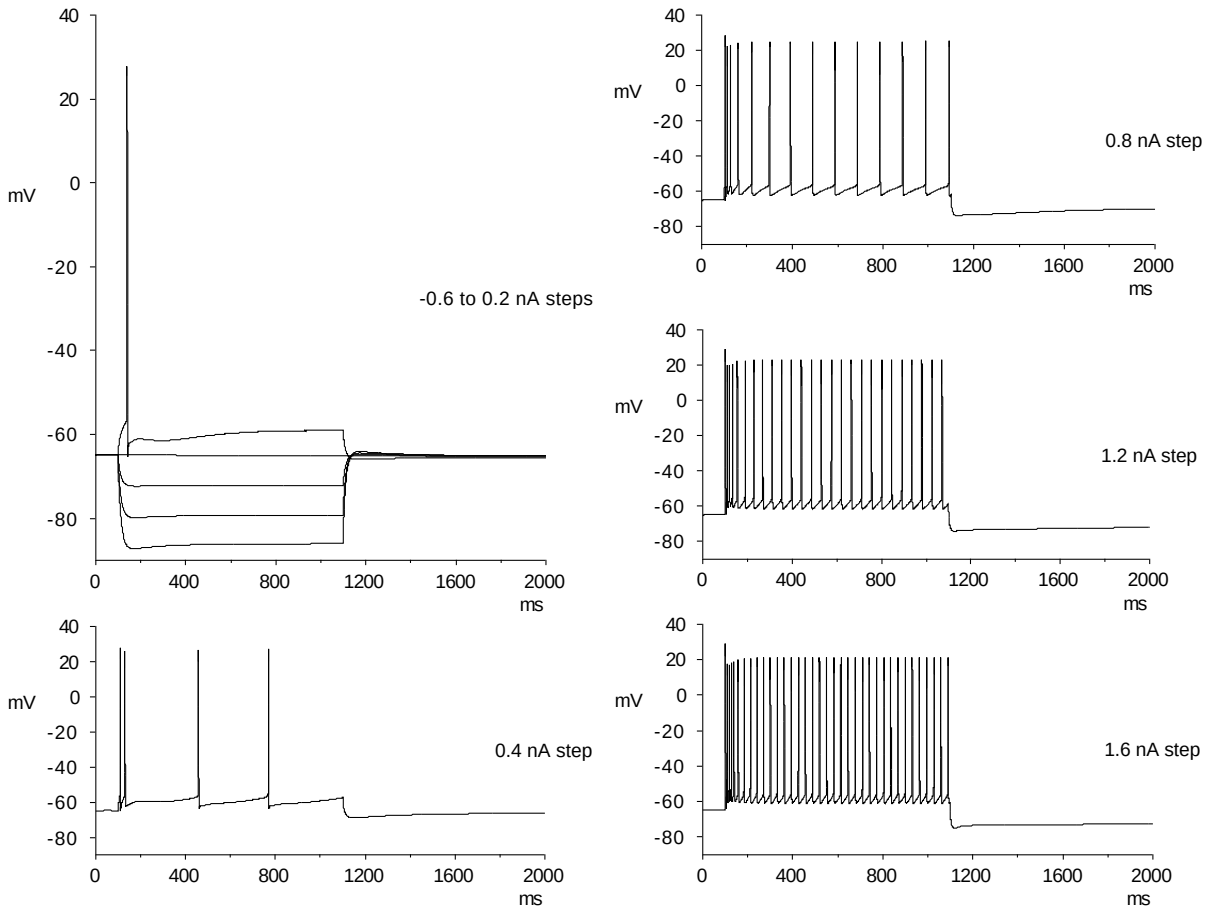

Figure 12: Basic responses to long current steps of the Working model under control conditions. Characteristics of these responses include depolarizing sags to hyperpolarizing current steps, fast initial spiking, followed by strong accommodation, and long lasting hyperpolarizations after spike trains. Also, the prominent fAHP after the spike (more evident in the 0.2nA and 0.4nA responses) disappears during the spike train as the firing frequency increases.

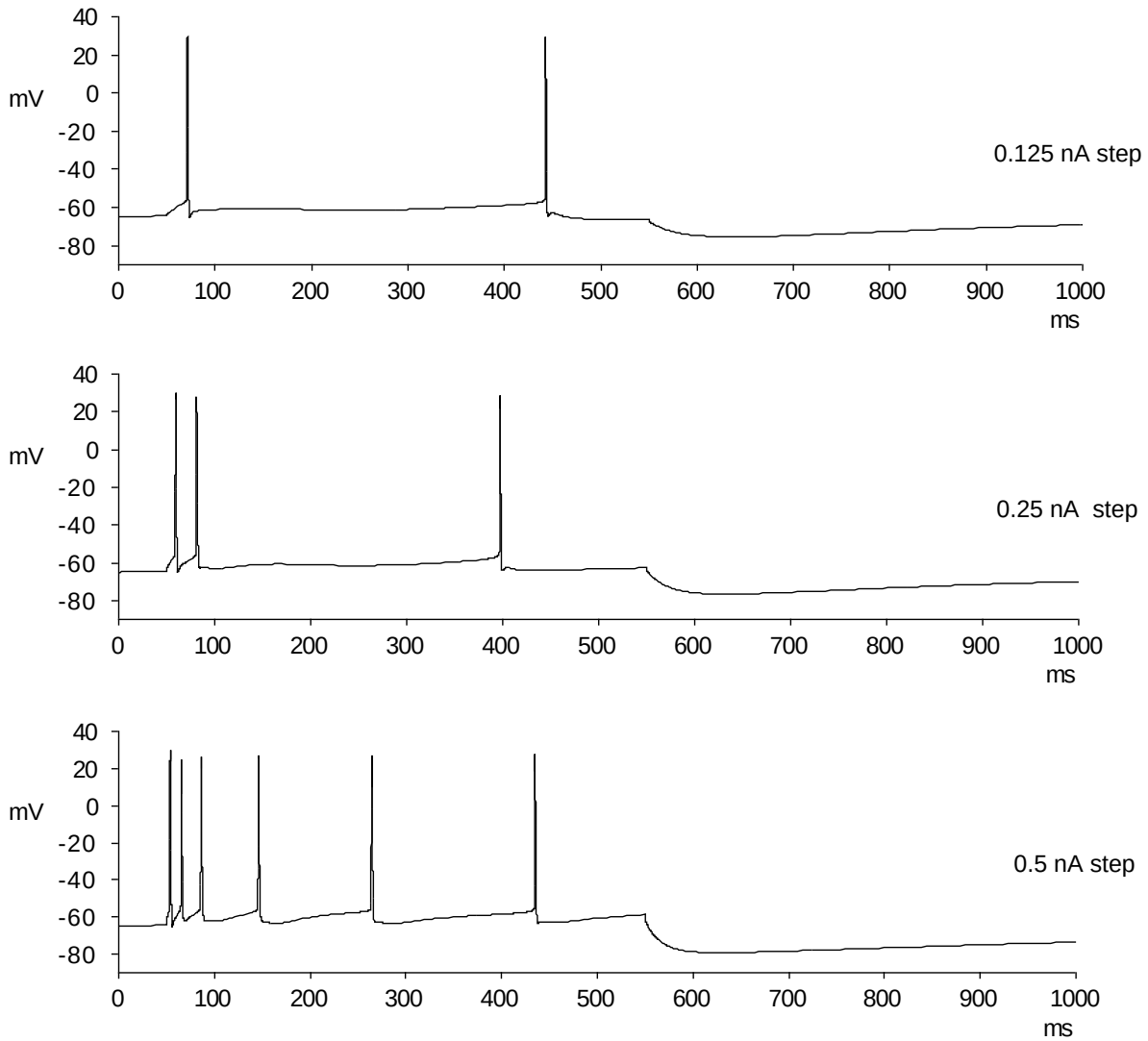

Figure 13: Simulations of the Working model of spike trains after setting R_m for both the soma and dendrites to 100kΩ cm^2, giving an R_{in} of about 210MΩ, thus corresponding more to parameters from whole cell patch recordings. The major differences are the higher gain for the cell with respect to the firing frequency as a function of stimulus intensity, and deeper sAHPs. Otherwise, the cell response is quite similar to that seen with the default linear parameters.

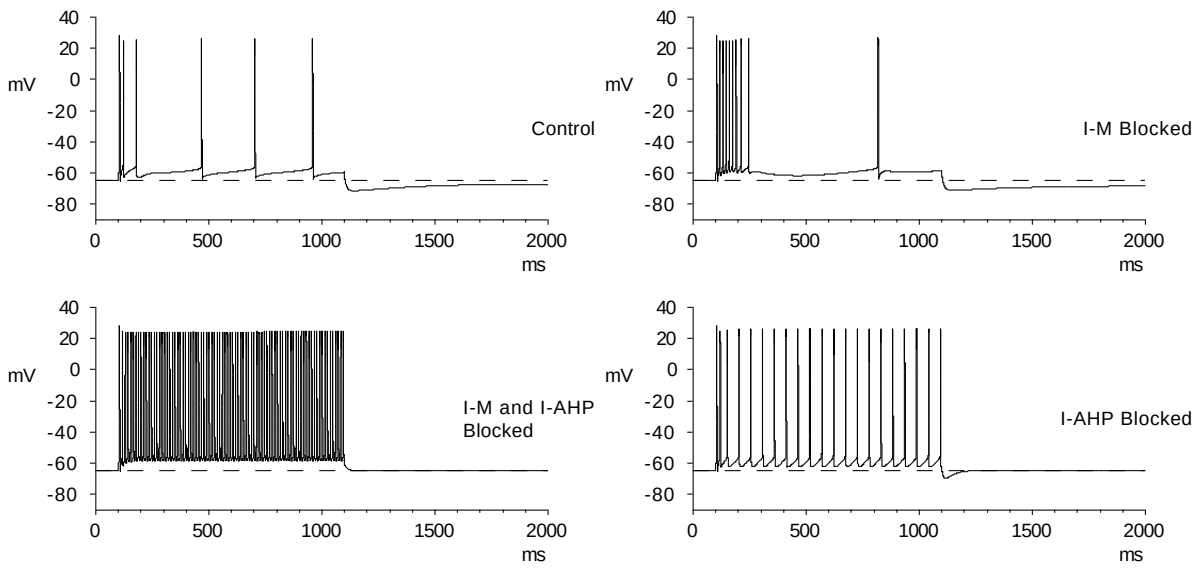

Figure 14: Responses of the Working model to long 0.5nA current steps, illustrating the roles of I_M and AHP in mediating the early and late phases of accommodation. The associated mAHP and and sAHP, or lack thereof, can also be appreciated in these simulations by comparing the after-hyperpolarizations with the resting potential of -65mV, marked by the dashed line. Note the reappearance of the fAHP in the later spike (at around 800 milliseconds) for the response when I_M is blocked.

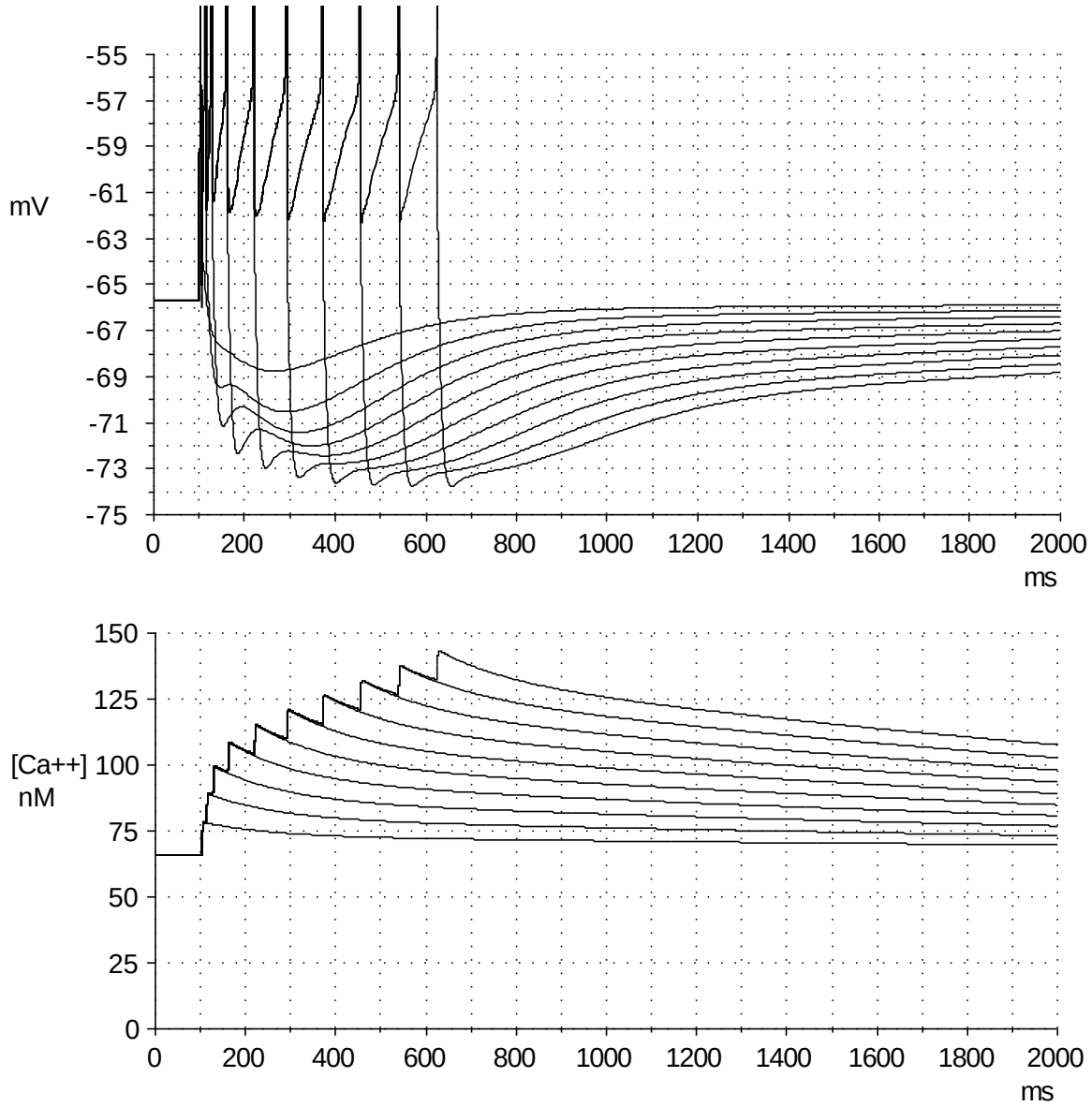

Figure 15:
Evolution of the mAHP, sAHP, and the average somatic $[Ca^{2+}]_{in}$ of the Working model under control conditions, in response to 0.85nA current steps. Durations of the steps were adjusted to evoke from one to ten spikes. For these simulations the "true" steady-state $[Ca^{2+}]_{in}$ of about 66nM was used as an initial condition (obtained after allowing the system to relax for about 20 seconds). The mAHP peak can be readily distinguished, preceeding the sAHP peak after each spike train. The peak of the sAHP for the shorter trains occurs about 200 milliseconds after the stimulus end. Note that the PHPs during the spike train are about six millivolts, starting from about -62mV until spike threshold between -56 and -55mV.

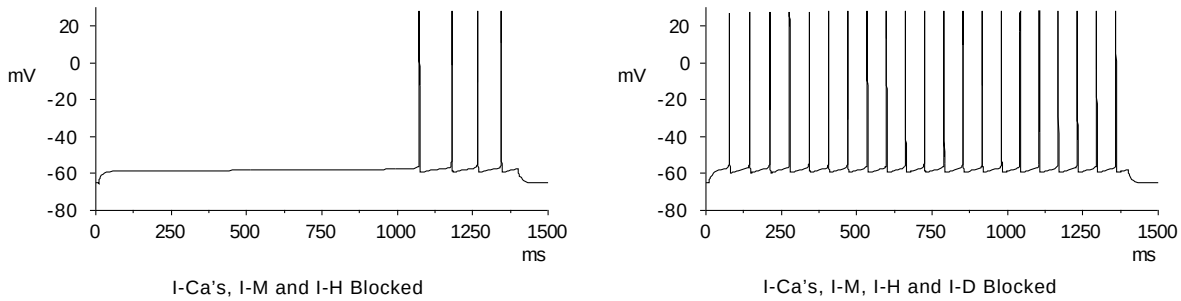

Figure 16: Repetitive firing in response to 0.19nA current step showing the delay in the initial spike mediated by I_D (cf. Figure 2e. in Storm, 1988b). In both traces Ca^{2+} currents, I_M and I_H were blocked, and I_D is blocked in the trace on the right. Although the resting potential of this model was -65mV, a virtual holding potential of -75mV was used to enhance I_D by partial deinactivation. This corresponds to the figure mentioned above in Storm, 1988, where the resting potential of the cell was -74mV.

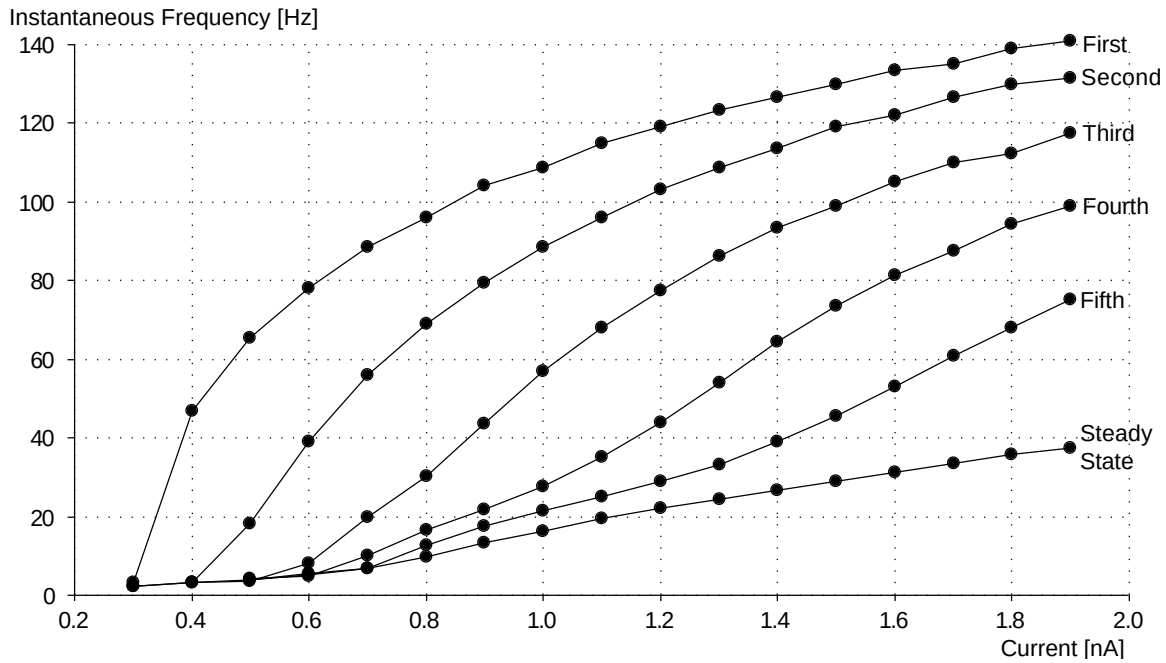

Figure 17:
f/I plot for the Working model under control conditions (compare with Lanthorn et al., 1984). Each trace is the instantaneous firing frequency for the spike interval indicated on the right, for different intensities of long (1000 millisecond) current steps.

Reference	Temp.	Cell Type/ Method	E_{rest} (mV)	R_{in} (MΩ)	τ_0 (ms)
Turner and Schwartzkroin, 1980		CA1/S		28±7	11±4
Brown et al., 1981	37.5°C	CA1/S		43±4	15±1
		CA3/S		39±3	19±2
		DGC/S		38±3	12±1
Thompson et al., 1985	37°C	CA1/S	-64±9	30±9	
	27°C		-60±7	52±13	
Stafstrom et al., 1992	32°C	DGC/S	-74±2	54±3	14±2
		DGC/P	-84±1	228±14	27±1
Spruston and Johnston, 1992	32°C	CA1/PP	-64±2	104±10	28±2
		CA3/PP	-66±1	135±8	66±4
		DGC/PP	-74±2	446±87	43±4
Buckmaster et al., 1993	35°C	CA3c, burst?/S	-62±0.9	52±3.5	16±1.2
Scharfman, 1993		CA3c, burst/S	-66±2	63±5	23±2
Major et al., 1994	20-24°C	CA3/P		190[1]	93[1]
Zhang et al., 1994	33°C	CA1/S	-66±1	38±2	
		CA1/P[2]	-60±1	59±2	
		CA1/P[3]	-63±1	51±3	
Jensen et al., 1996	33.5°C	CA1, non-burst/S	-63±3	25±8	8±2
		CA1, burst/S	-63±3	26±7	14±5
		CA1, all/S	-63±3	26±7	13±5
Fraser and MacVicar, 1996[4]	34-35°C	CA1/P	-65±0.1	149±3	20.7±0.4
Working Model			-65.7[5]	39	14

Table 1: Values of measured linear parameters from various sources, along with those for the Working model. For "Method", S = sharp microelectrode, P = whole-cell patch electrode, PP = perforated patch electrode. For this and subsequent tables, most values are rounded to 2 significant figures, and are followed by the reported standard deviation when available; a blank field means parameter not given or not applicable, "DGC" dentate granule cell. Measurements from CA1 and CA3 are all from pyramidal cells. Patch pipettes in both Major et al. and Fraser and MacVicar were filled with K-gluconate solutions. For the different temperatures tested by Thompson et al., and the different patch pipette filling solutions tested by Zhang et al., there was a statistically significant difference in the R_{in} values, but not the E_{rest}. In the different firing classifications used by Jensen et al., there was a significant difference in the value of τ_0 between bursting and non-bursting CA1 HPCs. Notes: 1 - Average of 4 cells. 2 - $KMeSO_4$ filled patch pipettes. 3 - K-gluconate filled patch pipettes. 4 - Data from 188 cells. 5 - "True" E_{rest} obtained after 20 second relaxation to steady-state from a holding potential of -65mV.

Reference	Temp.	Thresh.(H.P.) (mV)	Amplitude (mV)	dV/dt Rise (mV/ms)	dV/dt Fall (mV/ms)	Duration (ms)
Thompson et al., 1985	37°C	-50(-55)	78±10	394±90	105±21	.78±0.1
	27°C	-45(-55)	79±10	265±79	43±7	1.5±0.3
Andersen et al., 1986	34°C	-49(-65)				
Storm, 1987a	28-33°C	-55/-45(-60/-70)	98±8	238±16	85±19	
Spruston & Johnston, 1992	32°C	-55(-66)				
Buckmaster et al., 1993	35°C		66±1			2.6±.1
Scharfman, 1993		-47(-63)	85±2	410±25	87±5	1.7±0.2
Jensen et al., 1996	33.5°C	-56±3(-63±3)	89±5			
Working Model		-54(65)	78	467	98	.83

Table 2: Values of single spike parameters of regular spiking cells (except for that from Scharfman, which were quasi-bursting cells), compared with that for the Working model. Cell types are either CA1 pyramidal cells or CA3c cells (Buckmaster et al. and Scharfman), and recordings are either with sharp electrodes or perforated patch (Spruston and Johnston). In all cases parameters were taken from either the single spike in response to a brief current pulse or the initial spike in response to a sustained, near threshold stimulus. "Thresh.(H.P.)" refers to the spike threshold, with the holding potential in parentheses - note that this may or may not be the "true" resting potential. The values given for Storm, 1987a, are ranges. Spike threshold in Andersen et al. (1986) was defined as the point at which dV/dt was greater than 50mV/ms, for the Working model this point was taken as when dV/dt was greater than 12mV/ms, and the thresholds reported in Jensen et al. (1996) were apparently determined "by eye". Similarly, the remainder of the values were estimated by the author from figures in the cited reference. Spike amplitude was measured from threshold in all cases, except for Storm, where amplitude was referenced from the holding potential, and Buckmaster et al., who defined spike onset as the point at which $dV/dt > 12$mV/ms. The maximum rates of rise and fall were reported by Thompson et al., and used for the Working model. Storm used the 10-80% and 80-20% points (relative to spike threshold and peak), Scharfman the slope of lines fitted from the threshold to the peak and the peak back to the threshold voltage, as references for the rate of rise and fall, respectively. The spike duration was taken in Thompson et al. and the Working model as the width at half amplitude, for Buckmaster et al. as the time from spike onset to the recrossing of the onset voltage, and for Scharfman and Jensen et al. the time from spike threshold to the recrossing of the threshold voltage.

Reference	Cell	Temp.	Location	$\Delta[Ca^{2+}]$/spike (nM)	Decay τ (ms)
Jaffe et al., 1992	HPC	30°C	soma	2.1	$>500^{est}$
			60μm from soma	3.5	$>500^{est}$
			>250μm from soma	no change	
Spruston et al., 1995	HPC CA1	22-24°C	within 400μm of soma	60	500^{est}
Schiller et al., 1995	LV CPC	24°C	proximal dendrite	110	560
		34°C		110	300
Christie et al., 1995	HPC CA1	30°C	soma	11	2000^{est}
			1-50μm from soma	16	600^{est}
			50-200μm from soma	11-16	400^{est}
Working Model			soma	12	1000^{est}

Table 3: Values for $[Ca^{2+}]_{in}$ changes in response to current-evoked spikes from the literature and the Working model, expressed as $\Delta[Ca^{2+}]$/spike. Values marked with est are measured directly from figures in the cited reference. LV CPC - layer V cortical pyramidal cell.

Channel	Major Ion(s)	Gating Equation	E_{rev} (mV)	$\overline{g}$ (μS)	$\overline{p}$ (cm^3/s)	Major Functional Role
I_{Na}	Na^+	x	+65	1.2		Spike Upstroke
I_{CaN}	Ca^{2+}	m^2h	+135[1]		1e-8	Trigger I_{CT}, I_{AHP} Ca^{2+} Spikes
I_{CaL}	Ca^{2+}	m^2	+135[1]		3e-9	
I_{CaT}	Ca^{2+}	m^2h	+135[1]		3e-9	
I_D	K^+	x^4y^4	-95	0.05		Sub-threshold integration
I_{DR}	K^+	xy	-70	0.4		Spike repolarization
I_A	K^+	x^4y^3	-70	2.3		Spike repolarization
I_{CT}	K^+	x	-80	0.4		Repolarization of first spikes in train
I_M	K^+	x^2	-80	0.4		Medium adaptation
I_{AHP}	K^+	w^2	-85	0.02		Slow adaptation
I_H	K^+,Na^+	y	-17	0.003		Stability of E_{rest}

Table 4: Summary of the channels used in the Working model. The x particles in the gating expressions for I_{Na} and I_{CT} are the Markov gating particles shown in Figure 9, with parameters given in Tables 6 and 8. The parameters for the remaining particles referenced in the gating expressions, defined with the extended Hodgkin-Huxley model, are given in Table 5. The parameters $\overline{g}$ and $\overline{p}$ characterize ohmic and GHK current equation based constant-field conductance models, respectively. Note 1: Based on the Nernst potential equation with resting $[Ca^{2+}]_{in}$ of 50nM and $[Ca^{2+}]_{out}$ of 1.8mM - this overestimates the true driving force since the current for these channels is calculated using the GHK current equation.

Channel	Particle	order	z	γ	K (1/ms)	$V_{1/2}$ (mV)	τ_0 (ms)
I_{CaL}	m	2	4.6			-1	1.5
I_{CaN}	m	2	3.4			-21	1.5
	h	1	-2			-40	75
I_{CaT}	m	2	3			-36	1.5
	h	1	-5.2			-68	10
I_D	x	4	3			-63	1
	y	4	-2.5	0	2e-4	-73	0
I_{DR}	x	1	3	0.8	1.7e-1	-5	0.8
	y	1	-1			-68	300
I_A	x	4	2.8	0.85	8e-2	-41	1
	y	3	-3	1	4e-2	-49	2
I_M	x	2	6	0.6	3e-3	-45	8
I_H	y	1	-2			-98	180

Table 5: Parameters of the extended Hodgkin-Huxley model particles in the Working model. The number of particles of a given type assigned to a channel is given by the "order" parameter, as listed in the "Gating Equation" column in Table 4. An empty entry for K means that $1/K << \tau_0$, and thus the time constant for the particle is essentially voltage independent and equal to τ_0. In this case the entry for γ is blank since this parameter only effects the voltage dependent time constant. The parameters α_0 and β_0 described in Section 8.4.2 are 0 for all these models.

Transition	$1/\tau_{max}$ (1/ms)	k (mV)	$V_{1/2}$ (mV)	$1/\tau_{min}$ (1/ms)
$C_2 \rightarrow O$	0	1	-51	3
$O \rightarrow C_2$	0	-2	-57	3
$C_1 \rightarrow O$	0	1	-42	3
$O \rightarrow C_1$	0	-2	-51	3
$I \rightarrow C_1$	0.01	-1	-53	1
$C_1 \rightarrow C_2$	0.01	-1	-60	1
$O \rightarrow I$	n/a	n/a	n/a	3

Table 6: Parameters of the I_{Na} Markov gating in the Working model, according to Figure 9 and Equation 4. The $O \rightarrow I$ transition is voltage-independent and is equal to $3/ms$. The τ_{min} parameter represents a rate-limiting step: its inverse gives the maximum rate for a state transition. Likewise, the inverse of τ_{max} acts as a voltage-independent additive rate for a transition. In this version of the I_{Na} model, the rates for the transitions $I \rightarrow O$, $C_1 \rightarrow I$ and $C_2 \rightarrow C_1$ are assumed very small and thus ignored.

Transition	$1/\tau_{max}$ (1/ms)	k (mV)	$V_{1/2}$ (mV)	$1/\tau_{min}$ (1/ms)	α (ms^{-1} mM^{-n})	β (1/ms)	n
$O \rightarrow I$	0	-3.5	-64	10			
$I \rightarrow C$	0	-10	-120	0.1			
$C \rightarrow O$	1	7	-20	1000	1e6		3
$O \rightarrow C$	n/a	n/a	n/a	n/a		0.05	

Table 7: Parameters of the I_{CT} Markov gating in the Working model, according to Figure 9, Equations 4 (the τ_{max}, k, $V_{1/2}$ and τ_{min} parameters), and Equations 5 and 6 (the α, β and n parameters). Note that the $C \rightarrow O$ transition is defined (Equation 7) as the product of the $\alpha(V)$ (Equation 4) and $\alpha[Ca^{2+}]^n$. The exponent n in the units for α is the number of bound Ca^{2+} ions, as given in the table. Similar to the model of I_{Na}, for I_{CT} the rates for the transitions $I \rightarrow O$ and $C \rightarrow I$ are assumed very small and thus ignored.

Particle	order	α (ms^{-1} mM^{-n})	β (1/ms)	n	τ_0 (ms)
w	2	2e14	0.01	4	100

Table 8: Parameters of I_{AHP} Ca^{2+}-dependent gating particle w in the Working model, as defined by Equations 5 through 7. The exponent n in the units for α is the number of bound Ca^{2+} ions, as given in the table.